TEMPERATURE ROBUST
ACTIVE VIBRATION CONTROL OF A PLATE
USING PIEZOELECTRIC SENSORS AND ACTUATORS

A THESIS

by

VIVEK GUPTA

SUBMITTED TO HIMACHAL PRADESH UNIVERSITY
IN THE FACULTY OF PHYSICAL SCIENCES
IN FULFILLMENT OF THE REQUIREMENTS FOR THE DEGREE OF

DOCTOR OF PHILOSOPHY

IN

PHYSICS

JANUARY 2012

under the joint supervision of

Dr. Nagesh Thakur
Department of Physics,
Himachal Pradesh University,
Shimla.

Dr. Manu Sharma
Mechanical Engineering Branch,
University Institute Engineering & Tech.,
Panjab University, Chandigarh.

DEPARTMENT OF PHYSICS
HIMACHAL PRADESH UNIVERSITY
SHIMLA-171005

INDIA

ABSTRACT

In this thesis, a new scheme for active vibration control of a 'smart piezo structure' is proposed. The proposed scheme makes active vibration control technique robust to temperature variations. The whole scheme is analytically derived, understood using simulations and finally experimentally verified. This scheme has been made robust to temperature variations by including the temperature dependence of piezoelectric strain and permittivity coefficients in piezoelectric constitutive equations. Temperature dependence of these coefficients is material specific and there is no reliable analytical expression for this so far. Therefore, it is proposed that the temperature dependence of strain and permittivity coefficients be included in piezoelectric constitutive equations using experimental characterization of the piezoelectric material. In this work, piezoceramic PZT-5H is used as sensor and actuator. Actual experimental values of PZT-5H strain coefficient (d_{31}) and permittivity ($\in_{33}$) have been used for temperatures ranging from -75ºC to 160ºC. These values are obtained by experimental characterization of PZT-5H and the piezoelectric constitutive equations have been augmented using these values [78]. The variation of 'd_{31}' and '$\in_{33}$' with temperature is included in the piezoelectric constitutive equations using curve fit technique. It updates piezoelectric constitutive equations at each 'ambient temperature'. As a result, modal state vectors are accurately estimated and the control law applies required control voltages on PZT-5H actuator at all temperatures. Simulation studies show that it makes active vibration control technique robust to temperature variations. Experimental findings have confirmed this new scheme for active vibration control of a 'smart piezo structure'. To implement

this new scheme, firstly d-form augmented piezoelectric constitutive equations have been converted into e-form. Using e-form constitutive equations, a finite element model of smart two dimensional plate instrumented with piezoelectric patches is derived. Coupled equations of motion are uncoupled using 'modal analysis'. First three modal displacements and velocities are estimated using Kalman observer. First mode of smart cantilevered plate is actively controlled using 'negative velocity feedback' control law at various temperatures. Simulation results are presented using MATLAB. It is observed that active vibration control performance is not maintained at temperature away from 'reference temperature' of PZT-5H if temperature dependence of 'd_{31}' and '$\in_{33}$' is ignored. However, active control of vibrations becomes robust to temperature variations when temperature dependence of 'd_{31}' and '$\in_{33}$' is included in piezoelectric constitutive equations. Finally, experiments are performed at elevated temperatures which confirm simulation results and thus, the new scheme for active vibration control !

TABLE OF CONTENTS

NOMENCLATURE

Symbol	Description
$[\ ]$	Matrix
$[A]$	System state matrix
$[B]$	Control matrix
$[C]$	Output matrix
$[C']$	Damping matrix
$[c]$	Elasticity matrix
$[d]$	Piezoelectric strain coefficient matrix
$[e]$	Piezoelectric stress coefficient matrix
$[K]$	Stiffness matrix
$[M]$	Mass matrix
$[\in]$	Permittivity coefficient matrix
$\{\ \}$	Vector
$\{D\}$	Electric displacement vector
$\{E\}$	Electric field vector
$\{f^e\}$	External force vector on an element
$\{p\}$	Pyroelectric constant vector
$\{s\}$	State vector of the system

$\{x\},\{\dot{x}\},\{\ddot{x}\}$	Displacement vector, velocity vector, acceleration vector
$\{y\}$	Sensor output
$\{\alpha\}$	Coefficient of thermal expansion vector
$\{\gamma_{ij}\}$	Shear strain vector in j^{th} direction in the plane perpendicular to i^{th} direction
$\{\sigma\}$	Stress vector
$\{\sigma_{ij}\}$	Normal stress vector in j^{th} direction in the plane perpendicular to i^{th} direction
$\{\varepsilon\}$	Strain vector
$\{\varepsilon_{ij}\}$	Normal strain vector in j^{th} direction in the plane perpendicular to i^{th} direction
$\{\tau_{ij}\}$	Shear stress vector in j^{th} direction in the plane perpendicular to i^{th} direction
A	Area
a ,b, h	Length, breadth, thickness
c_{ijkl}	Elasticity stiffness constant
D_n	Electric displacement in n^{th} direction
d_{31}	Piezoelectric strain constant
d_{ij}	Piezoelectric strain constant
$\overline{d}_{nij}$	Change in piezoelectric strain coefficient per unit temperature
d_{nij}^{T}	Piezoelectric strain coefficient at constant temperature
E_n	Electric field in n^{th} direction

e_{31}	Piezoelectric stress constant
e_{ij}	Piezoelectric stress constant
e_{nkl}^{T}	Piezoelectric stress coefficient at constant temperature
$\bar{e}_{nkl}$	Change in piezoelectric stress coefficient per unit temperature
G_c	Controllability Gramian matrix
f	Force
I	Moment of inertia
k	Feedback control gain
K	Dielectric constant of piezoelectric material
L	Lagrangian
M	Moment
m_i	Modal mass of i^{th} eigen mode
p	Pyro electric constant
p_n^{σ}	Pyroelectric constant in n^{th} direction at constant stress
q	Charge applied on piezoelectric material
$s_{ijkl}^{E,T}$	Compliance at constant electric field and temperature
s_{ij}	Compliance
T	Temperature
ΔT	Change in temperature from 'reference temperature'
t	Time
u, v'', w	Displacements along x, y and z-axs

V	Voltage applied on piezo-actuator
v	Voltage generated in piezoelectric material
w_m	Natural frequency of the m^{th} mode of vibration
Y	Young's modulus of elasticity
α_{ij}^{E}	Coefficient of thermal expansion at constant electric field
α_{kl}	Coefficient of thermal expansion
σ	Stress
σ_{ij}	Normal stress in j^{th} direction in the plane perpendicular to i^{th} direction
ρ	Density
ν'	Poisson's ratio
λ_i	i^{th} eigen value
$\in_0$	Absolute permittivity
ε_{ij}	Normal strain in j^{th} direction in the plane perpendicular to i^{th} direction
$\in_{nm}^{T}$	Permittivity constant at constant temperature
$\bar{\in}_{nm}$	Change in permittivity constant per unit temperature
ω_j	Modal frequency
ζ_j	Modal damping ratio
$\eta_i(t)$	Time response of the i^{th} eigen mode

Subscripts

int	Property due to intrinsic effect

ext	Property due to extrinsic effect
s	Substrate
p	Piezoelectric
j	In the j^{th} direction

Superscripts

T	Transpose
int	Property due to intrinsic effect
ext	Property due to extrinsic effect

LIST OF FIGURES

LIST OF TABLES

ABBREVIATIONS

Symbol	Description
ACLD	Active Constrained Layer Damping
A/D	Analog to Digital
ANS	Assumed Natural Strain
ARE	Algebraic Riccati Equation
AVC	Active Vibration Control
CMPF	Combined Position Mode Function
DAQ	Data Acquisition
D/A	Digital to Analog
DC	Direct Current
EAS	Enhanced Assumed Strain
FEA	Finite Element Analysis
FEM	Finite Element Method
FFT	Fast Fourier Transform
FRF	Frequency Response Function
HSANS	Hybrid Stress Assumed Natural Strain
PVC	Passive Vibration Control
PVDF	Poly VinylDene Fluoride
PZT	Lead Zirconate Titanate
RHEAS	Refined Hybrid Enhanced Assumed Strain
SVD	Singular Value Decomposition

CHAPTER I

INTRODUCTION

Evolution of human civilization is saga of materials development viz. Stone age, Bronze age, Iron age etc. Use of natural materials with their inherent limitations in the native form continued up to the dawn of the 20^{th} century. Thereafter, ability to synthesize materials brought in its wake the development of smart materials. Smart materials are the materials whose one or more properties can be significantly changed in a controlled fashion using external stimuli such as stress, temperature, electric field, magnetic field, moisture etc. Smart materials when combined with modern day processors, has enabled human civilization to realize a new type of structures known as smart structures.

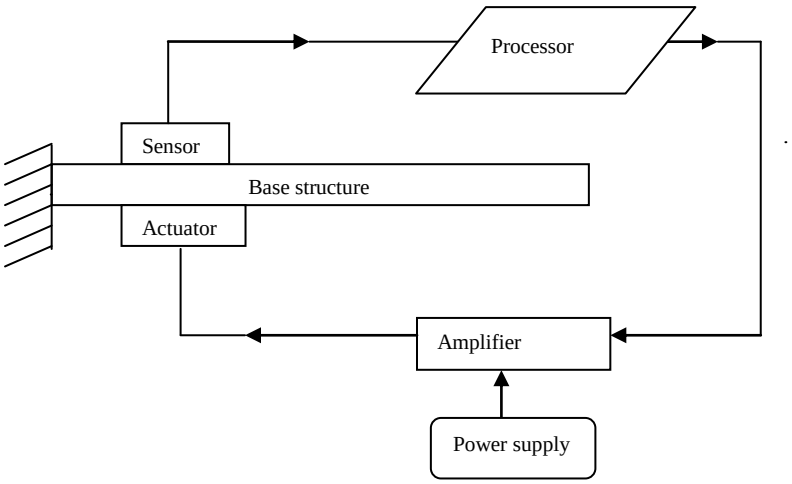

Figure 1.1: A schematic of a smart structure

A structure whose structural characteristics e.g. damping, shape etc. change automatically so as to adapt to environmental disturbances or to meet the mission

requirement is known as a ‘smart structure’. An external source of energy is used to control structural response of a ‘smart structure’. A ‘smart structure’ essentially consists of sensors to capture the dynamics of the structure, a processor to manipulate the sensor signals, actuators to obey the order of processor and a source of energy to actuate the actuators (Figure 1.1). Also known as intelligent/adaptive/active structure, a ‘smart structure’ can be used for vibration control, shape control, structural health monitoring, micro-sensing, nano-positioning, fuel injection etc. It has applications in space, automotive, optical, machine tool, medical, infrastructural systems etc. Development of smart structures has recently gained lot of interest due to: (i) increased interest of man in space exploration, nano-positioning, micro-sensing etc. (ii) advent of fast processors, real time operating systems etc. (iii) development of stable and high performance sensors and actuators and (iv) advances in control theory. Solid state sensors and actuators made up of smart materials are the basic building blocks of a ‘smart structure’. These are integrated into the structure either by surface bonding or embedding without causing any significant changes in the mass or stiffness of the basic structure. Some commonly used smart materials are: piezoelectric materials, shape memory alloys, electrostrictive materials, magnetostrictive materials, electro–rheological fluids etc. In present work, piezoelectric patches are used as sensors and actuators for active vibration control of a ‘smart structure’. Therefore, in the following sections, a brief introduction is given on ‘smart piezo structure’, ‘piezoelectricity’ and ‘active vibration control’.

1.1 Smart Piezo Structure

Realization of a ‘smart structure’ using smart piezoelectric materials has found tremendous interest of researchers all over the globe in the past two decades. A ‘smart

structure' wherein piezoelectric materials are used as sensors and actuators is known as 'smart piezo structure'. Among all the smart materials available for use in smart structures, only piezoelectric materials have the unique capability to be used effectively as both sensor and actuator elements. Piezoelectric sensors and actuators are being used extensively in smart structures due to their excellent electromechanical properties viz. fast response, easy fabrication, design flexibility, low weight, low cost, large operating bandwidth, low power consumption, generation of no magnetic field while converting electrical energy into mechanical energy etc. To understand the working of smart piezo structures, one needs to understand the phenomenon of piezoelectricity.

1.2 Piezoelectricity

The name piezoelectricity is made up of two parts 'piezo' and 'electricity'. Piezo is a Greek word for 'pressure'. Thus, piezoelectric effect means pressure-electric effect. Piezoelectricity is the ability of certain crystalline materials to develop an electric charge proportional to mechanical stress and vice versa. Piezoelectricity is a branch of crystal physics which demonstrates electromechanical interaction very nicely. Piezoelectric effect was discovered by Pierre and Jacques Curie. They published this discovery in 1880 and the opening paragraph of their paper was: ***"Those crystals having one or more axes whose ends are unlike, that is to say hemihedral crystals with oblique faces, have the special physical property of giving rise to two electric poles of opposite signs at the extremities of these axes when they are subjected to a change in temperature. This is the phenomenon known under the name of pyroelectricity. We have found a new method for the development of polar electricity in these same crystals, consisting in subjecting them to variations in pressure along their hemihedral axes"*** [1]**.** Curie

brothers found this effect in the plates made up of zinc blende, sodium chlorate, boracite, tourmaline, quartz, calamine, topaz, tartaric acid, cane suger and Rochelle salt. The converse of this piezoelectric effect was predicted by Gabriel Lippmann in 1881 and confirmed by the Curie brothers that same year.

Piezoelectric phenomenon may be more precisely defined in terms of direct and converse piezoelectric effects. In direct piezoelectric effect, application of mechanical load on piezoelectric material induces an electrical response. Measuring this electrical response, the mechanical state of deformation in the structure can be determined and monitored which leads to sensor applications. In converse piezoelectric effect, an electrical input in the piezoelectric material is converted into a corresponding mechanical strain. This leads to the actuator applications of piezoelectric materials wherein the state of deformation of the structure can be controlled or altered by applying the appropriate electrical input. These days, piezoelectric materials are the most popular smart materials. They are being studied extensively by researchers and used successfully in industry due to their wide range of applications such as electromechanical transducers etc. To get more insight into piezoelectric materials, following sections discuss piezoelectric phenomenon, piezoelectric ceramics, piezoelectric polymers, mathematical treatment of piezoelectricity and piezoelectric sensors and actuators.

1.2.1 *Piezoelectric Phenomenon*

Spatial arrangement of atoms within a material determines the physical properties of that material. In general, the atomic arrangement has three classifications: amorphous, polycrystalline and crystalline. Piezoceramics are crystalline in nature. The unit cell of a crystalline material consists of a group of positively and negatively charged ions. The

position of the center of the positive and negative charges is important because it determines the electromechanical properties of the material. A crystal wherein the centers of positive and negative charges coincide is said to be centrosymmetric (Figure 1.2a). For a crystal to exhibit the piezoelectric effect, its structure should have no centre of symmetry i.e. it should be non-centrosymmetric. A single crystal with this structure has anisotropic characteristics and the centers of positive and negative charges do not coincide even in the absence of external load (Figure 1.2b). Such a material is said to exhibit spontaneous polarization which provides a net electric dipole moment within the crystal unit cell. The material is said to be 'polar' and the dipoles aligned in the same direction arrange themselves into regions called domains.

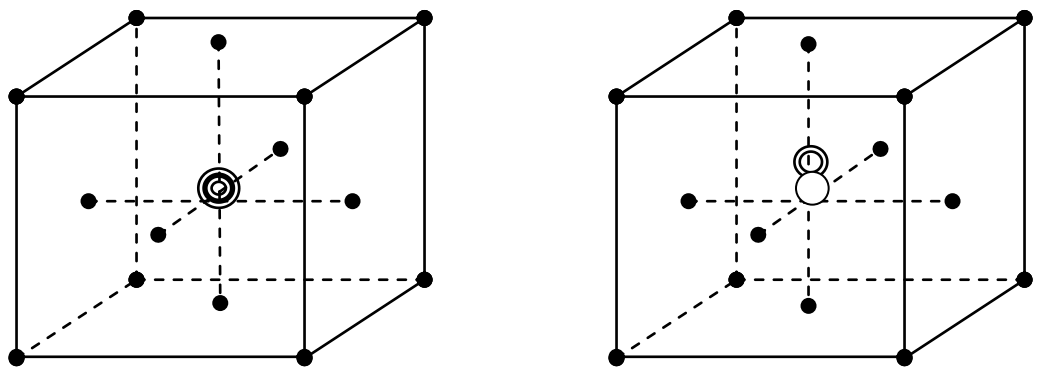

(a) Centrosymmetric unit cell **(b) Non-centrosymmetric unit cell**

Figure 1.2: Centrosymmetric and non-centrosymmetric unit cells (◎ : Overlapping centers of positive and negative charges, ○ : Centre of negative charge, ◎ : Centre of positive charge)

Generally, piezoceramic materials do not exhibit piezoelectricity above the Curie temperature. Piezoelectric materials have non-centrosymmetric unit cells below Curie temperature and a centrosymmetric structure above Curie temperature. The crystal

structure of a material changes at the Curie temperature from piezoelectric (non-symmetrical) to a non-piezoelectric (symmetrical) form. As a result, the material loses its piezoelectric properties [1]. Above Curie temperature, these crystals exhibit simple cubic symmetry wherein positive and negative charge sites coincide thereby having no dipoles present in the material. At this stage, the structure of the crystal lattice is called the perovskite structure. This state is called the paraelectric phase. When a non-centrosymmetric unit cell is deformed by a mechanical load, the separation between the positive and negative charge sites in each unit cell is altered. It leads to net polarization at the material surface (Figure 1.3). This is the cause of direct piezoelectric effect. This effect is reciprocal in nature. When non-centrosymmetric unit cell is exposed to an

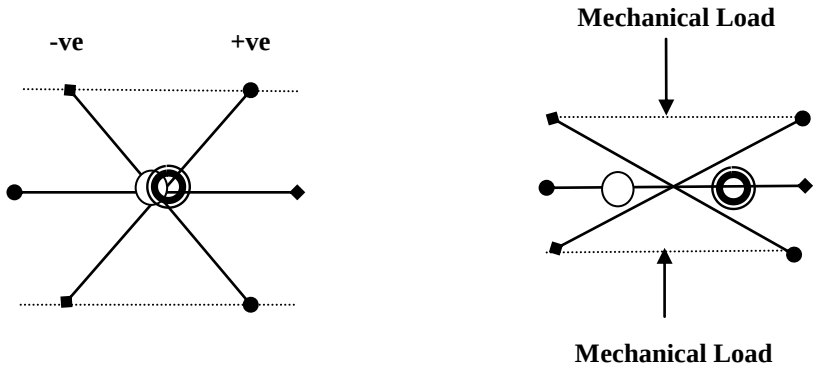

Figure 1.3: A schematic representation of direct piezoelectric effect. (a) Unperturbed molecule (b) Molecule subjected to an external mechanical load (○ : Centre of negative charge, ◉ : Centre of positive charge)

electric field, the positive and negative ions try to shift either farther apart or closer with respect to each other according to the polarity of the applied electric field. As a result, the movement of ions causes the unit cell to be stretched or contracted. This gives rise to converse piezoelectric effect. With careful measurements, one can observe that

mechanical variables are proportional to the corresponding electric variables within some range and vice versa. These variables are directional.

1.2.2 *Piezoelectric Ceramics and Piezoelectric Polymers*

As discussed in previous sub-section, piezoelectricity occurs naturally in crystalline materials with specific properties. For piezoelectric interaction to exist, it is necessary that certain axes of the medium intrinsically possess a one-wayness called polarity. Polarity needed to impart piezoelectric properties can be created in an isotropic ferroelectric polycrystalline ceramic more or less permanently by temporary application of a strong electric field. This process, called 'poling' is analogous to the magnetization of a permanent magnet. Piezoceramics or piezo polymers are artificially made piezoelectric materials with strong piezoelectric effects [2]. Barium titanate was the first man made piezo ceramic [3]. An advancement of great importance was the discovery of very strong and stable piezoelectric effects in lead zirconate titanate (PZT) solid solutions [4]. These days, PZTs are the most dominant piezoelectric ceramics.

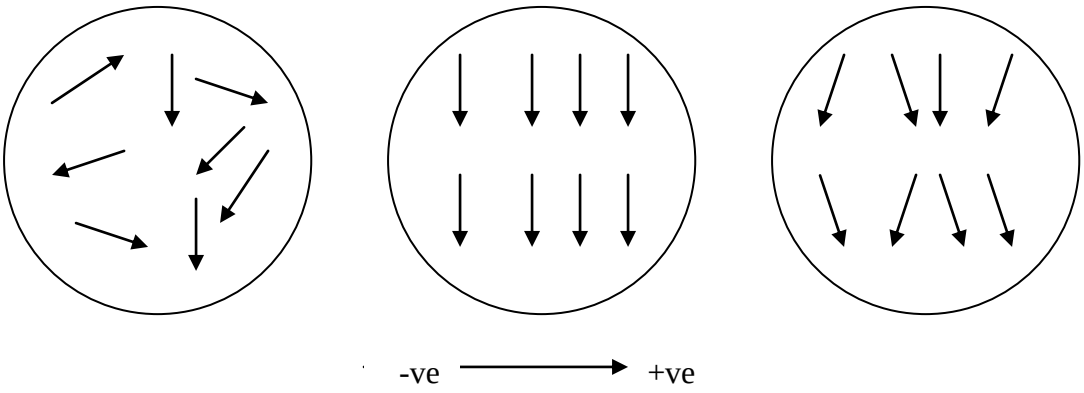

(a) Unpoled **(b) Being poled** **(c) Poled**

Figure 1.4: Poling process in piezoceramics

Piezoceramics are polycrystalline in nature and do not have piezoelectric characteristics in their original state. Piezoelectric effects are induced in these materials through simple poling in which application of high dc electric field at elevated temperatures results in polarization. Poling process forces polar axes of unit cells to orient parallel to the applied field. This imparts required permanent net polarization and mechanical deformation to the ceramic (Figure 1.4). Piezoceramic materials have linear properties at low electric fields and low mechanical stresses. They have nonlinear properties at high electric fields and high mechanical stresses.

Polyvinylidene fluoride (PVDF) is the most commonly used piezoelectric polymer. PVDF consists of long chains of repeating monomers. It is a ferroelectric polymer having the strongest known piezoelectric properties of all polymers. PVDF was discovered in 1948 but a strong piezoelectric effect in stretched and poled films of PVDF was discovered in 1969 [5]. PVDF provides less transducer power than PZT for actuator applications but is more sensitive than PZT as a sensor. The maximum actuation strain of PZT piezoceramics is about 1000 micro strains whereas PVDF piezopolymer can produce maximum actuation strain of 700 micro strains only. PVDF is flexible as compared to PZT which is usually brittle. PVDF is commercially available in the form of large and thin flexible sheets and can be made into any desirable shape.

1.2.3 *Mathematical Treatment of Piezoelectricity*

In 1894, Woldemar Voigt defined the relationship between piezoelectricity and the crystal structure. Combining the elements of symmetry of elastic tensors and electric vectors with geometrical symmetry elements of crystals, Voigt showed that 32 classes of crystal structure may show piezoelectric properties. For each of these 32 crystal classes,

there exists one value of possible 18 piezoelectric coefficients. Complete description of piezoelectric properties of a crystal involves treatment in terms of three different types of directional quantities: electric (field and polarization), elastic (stress and strain) and the piezoelectric coefficients (which relate electric and elastic quantities). Electric quantities can be mathematically represented as vector quantities (first order tensors) while elastic and piezoelectric constants can be represented as second and third order tensors. The fundamental piezoelectric relations which describe electromechanical interactions are known as 'constitutive equations'. These constitutive equations are analogous to that of ordinary solids. In ordinary solids, a stress $\{\sigma\}$ causes a proportional strain $\{\varepsilon\}$ related by elastic modulus matrix [Y] through a constitutive relationship defined by Hook's law as:

$$\{\sigma\}_{6\times1} = [Y]_{6\times6}\{\varepsilon\}_{6\times1} \tag{1.1}$$

Piezoelectricity is the additional creation of an electric charge by the applied stress. Also, charge is proportional to the force which in terms of electric displacement $\{D\}$ (charge per unit area) can be written as:

$$\{D\}_{3\times1} = [d]_{3\times6}\{\sigma\}_{6\times1} \tag{1.2}$$

This is direct piezoelectric effect. Matrix $[d]$ is known as 'piezoelectric strain constant matrix'. In converse piezoelectric effect, an electric field $\{E\}$ produces expansion or contraction strain depending upon the polarity i.e.

$$\{\varepsilon\}_{6\times1} = [d]^{T}_{3\times6}\{E\}_{3\times1} \tag{1.3}$$

Piezoelectric strain constant is numerically identical for both direct and converse piezoelectric effects. High value of piezoelectric strain constant *'d'* is desirable for

materials intended to develop motion or vibration such as sonar or ultrasonic transducers. Similarly, piezoelectric strain constant *'h'* and piezoelectric stress constants *'e'* and '*g'* are defined as:

$$\begin{aligned} \{E\}_{3\times1} &= -[h]_{3\times6}\{\varepsilon\}_{6\times1} \\ \{\sigma\}_{6\times1} &= -[e]^{T}_{3\times6}\{E\}_{3\times1} \\ \{E\}_{3\times1} &= -[g]_{3\times6}\{\sigma\}_{6\times1} \end{aligned} \tag{1.4}$$

Accordingly, direct and inverse piezoelectric effects can be written in the form of *d-form*, *e-form*, *g-form* and *h-form* piezoelectric constitutive equations [6]. Piezoelectric constant sign is taken as positive when a positive charge is induced in the positive direction of the axis under a positive (extensional) stress. Piezoelectric constitutive equations are the equations which relate elastic variables (stress and strain) to the electric variables (electric field and electric displacement). Since elastic, dielectric and piezoelectric constants of piezoelectric crystals and ceramics are expressed in terms of tensors, so *e-form* of piezoelectric constitutive equations for direct and inverse piezoelectric effects are written as [6]:

Direct Piezoelectric Effect: $$D_n = e_{nkl}\varepsilon_{kl} + \in^{\sigma}_{nm} E_m \tag{1.5}$$

Inverse Piezoelectric Effect: $$\sigma_{kl} = c_{ijkl}\varepsilon_{ij} - e^{T}_{nkl}E_n \tag{1.6}$$

where D_n is electric displacement in n^{th} direction, e_{nkl} is piezoelectric stress coefficient, ε_{kl} is normal strain in l^{th} direction in the plane perpendicular to k^{th} direction, $\in^{\sigma}_{nm}$ is permittivity coefficient at constant stress, E_m is electric field in m^{th} direction, σ_{kl} is normal stress in l^{th} direction in the plane perpendicular to k^{th} direction and c_{ijkl} is the elasticity stiffness constant. In matrix form, these equations are written as:

Direct Piezoelectric Effect: $$\{D\} = [e]\{\varepsilon\} + [\in]\{E\} \quad (1.7)$$

Inverse Piezoelectric Effect: $$\{\sigma\} = [c]\{\varepsilon\} - [e]^T \{E\} \quad (1.8)$$

where $\{D\}$ is electric displacement vector, $[e]$ is piezoelectric stress coefficient matrix, $\{\varepsilon\}$ is strain vector, $[\in]$ is permittivity coefficient matrix, $\{E\}$ is electric field vector, $\{\sigma\}$ is stress vector, $[c]$ is elasticity matrix and $[e]^T$ is the transpose of piezoelectric stress coefficient matrix. Equation (1.7) associated with direct piezoelectric effect serves as the principle for piezoelectric sensor and equation (1.8) associated with inverse piezoelectric effect serves as the principle for piezoelectric actuator.

1.2.4 *Piezoelectric Sensors and Actuators*

Just before the start of First World War, Paul Langevin conceived the idea of exciting quartz plates electrically to serve as emitters and receivers of high frequency sound waves under water. This kind of acoustic wave can penetrate sea water and it was used to locate enemy submarines. This was the first attempt to use piezoelectric material in some application. During World War II, Langevin's quartz transducer was replaced by a Rochelle salt transducer. These days, piezoelectric materials are used in devices such as electromechanical transducers, ultrasonic generators, ultrasonic interferometers, accelerometers, phonograph pickups, loudspeakers, sonar transmitter, sonar receiver, microprocessors, crystal filters, quartz crystal oscillators in clocks etc. Piezoelectric materials are most widely used as transducers. We can group the transducers into two classes: sensors (piezoelectric generators) and actuators (piezoelectric motors). Sensors convert mechanical energy into electrical energy while actuators convert electrical energy into mechanical energy (Figure 1.5).

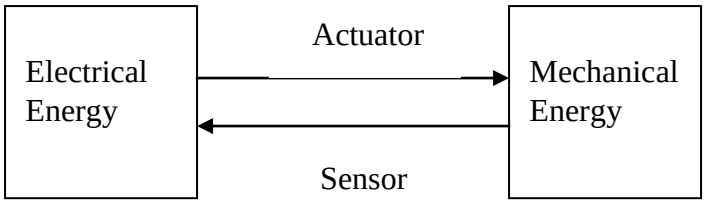

Figure 1.5: Piezoelectric transducer

Piezoelectric materials are used as sensors and actuators in the form of distributed layers, surface bonded patches, embedded patches, cylindrical stacks, piezo paint sensor, screen printed piezoelectric layer, active fibre composites, functionally graded piezo material etc. Surface mounted or embedded piezo patches can control a structure better than distributed one because the influence of each patch on the structure response can be individually controlled. A common geometry for piezoelectric actuators is a laminated structure. Number of piezoceramic layers may be stacked one over other. The number of layers that should be used depends on the design requirement viz. single layer (unimorph), double layers (bimorph), and multilayers (multimorph) (Figure 1.6).

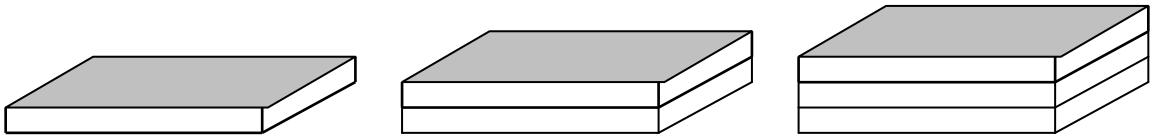

(a) Single layer **(b) Double layer** **(c) Multilayer**

Figure 1.6: Transducer structure

However, as the number of layers increases, the electric wiring between layers becomes more complicated and the deformation decreases with the addition of more

layers. So, multimorphs with more than four layers are usually impractical. Each laminated structure can be used as either actuator or sensor. That is, they can generate: (i) motions in longitudinal or transverse direction under an external electrical field and (ii) electrical charges when loaded mechanically.

Piezoceramic patches are bonded to the base structure using a layer of glue. A piezoelectric material subjected to an external electric field extends or contracts depending on the direction of the applied field and the internal polarization [1]. In a 'smart structure', electric field can be applied to actuate piezoceramic actuators in three different ways:

(i) Parallel to the poling direction of the piezoelectric actuator (Figure 1.7a). It produces extension in the piezoelectric actuator and thereby bending of the host structure. Such an actuator is called extension bending actuator [7]. If we obtain a displacement or force in the thickness or longitudinal direction, we say that the actuator works in the longitudinal or axial mode (d_{33} mode). If deformation under this electrical field is along the transverse direction, we say that actuator works in the transverse mode (d_{31} mode). Structural deformation in the transverse mode is much larger than the longitudinal mode. Therefore, d_{31} operation mode is popular in practice.

(ii) Perpendicular to the poling direction of the piezoelectric actuator (Figure 1.7b). It shears the piezoelectric patch causing shear actuation and thereby bending the host structure [8]. Shear actuation is more efficient than the extension actuation for stiff structures and thick piezoelectric actuators. Extension bending actuators produce boundary concentrated forces and moments in the structure whereas sandwich shear actuators induce distributed moments in the structure.

(iii) At a specific angle to the poling direction of the piezoelectric actuator (Figure 1.7c). It excites the structure in desired specific direction. Such an actuation is called directional actuation [9].

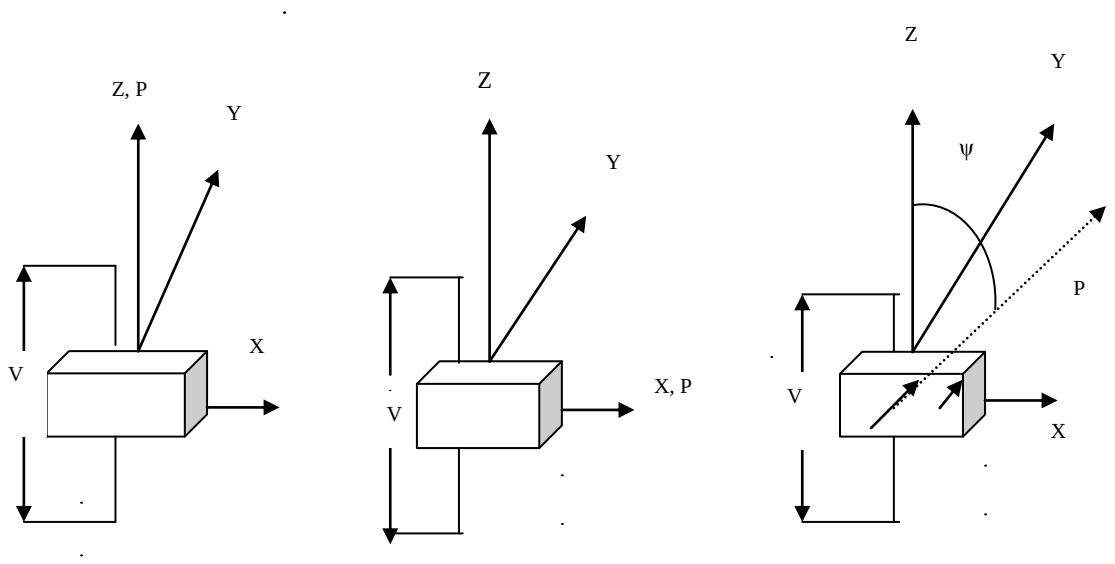

(a) Extension-bending **(b) Shear actuation** **(c) Directional actuation**

Figure 1.7: Various piezoelectric actuation techniques being realized by altering the direction between the applied electric potential 'V' and the poling direction 'P'

1.3 Vibration Control of Structures

Vibrations are basic phenomena in this universe. From electrons to heavenly bodies, everything experiences vibrations in one form or other. Day and night cycle is not possible without rotation of earth about its axis. Without heart beating and oscillatory motion of the lungs, no animal life is possible. We cannot speak without oscillatory motion of the larynx, we cannot hear if eardrums stop vibrating, we can not see if light waves do not undergo vibration, sound cannot travel without vibrating medium and we can not walk with out oscillating our legs.

Whereas vibrations are necessary for existence of life and many other human activities, vibrations sent as shock waves by earthquake or atmospheric turbulence can cause destruction. Vibrations emanating from moving parts of machines cause damage to machines. Noise generated by unwanted vibrations of machines creates nuisance. Vibrations coming on to the passenger seat of an automobile due to road roughness causes irritation, pain and discomfort to the rider. Structural vibrations in bridges, tall buildings, aeroplanes etc. can lead to fatigue failure of the structure. There is an unending list of ill effects caused by unwanted vibrations. Therefore, since time immemorial, man has been trying hard to control these unwanted structural vibrations by modifying mass, stiffness and damping of the structure. Starting from intuitive methods, advent of fast processors has enabled man to control structural vibrations even in real time. Vibration control of unwanted vibrations is still a challenge and vibration control methods have attracted many researchers. Vibrations can be controlled either by passive or active means. In the following sub-sections, these means are discussed.

1.3.1 *Passive Vibration Control (PVC)*

Vibration control is called passive vibration control (PVC) if no external source of energy is used to control structural vibrations. There are many ways to achieve passive vibration control viz.: (i) changing damping of the system by employing viscous or coulomb dampers, using constrained or unconstrained visco-elastic damping treatments etc. (ii) modifying stiffness and/or mass of the system in order to obtain desired dynamic characteristics of the system (iii) suitably designing a dynamic absorber to absorb vibrations of the system and (iv) designing a suitable isolation system for a system suffering from vibrations due to surroundings. If none of these techniques work then the

system is redesigned for the desired dynamic characteristics. With the advent of computers, it is possible to design a system with the desired dynamic characteristics at the computer level using suitable software. However, PVC may increase overall mass of the structure and is found to be unsuitable for controlling low frequency vibrations [10-11]. Also, this method does not suit applications such as in space structures where less weight is desired and low frequency vibrations are encountered.

1.3.2 *Active Vibration Control (AVC)*

Vibration control is called active vibration control if an external source of energy is employed to control the structural vibrations. It requires sensors to capture the dynamics of the structure, a processor to manipulate the sensor signals, actuators to apply a force opposing the excitation force and a source of energy to actuate the actuators. Vibration signal sensed by sensors is suitably processed by the processor and then fed back to the actuators. Passive vibration control is not able to suppress low frequency modes of vibration whereas active vibration control provides improved low frequency performance, reduction of size and programmable flexibility of design [11-13]. Therefore, in applications where less weight is required and low frequency vibrations are encountered, active vibration control technique can be used for controlling the unwanted vibrations [14].

Most common technique in AVC is feedback control. In feedback control, signal obtained from the error sensor is used as an input to the controller and the control effort is applied on the mechanical system via an active actuator. Block diagram of the feedback control is shown in Figure 1.8. Using a suitable modelling technique, equation of motion of the structure can be written as:

$$[M]\{\ddot{x}\}+[C']\{\dot{x}\}+[K]\{x\}=\{F(t)\} \tag{1.9}$$

where $[M]$ is mass matrix, $[C']$ is damping matrix, $[K]$ is stiffness matrix, $\{x\}$ is displacement vector, $\{\dot{x}\}$ is velocity vector, $\{\ddot{x}\}$ is acceleration vector and $\{F(t)\}$ is the force vector. A closed loop system wherein a control force proportional to velocity is applied, can be represented as:

$$[M]\{\ddot{x}\}+[C']\{\dot{x}\}+[K]\{x\}=\{F(t)\}-[C_1']\{\dot{x}\} \tag{1.10}$$

or $$[M]\{\ddot{x}\}+\left([C']+[C_1']\right)\{\dot{x}\}+[K]\{x\}=\{F(t)\} \tag{1.11}$$

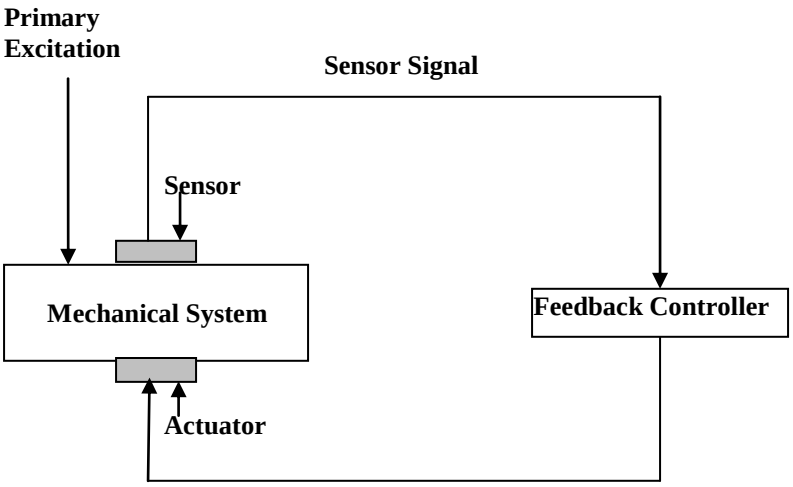

Figure 1.8: Feedback control system

Comparison of equations (1.9) and (1.11) shows that negative velocity feedback has increased the damping of the system. Electrical output of the sensor can be manipulated to apply a force proportional to displacement, velocity and acceleration. Then equation of motion becomes:

$$\left([M]+[C_0']\right)\{\ddot{x}\}+\left([C']+[C_1']\right)\{\dot{x}\}+\left([K]+[C_2']\right)\{x\}=\{F(t)\} \tag{1.12}$$

From equations (1.9)-(1.12), it is clear that active vibration control technique can alter effective mass, stiffness and damping of the mechanical system. In this way, vibrations can be controlled by active means using external source of energy. Helicopters, aeroplanes, satellites and other space structures have to be light weight. Their Structural materials have low mass density (like aluminium) and very low internal damping. Low damping of the structure makes the space vehicle prone to structural instability. In these structures, passive vibration control is unsuitable due to weight restrictions. Moreover, a space vehicle may encounter unforeseen external disturbances and its structural system may considerably change during its working. Vibration control system in such applications should be robust to unforeseen disturbances and structural changes. Active vibration control system suits well for such applications. Therefore, these structures should be smart structures which can cope with any type of unforeseen conditions. PVC has been employed since decades and is a well developed technology whereas AVC is still not commercially viable and is an infant. In the following section, more insight into the world of 'active vibration control' is presented.

1.4 Active Vibration Control of a 'Smart Structure' using Piezoceramic Sensors and Actuators: State-of-the-Art

In recent years, there has been considerable interest in the analysis and design of smart structures and vibration control is an important area of research in smart structures. An efficient way of implementing active vibration control is with the use of piezoelectric materials as sensors and actuators in smart structures due to their excellent properties. Before active vibration control technique is experimentally employed, one has to analyze the problem analytically.

1.4.1 *Analytical Development*

When active vibration control is to be performed on a structure using piezoceramic sensors and actuators, one has to:

1. understand the sensor-actuator mechanics
2. place sensors and actuators suitably on host structure
3. mathematically model the whole dynamic system using a suitable modeling technique and
4. apply a suitable control law.

In AVC, piezoelectric materials can be used as self-sensing actuators, extension-bending actuators, shear actuators and modal sensors/actuators depending upon the design and requirement of the 'smart structure'. Interaction of sensor and actuator with the host structure can be captured using piezoelectric constitutive equations (1.7) and (1.8). AVC performance also depends upon the placement of piezoelectric sensors and actuators on a 'smart structure'. Limited number of sensor and actuators are to be placed over the structure where lots of options are available. Unwise placement of sensors and actuators over a 'smart structure' can make the structure unstable. Also, sensors and actuators should be so placed that it best suits the end application of the 'smart structure'. Keeping in mind the end application of the 'smart structure', a criterion can be fixed to find the sensor-actuator locations to maximize the performance of AVC. Such a criterion is referred to as 'optimization criterion'. Once 'optimization criterion' is fixed, desired sensor-actuator locations can be found using a suitable search algorithm called 'optimization technique'. Such a placement of sensors and actuators which is done by optimizing some fixed criterion is called 'optimal placement'.

When the design and placement of sensors and actuators is finalized, next task is to model the 'smart structure' mathematically. Various tools like Hamilton's principle, finite element method, modal testing, system identification etc. can be used to find the equations of motion of a 'smart structure'. The resulting equation of motion is obtained as:

$$[M]\{\ddot{x}\}+\left[C^{'}\right]\{\dot{x}\}+[K]\{x\}=\{F\} \tag{1.13}$$

Equation (1.13) represents a coupled system of equations. Analysis of such a system would become easier if these coupled equations are converted into uncoupled equations. In that case, single degree of freedom tools can be used to analyze the actual multi degree of freedom system. So, coupled equations (1.13) are converted into uncoupled equations using 'modal analysis'. In order to control the response of a system using modern control theories, uncoupled equations of motion are written in a state-space form. Now, the response of 'smart structure' under various situations can be simulated using suitable software packages. Simulation analysis of a mathematical model derived using appropriate modeling technique can be carried out by writing computer code in MATLAB, MATHEMATICA, VAPAS, DYNADID2D etc. Commercial finite element packages such as ANSYS/Multiphysics, ABAQUS, MSC/NASTRAN, COSAR etc. are also available to model smart piezo structures.

Once equation of motion of 'smart structure' is obtained, its vibration response can be controlled using suitable control technique. Vibrations of 'smart structure' are controlled by applying suitable voltage signals to the actuators. Voltage to be applied to the actuators is calculated using a control law. Actual structural vibrations consist of multiple modes. It is neither required nor effective to control all the vibration modes of a given

structure. Depending upon the nature of 'smart piezo structure', modes and frequency ranges of interest, the control law is decided. Control action simulations can be carried out in ANSYS, MATLAB/Simulink, MATLAB/Control System Toolbox, SCILAB etc. Several simulations need to be carried out to see the effectiveness of control law and if the results are encouraging, active vibration control scheme is experimentally implemented. Simulation results on active vibration control of a 'smart piezo structure' are shown in Figure 1.9 using an effective control law. This figure demonstrates the beauty of active vibration control scheme.

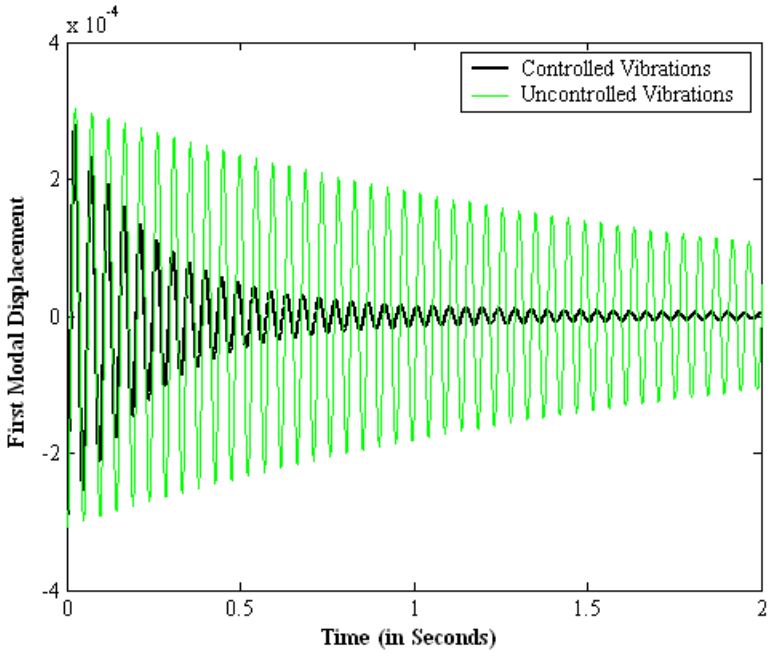

Figure 1.9: Active vibration control of a 'smart structure'

1.4.2 *Experimental Implementation*

For practical implementation of the active vibration control scheme, an experimental setup consisting of following is required:

1. Host Structure
2. Sensors and Actuators
3. Sensor Conditioning Device
4. Frequency Filter
5. Analog to Digital Card
6. Processor
7. Actuation Amplifier

First of all, piezoceramic sensor and actuators are bonded or embedded at optimal locations using an epoxy adhesive on the host whose structural vibrations are to be controlled using active means. Poling directions of piezoceramics are fine soldered to thin connecting wires. Sensor signal from piezoceramic sensors is fed into multi channel sensor signal conditioning system wherein it is amplified using a piezoelectric charge amplifier after suitable conditioning. Unwanted frequencies present in sensor signal are filtered out by a frequency filter. Resulting sensor signal is fed into 'Real Time System' via analog to digital data acquisition card. 'Real Time System' minimizes time delays. Control program written in a PC is downloaded into 'Real Time System' and is executed there. After real time manipulation of sensor signal in 'Real Time System' as per the control program, digital to analog data acquisition card outputs the desired control signal. This control signal is fed into multi channel piezo actuator system where it is amplified using a voltage amplifier. Amplified control signals obtained from the piezo actuator system are now applied on the actuators. These external control voltages actuate the actuators according to the control algorithm and structural vibrations are thus controlled

using active means. To implement AVC control algorithm experimentally, LabVIEW software can be used.

In this entire exercise, designer faces several challenges. To control structural vibrations using AVC scheme, piezoelectric sensors and actuators are to be properly understood. It forms the basis of coupling between the sensors, actuators and the structure to be controlled. Performance of piezoceramic sensors and actuators is sensitive to thermal, hygro, non-linearities, fatigue and ageing effects etc. Smart structure is intended to work in real life environment where these effects are encountered. Electromechanical interaction of piezoelectric sensors and actuators in real life environment has not been well understood. This is the real and actual potential hindrance to achieve AVC in real life situations. Once interaction of piezoelectric sensors and actuators is properly understood, optimal locations of the sensor and actuator are decided by optimizing a performance index. Next task is to make a good mathematical model of the 'smart structure'. Getting a suitable mathematical model is a tough task. As of now, active vibration control is applied on simple two dimensional structures and rarely on real life structures. It is difficult to model a real life structure because of: (i) complex three dimensional shape (ii) complex and large boundary conditions and (iii) ever evolving nature of real life structures. Mathematical models robust to thermal, hygro, non-linearities, fatigue and ageing effects are required. Once mathematical model is ready, a suitable control approach is used to control the vibrations of a 'smart structure'. This field demands small control algorithms which: (i) can be completed in stipulated time (ii) are robust to parametric uncertainties and (iii) adaptive to different environmental changes. Several control approaches are available and one has to decide for the one which is best

suited for the end application. After suitable control approach is decided, several simulations are carried out and viability of proposed AVC scheme is ascertained. Real time processor should be fast enough to carry out the control algorithm within the allotted sampling time. Practical implementation of active vibration control has to be cost effective. Human civilization needs to develop smart structures for controlling unwanted structural vibrations. With this introduction to the world of smart structures, one can proceed to implement vibration control scheme by active means using piezoelectric sensors and actuators.

CHAPTER II

REVIEW OF LITERATURE AND SCOPE OF WORK

An idea to use piezoelectric sensors and actuators in active vibration control was conceived in 1980 [15]. However, pioneer works in mid and late eighties [7,16-18] set the platform for researchers in this field all over the globe. Literature on active vibration control can be segregated into:

- Techniques to use piezoelectric materials as sensors and actuators
- Techniques to model real life environmental effects
- Optimal placement of piezoelectric sensors and actuators
- Techniques to write equations of motion of a 'smart structure'
- Techniques to control structural vibrations
- Software to implement active vibration control scheme

In following sections, these techniques are discussed one by one. The scope of present work is an outcome of this literature review and it is discussed in last sections.

2.1 Techniques to Use Piezoelectric Materials as Sensors and Actuators

Piezoelectric materials can be used as sensors and actuators in the form of distributed layers [16-17], surface bonded patches [7, 19], embedded patches [20], cylindrical stacks [21], piezo paint sensor [22], screen printed piezoelectric layer [23], active fibre composites [9], functionally graded piezo material [24] etc. However, surface mounted or embedded piezo patches can control a structure better than distributed one because the influence of each patch on the structural response can be individually controlled [25]. In a 'smart structure', piezoelectric materials can be used as self-sensing actuators, extension-

bending actuators, shear actuators and modal sensors/actuators. In the following sub-sections, state-of-the-art to implement these designs is discussed.

2.1.1 *Self-Sensing Actuators*

A single piezoelectric patch can exhibit direct as well as inverse piezoelectric effect simultaneously. Hence, a single piezoelectric patch can be used as sensor/actuator simultaneously. Actuator, which can be used to sense as well is called concurrent sensor. Self-sensing/concurrent-sensing concept ensures perfect sensor-actuator collocation which leads to better control stability, less weight and low cost of the 'smart structure' [26-27].

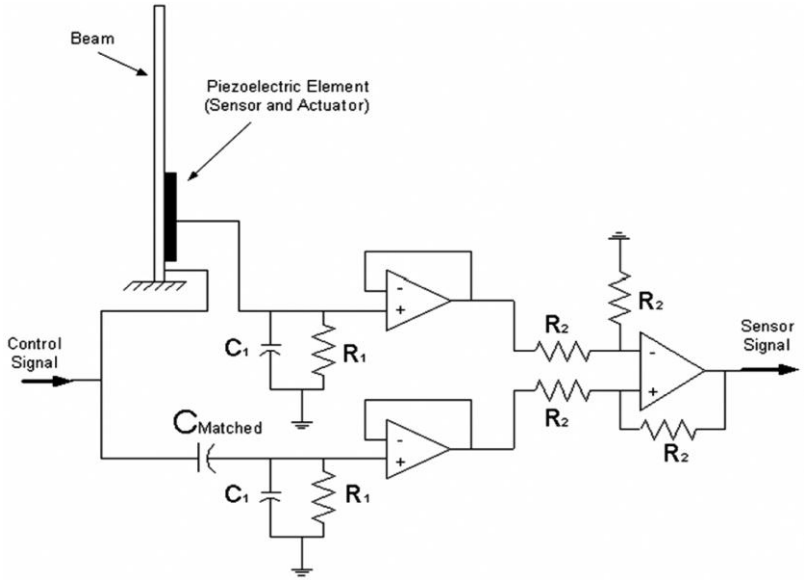

Figure 2.1: Self-sensing actuator with a bridge circuit

In self-sensing piezoelectric actuators, main challenge is to separate sensor signal from the control signal. It can be done using a bridge circuit. Piezoelectric is introduced in bridge circuit in the form of a voltage source due to control signal and a pure capacitor

in series. The circuit is divided into two parts using the 'principal of superposition': one with control signal and second with control plus sensing signal (Figure 2.1). Bridge balance condition is achieved by introducing a matching capacitance ($C_{Matched}$). When perfectly balanced, this circuit acts as a simplified voltage divider which gives the difference between two parts leaving only sensor signal as out put [28]. This sensor signal is then manipulated, amplified and fed back to actuator with suitable gains so as to induce control action. The bridge circuit should extract accurate mechanical strain rate signal i.e. sensor signal [29]. Performance of self-sensing scheme also depends upon electromechanical coupling effects between piezoelectric material and the structural vibrations [30]. Due to thermal dependence of piezoelectric capacitance, a perfect match of time constant cannot be maintained under varying thermal conditions. Hence as the temperature changes, capacitance of piezoelectric patch changes and match condition is lost. In such a situation, self-sensing cannot be done [31]. Match condition can be achieved if a set of capacitors is used such that a particular capacitor enters into the bridge circuit at a particular range of temperature. Such a bridge circuit design enhances the stable thermal operating range by 95°C (from 70°C to 165°C) [32].

2.1.2 *Extension-Bending and Shear Actuators*

A piezoelectric material subjected to an external electric field extends or contracts depending on the direction of the applied field and the internal polarization [2]. Mostly for structural vibration control, electric field is applied parallel to the poling direction of the piezoelectric actuator [7, 18]. It produces extension in the piezoelectric actuator and thereby bending the host structure. Such an actuator is called extension-bending actuator. It is also possible to excite the structure by applying electric field perpendicular to the

poling direction of the piezoelectric actuator [8, 33]. It shears the piezoelectric patch causing shear actuation and thereby bending the host structure. Extension actuators are effective when they are long and placed near the clamped end of beam whereas shear actuators are effective even for very short lengths and over a long range of position [34]. Shear actuation is more efficient in actively controlling the vibration for the same control effort. It is possible to model both the actuation mechanism in a unified way if two electric fields i.e. one along the direction of polarization and another perpendicular to the direction of polarization are substituted in the constitutive equations of piezoelectricity [20]. Direction of the stresses applied by piezo-actuators on the host structure is a function of : (i) the angle 'ϕ' between the applied electric field and the poling axis and (ii) fibre orientation 'ψ' in case of composite piezoelectric material. Therefore while modeling a 'smart structure' with anisotropic piezoelectric material, 'ψ' and 'ϕ' can not be ignored [9, 35]. Ignorance of this anisotropic property of such piezo-actuators will cause underestimation of control voltages [36].

2.1.3 *Modal Sensors/Actuators*

Many times, only some particular structural modes need to be controlled. To do so, the mathematical model (say finite element model) is usually converted into modal domain by using following orthonormal modal transformation:

$$\{x\}_{nx1} = [U]_{nxm} \{\eta\}_{mx1} \tag{2.1}$$

where $\{x\}$ is a vector of degrees of freedom of the structure, $[U]$ is orthonormal modal transformation matrix, $\{\eta\}$ is vector of modal coordinates, '*n*' is degrees of freedom / total number of modes of the system and '*m*' is the number of modes to be considered [37] . This converts coupled differential equations into uncoupled ones. Now, it becomes

quite natural to develop a sensor technology which senses only a particular mode. Such a sensor is called modal-sensor and its signal is manipulated, amplified and then fed back to so called modal-actuator. Use of independent modal sensor/actuator reduces the required number of sensors/actuators, dimensionality of the controller and required control energy [38]. These can be used for independent control of structural modes i.e. independent modal space control [39]. Interaction between the actuator and structural vibrations under closed circuit conditions induces modal coupling and hence higher modes get excited [40]. This is called 'spillover effect' and it degrades active vibration control performance. To avoid these effects, spatially distributed piezoelectric modal sensors/actuators for beam structure can be used [41]. Spatially distributed self-sensing piezoelectric actuators can also be used for modal control of a cantilevered beam [42]. Design of spatially distributed modal sensor/actuator is based upon structural mode shapes and is used for simple structures only. Modal sensors/actuators using an array of piezoelectric patches and feedback gain design can be used for complex structures [43]. Such sensors/actuators are called discrete modal sensors/actuators. Also, same array of piezoelectric patches can be given multiple weights and can act as a modal sensor/actuator for multiple modes simultaneously and independently. These schemes can be realized using different design and implementation techniques [44].

2.2 Techniques to Model Real Life Environmental Effects

Performance of piezoelectric sensors and actuators is sensitive to thermal, hygro, non-linearities, fatigue, ageing effects etc. A 'smart structure' instrumented with piezoelectric patches is intended to work in real life environment where these effects are encountered. Electromechanical interaction of piezoelectric sensors and actuators in real life

environment is not well understood. This is the real and actual potential hindrance to achieve AVC in real life situations. Therefore, mathematical models robust to these effects are desired. In the following sub-sections, techniques to model thermal, hygro, non-linearities, fatigue and ageing effects in piezoelectric sensors and actuators are discussed.

2.2.1 *Temperature Effects*

This effect is the most encountered effect during the operation of a 'smart piezo structure'. Piezoelectric materials are processed and standardized at a stress-free temperature called 'reference temperature'. Equations (1.7) and (1.8) are applicable when operating temperature, termed as 'ambient temperature' is same as 'reference temperature'. Mostly, researchers have attempted AVC at 'reference temperature' using these constitutive equations [7, 18, 45-47]. However in real life situation, 'smart piezo structure' may have to work at 'ambient temperature' other than 'reference temperature'. It would induce thermal stresses in the piezoelectric material. The theory of piezoelectricity with inclusion of thermal effects is known as piezothermoelasticity and is well established in literature [48-53]. Piezothermoelastic studies have also been extended to design smart piezo structures operating at ambient temperatures other than 'reference temperature' [54-55]. Most of the research is concentrated on developing piezothermoelastic finite element models of smart piezo structures [56-62]. Developments in piezothermoelasticity in relevance to smart piezo structures are also well documented [63-65]. When 'ambient temperature' is other than 'reference temperature', thermal effect can affect the response of a 'smart piezo structure' in three distinct ways: (i) 'thermal strain effect' i.e. introduction of thermal stresses in 'smart

structure' as a result of different thermal expansion coefficients (ii) 'pyroelectric effect' i.e. generation of electric displacement / voltage on piezoelectric material and (iii) change in elastic, piezoelectric & dielectric properties of 'smart structure'. AVC performance is influenced by thermal strain and pyroelectric effects [66-70]. These effects induce only static displacement in a 'smart piezo structure' [71-72]. Influence of thermal stresses upon isotropic host material can be ignored in case of steel, aluminum and titanium alloys within temperature range of ±200°C.

A 'smart piezo structure' can be excited by giving a thermal load i.e. subjecting it to temperature change for some time and can be controlled by simple negative velocity feedback [9, 19, 71]. Smart piezo structures subjected to heat flux are analyzed using the concept of entropy which is a function of strain, electric field and temperature. Helmholtz free energy (2.2) can be formulated as [73]:

$$F_H = \frac{1}{2} K_{ij} \varepsilon_i \varepsilon_j - e_{ij} E_i \varepsilon_k - \frac{1}{2} \in_{lk} E_l E_k - p_l E_l \theta - \alpha_i \varepsilon_i \theta - \frac{1}{2} \beta \theta^2 \tag{2.2}$$

where F_H is Helmholtz free energy, K_{ij} is stiffness tensor, ε_i is strain vector, e_{ij} is piezoelectric stress coefficient, E_i is electric field vector, $\in_{lk}$ is piezoelectric permittivity coefficient, p_l is pyroelectric constant, θ is the temperature, α_i is the coefficient of thermal expansion and β is the ratio of heat capacity to 'reference temperature'. Variation of Helmholtz free energy w.r.t. mechanical displacements, electric field and temperature would give equation of motion of a 'smart structure', sensor-actuator equation and heat transfer equation respectively. In all piezothermoelastic studies of smart piezo structures referred above, influence of temperature on active structural

vibration control has been theoretically investigated using linear piezoelectric constitutive equations:

$$\{D\} = [e]\{\varepsilon\} + [\in]\{E\} + \{p\}\Delta T \tag{2.3}$$

$$\{\sigma\} = [c]\{\varepsilon\} - [e]^T \{E\} - [c]\{\alpha\}\Delta T \tag{2.4}$$

where $\{p\}$ is pyroelectric constant vector, $\{\alpha\}$ is thermal expansion vector and ΔT is the change in temperature from 'reference temperature'. Constitutive equations (2.3) and (2.4) address thermal strain and pyroelectric effects only. Changes in elastic, piezoelectric and dielectric properties of 'smart piezo structure' at ambient temperatures other than 'reference temperature' are ignored. It has been experimentally found that piezoelectric sensor and actuator perform differently at different ambient temperatures [21, 24, 74, 75]. Dynamic transfer function between voltage applied to actuator and the voltage measured by sensor changes with temperature. Repeated thermal cycles cause reduction in frequency, stiffness, capacitance and dynamic performance of sensor [76]. Reduction in stiffness with increase in temperature causes increase in vibration amplitude of the actuator [24]. Change in temperature is not attributed only to the environmental conditions but smart material manufacturing processes can also induce temperature changes. Manufacturing process of thermoplastic composites embedded with PZT patches involves higher temperature treatments. It causes significant losses in PZT generated voltage even within safe temperature limits. However, these losses can be minimized if patch location is at about $1/4^{th}$ of the composite plate thickness [77]. These experimental findings can not be explained by constitutive equations (2.3) and (2.4). In these constitutive equations, piezoelectric stress coefficients (e_{31}, e_{33}, e_{15}) and

permittivity $(\in_{33})$ are measured at 'reference temperature' only and are assumed not to vary away from 'reference temperature'. In other words, piezoelectric stress coefficients and permittivity are assumed constant at all temperatures. Sensing and actuation behaviour of piezoelectric materials depend upon their strain/stress coefficients which are different at different ambient temperatures [2]. Experimental characterization of piezoceramic PZT-5H reveals that: (i) magnitude of piezoelectric strain coefficient (d_{31}) increases linearly with temperature and (ii) permittivity $(\in_{33})$ increases non-linearly with temperature [78]. These linear variations of 'd_{31}' cause as much as 75% decrease in strain output by piezoelectric actuator within temperature range of -150 to 100°C [78]. Therefore while actively controlling structural vibrations at temperatures away from reference temperature, influence of temperature on piezoelectric strain coefficient (d_{31}) and permittivity $(\in_{33})$ can not be ignored. Constitutive equations which take into account the temperature dependence of 'd_{31}' and '$\in_{33}$', should be used. When temperature dependence of 'd_{31}' and '$\in_{33}$' is considered, augmented constitutive equations are [78]:

$$\varepsilon_{ij} = s_{ijkl}^{E,T}\sigma_{kl} + d_{nij}^{T}E_n + \bar{d}_{nij}E_n\Delta T + \alpha_{ij}^{E}\Delta T \tag{2.5}$$

$$D_n = d_{nij}^{T}\sigma_{ij} + \bar{d}_{nij}\sigma_{ij}\Delta T + \in_{nm}^{\sigma,T} E_m + \bar{\in}_{nm}E_m\Delta T + p_n^{\sigma}\Delta T \tag{2.6}$$

where $s_{ijkl}^{E,T}$ is the compliance at constant electric field and temperature, d_{nij}^{T} is piezoelectric strain coefficient at constant temperature, $\bar{d}_{nij}$ is change in piezoelectric strain coefficient per unit temperature, α_{ij}^{E} is coefficient of thermal expansion at constant electric field, $\in_{nm}^{\sigma,T}$ is permittivity coefficient at constant stress and temperature, $\bar{\in}_{nm}$ is

change in permittivity coefficient per unit temperature and p_n^{σ} is pyroelectric constant in n^{th} direction at constant stress. In augmented constitutive equations (2.5) and (2.6), temperature dependent parts '$\bar{d}_{nij}$' and '$\bar{\in}_{nm}$' can be experimentally measured for different temperatures [78]. Simulation studies using these augmented constitutive equations show that: (i) higher stresses are induced in PZT-5H at temperature higher than 'reference temperature' (ii) stresses are reduced at temperature lower than 'reference temperature' [79] and (iii) power consumption in a 'smart piezo structure' is different at different ambient temperatures [80]. Temperature dependent relations for permittivity, elastic compliance and piezoelectric constants are also derived using thermo dynamic relations [81]. Sensitivity analysis can be used to find out the impact of variation in the elements of elastic constant matrix, piezoelectric constant matrix and dielectric constant matrix on smart structural response. For example, if piezoelectric polarized in z-direction is subjected to electric field along the same direction then change in 'e_{31}' has most impact on the response of 'smart structure' as compared to change in 'e_{33}' and 'e_{15}' [82].

2.2.2 *Hygro Effects*

Moisture is another environmental factor which affects AVC performance. Moisture/hygro effect can modify structural stiffness and piezoelectric behavior resulting in different control performance. In situations where effect of moisture and temperature is appreciable, moisture-temperature dependent form of the constitutive equations (2.7) and (2.8) can be used [83].

$$\sigma_{ij} = c_{ijkl}\left(\varepsilon_{kl} - \alpha_{kl}\Delta T - \beta_{kl}\Delta\gamma\right) - e_{kij}E_k \tag{2.7}$$

$$D_j = e_{jkl}\varepsilon_{kl} + \in_{jk} E_k + p\Delta T + \chi\Delta\gamma \tag{2.8}$$

where β_{kl} is the coefficient of moisture expansion, χ is the moisture electric constant and $\Delta\gamma$ is the change in moisture concentration. Using the 'principal of virtual work', finite element equations of motion can be derived. These equations of motion have one extra stiffness matrix due to stresses developed by temperature and moisture and, one extra load vector due to hygro-thermal loading [9].

2.2.3 *Non-Linearities, Fatigue and Ageing Effects*

Piezoelectric materials exhibit non-linearities called hysteresis when driven by high electric field or when high mechanical stress is applied. It non-linearly increases the dielectric, piezoelectric and elastic coefficients of the piezoelectric material [84-86]. Hysteresis effects are attributed to: (i) intrinsic contributions due to elastic deformation of the crystal cell and (ii) extrinsic contributions due to rotation of dipoles formed by the presence of defects. Intrinsic contributions are perfectly linear while extrinsic contributions are non-linear. These non-linearities can be introduced in the piezoelectric constitutive equations [87]:

$$\varepsilon = \left[s_{\text{int}} + s_{ext}\, g(\sigma)\right](1-\nu')\sigma + 2\left[d_{\text{int}} + d_{ext}\, f(E)\right]E \tag{2.9}$$

$$D = \left[d_{\text{int}} + d_{ext}\, g(\sigma)\right]\sigma + \left[\in_{\text{int}} + \in_{ext} f(E)\right]E \tag{2.10}$$

where s, d and $\in$ are compliance, piezoelectric strain coefficient and permittivity coefficients due to intrinsic and extrinsic effects. $g(\sigma)$ is monotonous increasing function of stress 'σ', $f(E)$ is monotonous increasing function electric field 'E' and ν' is the Poisson's ratio. Need of an accurate constitutive equation incorporating hysterisis effects can be avoided if current or charge source is used instead of voltage

source to drive the actuators [88]. It reduces vibrations and hysterisis as well. By regulating the charge or current, fivefold reduction in hysterisis can be achieved [89]. It causes change in dynamics of the 'smart piezo structure' [90]. AVC performance is also influenced by repeated fatigue loading of the actuator. However, it can be ignored if the strain levels do not cross 60% of the static strain limit [76]. Piezoelectric materials suffer a long term ageing after polarization even without external stresses [21]. Ageing can be estimated by experimental characterization of the ageing process. 'd_{31}' coefficient and dielectric constant of piezoceramic PZT-5H has ageing rate of -4.4% and -1.34% per time decade respectively after polarization without any external stresses [23]. Therefore, AVC design should also incorporate ageing process over the life time of device.

2.3 Optimal Placement of Piezoelectric Sensors and Actuators

Active vibration control performance depends upon the placement of piezoelectric sensors and actuators. When a designer of 'smart structure' has to place limited number of sensor/actuator patches over the structure, lot of options are available. Unwise placement of even collocated sensor-actuator pairs over a 'smart structure' controlled by negative velocity feedback can make it unstable [91] and a wise placement of even non-collocated sensor-actuator pairs over a structure can make it stable [92]. It is therefore important that the option for placement so selected should not make the structure unstable. Also, it would be better if sensors and actuators are so placed that it best suits the end application of 'smart structure'. Keeping in mind the end application of 'smart structure', a criterion can be fixed for sensor/actuator locations to maximize the AVC performance. Such a criterion is referred to as 'optimization criterion'. Once 'optimization criterion' is fixed, desired sensor/actuator locations can be found using a

suitable search algorithm called ‘optimization technique’. Such placement of sensors and actuators which is done by optimizing some fixed criterion is called ‘optimal placement’. Optimization techniques like Univariate Search Method [93], Modified Method of Feasible Direction [94], Simulated Annealing [95], Tabu Search [96], Genetic Algorithms [97], Sensitivity Analysis [98], Gradient Algorithm [99], Invasive Weed Optimization [100] etc. are used to find the optimal sensor/actuator locations. Optimal placement of sensors and actuators over a structure can be different for different criteria. An optimization criterion can be based upon: maximization of modal forces/moments applied by the actuator, maximization of the deflection of host structure, minimization of control effort, maximization of degree of controllability/observability of the modes of interest, minimizing spillover effects etc. Researchers have used many ‘optimization criteria’ and ‘optimization techniques’ to find optimal locations. Optimization techniques used to find optimal piezoelectric sensor/actuator locations on a ‘smart structure’ are well documented [101]. In a similar review, ‘optimization criteria’ used by researchers for placement of piezoelectric, shape memory alloys and magnetostrictive actuators on a ‘smart structure’ have been discussed [102]. In following sections, ‘state-of-the-art’ for optimal placement of piezoelectric sensors and actuators based upon above mentioned six criteria is presented one by one.

2.3.1 *Maximizing Modal Forces/Moments Applied by Piezoelectric Actuators*

Piezoelectric actuators are desired to strain the host structure in a direction opposite to the strains developing in the host structure. So, it can be reasoned that piezoelectric actuators should be placed in the regions of high average strains and away from the areas of zero strain (strain nodes). If an electric field is applied across piezoelectric actuators in

the same direction as shown in Figure 2.2a, the host structure will be deformed in extension mode. If the field is applied across piezoelectric actuators in the opposite directions as shown in Figure 2.2b, the host structure will be deformed in bending mode [7]. For control of first mode of a cantilevered beam, collocated actuator pair should be placed near the root. For second mode control, actuators should not be placed at a distance 0.216 of beam length from the root as this is a location of zero strain node. Segmented actuators at the opposite sides of zero strain node and driven 180° out of phase would suit to control such modes [7].

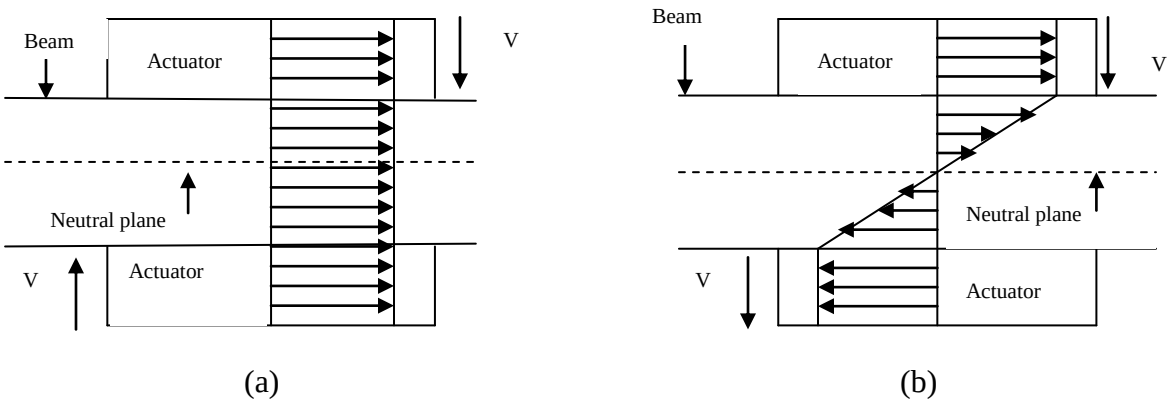

Figure 2.2: A sketch of the surface bonded piezoelectric-host strain distribution during (a) extension and (b) bending mode of the collocated piezoelectric actuator pair

Actuators can be so placed such that modal force available to modes of interest is maximized. To achieve this goal, second order differential equations of motion are written in modal domain. When a plate is controlled using independent modal space control, modal force applied by an actuator to excite j^{th} mode depends upon the location of the actuator and is given by [103]:

$$Q_j(t) = -a_p b_p \left(\frac{h_s + h_p}{2} \right) L\left[\psi_j\right] v_j(t) \tag{2.11}$$

where a_p is the length of piezoelectric patch, b_p is the breadth of piezoelectric patch, h_s is the height of substrate, h_p is the height of piezoelectric patch, $\left[\psi_j\right]$ is normalized modal function, $v_j(t)$ is the voltage applied on j^{th} piezo actuator and operator $L = e_{31}\left\{(\partial^2/\partial x^2) + (\partial^2/\partial y^2)\right\}$ for isotropic piezoelectric material. The vector which gets multiplied by actuator control voltage that is $L\left[\psi_j\right]$ is maximized to achieve maximum modal force objective. Optimal location thus obtained is where the sum of modal strains in '*x*' and '*y*' directions is maximum. Optimal placements of two actuators on a cantilevered plate are adjacent to each other at mid point of the cantilevered edge for first mode. For control of second mode, both actuators are placed at extreme corners of the cantilevered edge. For control of third mode, one actuator is placed at a distance of 0.25 times length of cantilevered edge on the cantilevered edge and second actuator is placed at a distance of 0.75 times length of cantilevered edge on the cantilevered edge [103]. Piezoelectric actuators apply moments and thus strains on the structure (as shown in Figure 2.2). Moments applied by piezoelectric actuator on the structure are function of actuator placement and thickness and are calculated as [104]:

$$M = -2b_s Y_p d_{31} \int_{(h_s - h_p)/2}^{(h_s + h_p)/2} E_z y dy = -2b_s \int_0^d \sigma_x y dy \tag{2.12}$$

where b_s is the width of beam, Y_p is modulus of elasticity of piezoelectric and *d* is the distance from actuator centerline to beam centerline. Thus, moments applied can be optimized so as to get optimal thickness and placement of actuator. Such optimal

thickness and placement of actuator would apply maximum moments on the structure and thus result in maximum curvature of the host structure. Therefore, curvature of the host structure (2.13) which is a function of modulus ratio of piezoelectric and host structure can be optimized [104]:

$$\frac{d^2y}{dx^2}=\left(\frac{1}{d}\right)\frac{d_{31}E_z(6\rho_a\rho_c)}{\rho_Y(1-\rho_a\rho_c^2-2\rho_a^3)+(6\rho_a\rho_c^2+2\rho_a^3)} \tag{2.13}$$

where $\rho_a=\frac{h_p}{2d}$, $\rho_c=\frac{h_s}{2d}$, $\rho_Y=\frac{Y_s}{Y_p}$ and Y_s is the modulus of elasticity of substrate. Plots showing optimal thickness versus modulus ratio for a given actuator location and optimal actuator location versus modulus ratio for given actuator thickness can be obtained for an embedded piezoelectric actuator. Also, such plot showing optimal thickness versus modulus ratio of a surface bounded piezoelectric actuator can be obtained. So for a given modulus ratio, optimal thickness as well as location of actuator with respect to neutral plane of the host structure can be obtained [104].

2.3.2 *Maximizing Deflection of the Host Structure*

When an external voltage is applied on the surface bonded piezoelectric actuator, it produces transverse deflections in the host structure. Transverse deflection of the host structure is a function of actuator placement. So, transverse deflection of the host structure can be used as criterion for optimal placement of actuators [105-109]. Using assumed mode shapes method, the dynamic transverse deflection of the beam with surface bonded piezoelectric patches is given by [110]:

$$w(x,t)=\sum_{i=1}^{\infty}\psi_i(x)\eta_i(t) \tag{2.14}$$

where $\psi_i(x)$ is normalized modal function and $\eta_i(t)$ is corresponding modal coordinate. Also, output sensor voltage is given by [110]:

$$V_{sensor} = e_{31} b_p d \int_{x_1}^{x_2} \frac{\partial^2 w(x,t)}{\partial x^2} dx \tag{2.15}$$

where x_1 and x_2 are the sensor co-ordinates along x-axis. Optimal position of actuator is where the system's strain value is highest. Highest strain value corresponds to the position where beam's curvature is highest. Optimal position of sensor is where V_{sensor} maximizes. Then the optimal position of collocated sensor-actuator pair is ascertained by the following equation [110]:

$$\frac{\partial^3 w(x,t)}{\partial x^3} = 0 \tag{2.16}$$

Maximum deflection of host structure can be written as sum of average angular displacements of adjacent edges of the actuator relative to opposite edges [111]:

$$w_{\max,j} = \frac{1}{\omega_j^2} \frac{a_0}{2\zeta_j m_j} \left| \left(\theta_1 a_p + \theta_2 b_p \right)_j \right| \tag{2.17}$$

where ω_j is the frequency of j^{th} mode, a_0 is the amplitude of external excitation, ζ_j is the damping ratio of j^{th} mode, m_j is modal mass of j^{th} mode and θ_1 & θ_2 are average angular displacements of length and breadth vector about *x* and *y* axes respectively. This summation can be optimized to find optimal position as well as orientation of the actuator. For simply supported plates, optimal actuator position is exactly at the anti-node of mode of interest. For cantilevered plate optimal actuator positions are close to the mid-span of cantilevered edge for the fundamental mode and near the corner of the cantilevered edge for second and third modes. For fourth and fifth modes, it is

recommended to place actuators at anti-nodes [111]. Similarly in case of cantilevered beam, dynamic deflection can be taken as criterion to decide optimal position and length of the piezoelectric actuator pair. Beam dynamic deflection (2.18) is a function of partial derivative of beam mode shapes with respect to length coordinate of the beam [112]:

$$w = \sum_{j=1}^{\infty} \eta_j \left. \frac{\partial \eta_j}{\partial \tilde{x}} \right|_{\alpha_1}^{\alpha_2} M_0 \frac{\left(\Omega \sin Z_j t - Z_j \sin \Omega t \right)}{Z_j \left(\Omega^2 - Z_j^2 \right)} \tag{2.18}$$

where η_j is j^{th} eigen mode of the beam, $\tilde{x}$ is normalized length coordinate of the beam, $\alpha_1 = x_p - \frac{l_p}{2}$, $\alpha_1 = x_p + \frac{l_p}{2}$, x_p is normalized position of actuator, l_p is normalized length of actuator, M_0 is maximum value of actuator moment, Ω is dimensionless loading frequency, $Z_j = \frac{\omega_j^2 \mu}{Y_s I_s} L_s^4$, μ is mass per unit length of the beam, L_s is length of beam and I_s is moment of inertia of the beam, . Effects of position and size of the actuator takes place in the term $\frac{\partial \eta_j}{\partial \tilde{x}}$. Therefore, this derivative can be partially differentiated and optimized to find optimal position of the actuator when its length is fixed. Optimal position thus obtained is located on the beam where opposite edges of actuators correspond to points of equal curvature of beam mode. Similarly, optimal length of the actuator (when position is fixed) corresponds to beam positions where opposite edges of the actuator have opposite curvatures. Optimal position as well as length of the actuator is achieved when it is placed between two consecutive points where the curvatures become zero. This location is anti-node of the mode and is strained the

highest [112]. Maximum plate deflection at a particular mode *(j,k)* can be expressed as a function of product of two sine functions of actuator position coordinates [113]:

$$|w_{\max}| = \sum_{j=1}^{\infty}\sum_{k=1}^{\infty}\left|A_{jk}\right|\sin^2\left(j\pi\alpha_0\right)\sin^2\left(k\pi\beta_0\right) \tag{2.19}$$

where function A_{jk} depends upon plate and piezoelectric actuator material properties, $\alpha_0 = \frac{\alpha_1+\alpha_2}{2}$, $\beta_0 = \frac{\beta_1+\beta_2}{2}$ and $\alpha_1, \alpha_2, \beta_1, \beta_2$ are normalized coordinates of four corners of piezo-actuator. The product function (2.20) is named as 'position mode function' (PMF) and can be partially differentiated to find optimal actuator location [113]:

$$\chi_{jk} = \sin^2\left(j\pi\alpha_0\right)\sin^2\left(k\pi\beta_0\right) \tag{2.20}$$

Optimal locations thus obtained are at the antinodes of respective vibration modes [113]. Optimal actuator locations to excite several modes simultaneously are obtained by taking combined position mode function (CPMF) which is summation of position mode functions of participating modes [113]. Modal displacement of a structure is a function of actuator placement and therefore an influence matrix of actuators can be constructed. To excite some modes only, rows of influence matrix corresponding to modes of interest can be maximized and remaining rows minimized. Sensor-actuator pair must be located near the centre line along the fixed edge of cantilevered plate to damp the first mode. To damp second mode, optimal location is when one edge of the sensor-actuator pair is on free edge of the plate and other edge is on the cantilevered edge of the plate. To control the first two modes simultaneously, one sensor-actuator pair is placed at the centre line along the cantilevered edge and other is placed adjacent to it along the cantilevered edge [114].

2.3.3 *Minimizing Control Effort/Maximizing Energy Dissipated*

In active vibration control, external source of energy is utilized to cause deflection of the structure. The dynamic equations of motion of 'smart structure' in modal domain are written as [115]:

$$\ddot{\eta}_j + c_j^{'}\dot{\eta}_j + \omega_j^2\eta_j = B_a V_{act} \tag{2.21}$$

where $c_j^{'} = 2\zeta_j\omega_j$, ζ_j is modal damping ratio, ω_j is modal frequency, $[B] = \begin{bmatrix} 0 \\ B_a \end{bmatrix}$ is control matrix and V_{act} is external control voltage applied on actuator. In state-space form, system (2.21) can be written as [92]:

$$\begin{aligned} \{\dot{s}\} &= [A]\{s\} + [B]V_{act} \\ \{y\} &= [C]\{s\} \end{aligned} \tag{2.22}$$

where $\{s\}$ is state vector of the system, $[A]$ is system state matrix, $\{y\}$ is sensor output and $[C] = [0 \quad B_v]$ is output matrix of the system. Active damping control law to increase energy dissipation through negative velocity feedback is [92]:

$$V_{act} = -k\{y\} = -kB_v\dot{\eta} \tag{2.23}$$

where k is feedback control gain. Electrical energy spent in structural vibration suppression is a function of actuator placement and is given by [116-117]:

$$J_e = \int_0^\infty {V_{act}}^T R V_{act} dt \tag{2.24}$$

where 'R' is the weighing matrix and is real symmetric positive definite. It is desired that minimum energy is spent in structural vibration suppression. Therefore, minimization of J_e can be used as a criterion for optimal placement with constraint of

minimum vibration suppression level. Using equation (2.24), optimal value of J_e is [117]:

$$J_e = -x^T(0)Px(0) \tag{2.25}$$

where matrix P is the solution of Lyapunov equation and $x(0)$ is the initial condition. Using above criterion, minimum energy is used to control the transverse vibrations of a cantilevered beam when actuator is placed near the root [18]. Optimal distribution of piezoelectric layer over cantilevered plate coincides with areas of high strain for first and third modes. Second and fourth modes which are anti-symmetric, have asymmetric distribution of piezoelectric layer. There is a critical coverage ratio over which additional treatment of active layer is not profitable. For single (second and fourth) as well as for multiple modes, split distribution of piezoelectric layer is the optimal distribution [116]. Equation (2.23), when substituted in (2.21) reduces the dynamic equation of motion of 'smart structure' to:

$$\ddot{\eta}_j + \left(c_j^{'} + B_a k B_v\right)\dot{\eta}_j + \omega_j^2 \eta_j = 0 \tag{2.26}$$

The closed loop system is stable if the location of collocated sensor-actuator is selected so that generalized damping matrix $\left(c_j^{'} + B_a k B_v\right)$ is positive definite. However, in case of non-collocated sensor-actuator pair this condition may not be necessarily achieved [92]. In such situation, asymmetric generalized damping matrix $\left(c_j^{'} + B_a k B_v\right)$ can be decomposed as a summation of a symmetric (C_d) and a skew-symmetric matrix (C_g) such that [92]:

$$C_d = c_j^{'} + D_c \quad ; \quad D_c = \frac{1}{2}[B_a k B_v + (B_a k B_v)^T] \tag{2.27}$$

$$C_g = \frac{1}{2}[B_a k B_v - (B_a k B_v)^T] \tag{2.28}$$

The closed loop system would remain asymptotically stable with infinite gain margin provided that the symmetric part 'C_d' of the generalized damping matrix is positive definite. Skew-symmetric matrix 'C_g' does not influence the system stability at all. Hence to find the optimal sensor/actuator locations for structural vibration control, one should only ensure the positive definiteness of symmetric matrix 'C_d' [92]. It is further desired that 'smart structure' dissipates energy as fast as possible. Energy dissipated by active vibration control of a 'smart structure' is [92, 118-119]:

$$J_d = -\int_0^\infty \dot{x}^T Q x dt \tag{2.29}$$

where $Q = \begin{bmatrix} 0 & 0 \\ 0 & D_c \end{bmatrix}$. Energy dissipated as given by equation (2.29) depends upon piezoelectric placement as well as on feedback gain. So, piezoelectric placements as well as control gains need to be optimized simultaneously so that energy dissipated by the system is maximized. With velocity feedback 'D_c' should always be positive definite and with state feedback, the real eigenvalues of closed loop system matrix should be negative [92]. Using equation (2.29) optimal value of J_d can be obtained [118-119] as:

$$J_d = -x^T(0) P x(0) \tag{2.30}$$

where matrix *P* is the solution of Lyapunov equation. For control of first four modes using equation (2.30), optimal location of collocated sensor-actuator pair comes out near beam root for velocity feedback control and at root for state feedback control [118]. Optimal placement of one collocated sensor-actuator pair is at 0.153 times beam length

from beam root for velocity feedback control. One collocated sensor-actuator pair is at 0.15 times beam length and second at 0.71 times beam length from beam root for velocity feedback control when two collocated sensor-actuator pairs are used. If three collocated sensor-actuator pairs are used then optimal placements are: (i) first pair at 0.158 (ii) second pair at 0.359 and (iii) third pair at 0.828 times beam length from beam root for velocity feedback control [119]. A criterion for the simultaneous minimization of energy spent by the actuators and maximization of energy dissipated by the structure can be obtained by using performance index of LQR optimal control as [92, 118, 120, 121]:

$$J_{ed} = \int_0^\infty (\dot{x}^T Q x + V_{act}{}^T R V_{act}) dt \tag{2.31}$$

Equation (2.31) can be minimized to find the optimal location of the actuator patch. Using (2.31) optimal value of J_{ed} can be written as [92, 118]:

$$J_{ed} = x^T(0) P x(0) \tag{2.32}$$

where matrix P is the solution of algebraic Riccati equation (ARE). Using criterion (2.32) to control first four modes of a cantilevered beam simultaneously, actuator is placed at 0.059 times beam length and sensor at 0.067 times beam length from beam root for velocity feedback control. For state feedback control, actuator is placed at 0.042 times beam length and sensor at 0.223 times beam length. Optimal placement of collocated sensor-actuator pair is at 0.125 times beam length for velocity feedback control [92]. The optimal solutions given by equations (2.25), (2.30) and (2.32) depend upon actuator locations and the initial states. These initial states may not be known. Therefore, a procedure which minimizes the trace of matrix P instead of solving equations (2.25), (2.30) and (2.32) can be used. The optimization criterion thus becomes [122]:

$$\text{Minimize } J = tr\left[P\right] \tag{2.33}$$

where *tr*[.] denotes the trace of matrix. The trace is also the sum of eigenvalues of the matrix. Placement of sensor-actuator which minimizes the trace of matrix [*P*] would be optimal from a possible set of locations for controlling the structural vibrations [123-129]. When LQR performance index is optimized using this method, the optimal locations of ten sensor-actuator pairs over a cantilevered plate to control first six natural modes are at regions of high modal strain energies. Five sensor-actuator pairs are placed at maximum modal strain energies of first two modes, two at maximum modal strain energies of fourth mode and three around the centre of the plate [129]. Optimal locations of four collocated piezoelectric actuator pairs on a plate shaped wing are: two at the leading and the trailing edge of the root, one at the edge of the tip and one at the mid cord of the out board region. Actuators placed at the tip, leading edge and at the trailing edge of the root are also thicker than the remaining two [123]. For control of first mode of a cantilevered beam, optimal actuator patch location is at root. One sensor is placed at a distance of 0.37 times beam length and second at 0.66 times beam length from the root [125]. Minimum control energy can also be ensured by minimizing [130]:

$$Z = tr[F^{-T}F^{-1}] \tag{2.34}$$

where $F = m^{-1}\psi^{T}$, m is modal mass matrix and ψ is normalized modal function.

2.3.4 *Maximizing Degree of Controllability*

Regardless of the control algorithm being applied, necessary condition for effective active vibration control is that the 'smart structure' should be controllable. A closed-loop system (2.22) is completely controllable if every state variable can be affected in such a way so as to cause it to reach a particular value within a finite amount of time by some

unconstrained control. If one state variable cannot be affected in this way, the system is said to be uncontrollable [131]. Controllability is a function of system dynamics and, the location and number of actuators. Control influence matrix '*B'* is determined by actuator locations on the 'smart structure'. A standard check for the controllability of a system is 'rank test' of a matrix '*R*' such that [131]:

$$R = [B \quad AB \quad A^2B \quad A^3B \quad ..... \quad A^{2n-1}B]_{2n\times 2n} \tag{2.35}$$

Closed-loop system (2.22) is completely state controllable if and only if $2n \times 2n$ matrix *R* is full rank [131]. Rank of a matrix is the number of independent rows (or columns) of the matrix when the rows (columns) are treated like vectors. Matrix *R* is called the 'controllability matrix' for the matrix pair [*A B*] where *A* is system state matrix and *B* is control influence matrix. Controllability of a system only tells us whether the system is controllable or not. Degree of controllability of a system can be increased with proper placement of actuators using various techniques. In a 'smart structure', optimal actuator locations are where electrical energy consumed is smallest and modal forces generated are the largest. Criterion (2.24) ensures actuator locations where energy required to control structural vibrations is minimum. Using this criterion, the optimal control energy is obtained as [132]:

$$J_e = [e^{At_1}\{x_0\} - \{x_{t_1}\}]^T G_C^{-1}(t)[e^{At_1}\{x_0\} - \{x_{t_1}\}] \tag{2.36}$$

where aim is to bring the modal system to a desired state $\{x_{t_1}\}$ from initial state $\{x_0\}$ after some time 't_1' and 'G_c' is the controllability Gramian matrix defined as [132]:

$$G_c(t) = \int_0^{t_1} e^{At} BB^T e^{A^T t} dt \tag{2.37}$$

Controllability Grammian matrix (2.37) is a measure of the degree of controllability of a system. Effects of actuator are contained in G_c by way of matrix 'B'. Minimization of control energy (2.36) means minimization of G_c^{-1}. In other words, minimum control energy would be used in structural vibration control if determinant of controllability Gramian matrix is maximized. Eigenvalues of controllability Grammian matrix are also a measure of the degree of controllability. Higher the eigenvalues of controllability Grammian matrix, higher is the controllability. If any eigenvalue of controllability Grammian is very less then the corresponding mode is difficult to control and would require huge amount of control energy for attenuation. Therefore, configuration of actuators which maximizes the performance index given by equation (2.38) would require minimal control effort to suppress structural vibrations [133].

$$J_e = \left(\sum_{j=1}^{2n} \lambda_j \right) \sqrt[2n]{\prod_{j=1}^{2n} \left(\lambda_j \right)} \tag{2.38}$$

where *n* is the number of first-modes to be controlled and λ_j is the j^{th} eigen value of controllability Grammian. Criterion (2.38) is equivalent to maximizing the performance index [134]:

$$J_e = tr\left[G_c \right] * (\det G_c)^{1/2n} \tag{2.39}$$

Based on criterion (2.38), optimal location of four actuators to control five modes of cantilevered plate is: two actuators at extreme corners of cantilevered edge and other two actuators placed adjacent to each other near centre of the plate [133]. Criterion (2.38) ensures global controllability of the system for the first *n* eigen modes. To control each

mode individually by applying minimal control effort, each diagonal term of G_c can be maximized i.e. performance index should be [134]:

$$J_e = \max.\left\{(G_c)_{11}, (G_c)_{22}, ..., (G_c)_{nn}\right\} \tag{2.40}$$

where $(G_c)_{ii}$ are the diagonal elements of G_c. Number of uncontrollable modes is equal to the number of very small singular values of controllability Grammian matrix [135]. So, minimal singular value of controllability Grammian can also be maximized to search for optimal location of actuators [136-137]. Optimal actuator locations for i^{th} mode can also be found using a measure of 'modal controllability' defined as [115, 136, 138-140]:

$$\delta = \| f_i \| \tag{2.41}$$

where $f_i^T = \dfrac{q_i^T B}{\|q_i\|}$ and q_i is the normalized eigen vector of the i^{th} mode. Simultaneous maximization of minimal singular value of controllability Grammian and 'modal controllability' of the i^{th} mode, gives optimal actuator locations between nodal lines for simply supported plate [136].

A square matrix can always be decomposed in the form of $U_1 W U_2$ where U_1 and U_2 are unitary matrices and W is a diagonal matrix with singular values as the diagonal elements [141]. This is called singular value decomposition (SVD). Singular values of control influence matrix B determines the magnitude of control forces. These singular values are found by performing singular value decomposition (SVD) of B. Therefore, to achieve maximum control forces, product of singular values can be taken as controllability index [142]:

$$\Gamma = \prod_{i=1}^{n} \kappa_i \tag{2.42}$$

where κ_i are the singular values of matrix *B*. Higher the controllability index Γ, smaller will be the required actuator voltages for vibration suppression. Therefore, maximization of controllability index gives optimal location of the actuator [143-145]. For control of first mode of simply supported beam, optimal location is at the mid-span (anti-node) of the beam. For simultaneous control of first two modes, there are two optimal locations at distance of approximately 0.3 times 'beam length' from both ends. Similarly, there are three optimal locations when first three modes are controlled simultaneously at distance of approximately 0.27, 0.50, 0.73 times 'beam length' from left end. Similarly for cantilevered beam, optimal location is at the root for first mode. For simultaneous control of first two modes, optimal location is at 0.56 times 'beam length' from the root. For simultaneous control of first three modes, optimal location is at distance of 0.70 times 'beam length' from the root. If free end of the cantilevered beam is propped then optimal location for control of first mode is at 0.3 times 'beam length' from the root. For simultaneous control of first two modes, optimal location is at 0.73 times 'beam length' from the root. For simultaneous control of three modes, optimal location is at 0.53 times 'beam length' from the root [143].

Transfer function (*G*) between actuator voltage and plate deflection gives the response characteristics of the system. Degree of controllability can be quantitatively measured using H_2 norm of the transfer function. H_2 norm of the transfer function is defined as the expected root-mean-square value of the output when the input is a unit variance white noise. Square of H_2 norm of the transfer function in modal form is [146]:

$$\|G_i\|_2^2 = \frac{1}{2\pi}\int_{-\infty}^{+\infty} tr\{G(r_1)G^*(r_1)\}dw \tag{2.43}$$

where $\|G_i\|_2$ is H_2 norm of the transfer function for i^{th} mode, r_1 is the location of piezoelectric actuator and superscript (*) denotes the complex conjugate. The integration is with respect to frequency *w*. Modal controllability is a measure of controller authority over i^{th} mode and can be defined as [146]:

$$M_i(r_1) = \left(\frac{f_i(r_1)}{\alpha_i}\times 100\right)\% \tag{2.44}$$

where $f_i(r_1) = \|G_i\|_2$ and $\alpha_i = \max f_i(r_1)$. Square of H_2 norm of the transfer function in spatial form is [146]:

$$\langle\langle G\rangle\rangle_2^2 = \frac{1}{2\pi}\int_{-\infty}^{+\infty}\int_R tr\{G(r_1)G^*(r_1)\}drdw \tag{2.45}$$

where $\langle\langle G\rangle\rangle_2^2$ is H_2 norm of the transfer function in spatial form and R is the spatial domain of the 'smart structure'. *r* is the length coordinate of base structure. Spatial controllability is a measure of controller authority over the entire structural modes in an average sense and is defined as [146]:

$$S(r_1) = \left(\frac{1}{\beta}\sqrt{\sum_{i=1}^{n} f_i(r_1)}\right)\times 100\% \tag{2.46}$$

where $\beta = \max\sum_{i=1}^{n} f_i(r_1)$ and n is the number of low frequency modes considered. Spatial H_2 norm is different than modal H_2 norm in the sense that it introduces an

additional average operation over the spatial domain *R*. Spatial H_2 norm is related to modal H_2 norm as [146]:

$$\left\langle\left\langle G\right\rangle\right\rangle_2^2 = \sum_{i=1}^{J} \left\|G_i\right\|_2^2 \tag{2.47}$$

Optimal piezoelectric actuator locations can be found by either maximizing modal controllability (2.44) or spatial controllability (2.46) [146-152]. Using criterion (2.44), first and second modes are completely controllable if actuator is placed at the root of the beam, third mode is completely controllable if actuator is placed at 0.735 times beam length from the root of the beam and fourth mode is completely controllable if actuator is placed at 0.829 times beam length from the root of the beam [146]. For control of first mode of a simply supported plate, optimal placement of actuator is in the middle of the plate [148]. Optimal piezo actuator location can also be obtained where the spatial controllability is maximized and modal controllability is guaranteed for each mode of interest [153].

2.3.5 *Maximizing Degree of Observability*

Every state variable in the system has some effect on the output of the system. A closed-loop system (2.22) is said to be completely observable if examination of the system output determines information about each of the state variables. If one state variable cannot be observed in this way, the system is said to be unobservable [131]. Observability is a function of system dynamics and, location and number of sensors. The output influence matrix *C* is determined by the position of sensors on the 'smart structure'. The standard check for the observability of a system is 'rank test' of a matrix *O* where [131]:

$$O = [C \quad CA \quad CA^2 \quad CA^3 \quad .... \quad CA^{2n-1}]^T_{2n\times 2n} \tag{2.48}$$

The system is completely state controllable if and only if $2n \times 2n$ matrix O is full rank. Matrix *O* is called the 'observability matrix' for the matrix pair [*A C*]. Observability of a system only tells us weather the system is observable or not. Degree of observability depends upon the location of sensors and can be increased with proper placement of sensors using various methods. Optimal location of sensors is determined using the same methodology as is used for actuators [134]. In a 'smart structure', optimal sensor locations are where vibration amplitudes or the changes in vibration mode shapes of host structure is relatively large [154] i.e. system output index (2.49) is as large as possible [132]:

$$J_o = \int_0^\infty \{Y\}^T \{Y\} dt \tag{2.49}$$

where *Y* is system output matrix. Measure of observability is the observability Gramian matrix G_o defined as [132]:

$$G_o(t) = \int_0^\infty e^{At} C C^T e^{A^T t} dt \tag{2.50}$$

Effects of sensor are contained in G_o by way of matrix *C*. Information about observability is hidden in eigenvalues of the observability Grammian matrix. If the i^{th} eigenvalue of G_o is small, it means that the i^{th} mode will not be well observed. Therefore, sensor location is so selected that eigenvalues of observability Grammian matrix corresponding to desired modes are maximized [134]. To maximize these eigenvalues, maximization of following measure can be done [132, 155]:

$$J_o = tr\left[G_o\right] * \left(\left|G_o\right|\right)^{1/2n} \tag{2.51}$$

where n is the number of first modes to be observed. Criterion (2.51) ensures global observability of the system for the first n eigen modes. To observe each mode individually, diagonal terms of G_o can be maximized i.e. performance index should be [134]:

$$J_o = \max.\left\{\left(G_o\right)_{11}, \left(G_o\right)_{22}, ..., \left(G_o\right)_{nn}\right\} \tag{2.52}$$

where $\left(G_o\right)_{ii}$ are the diagonal elements of G_o. Optimal sensor locations can also be found using a measure of 'modal observability' of the i^{th} mode [156] which is defined as [138]:

$$\delta = \left\| f_i \right\| \tag{2.53}$$

where $f_i^T = \dfrac{q_i^T C}{\left\|q_i\right\|}$ and q_i is the normalized eigen vector of the i^{th} mode. For a collocated sensor-actuator system: (i) measure of modal observability is equivalent to the measure of modal controllability [156, 157] (ii) optimal sensor locations are same as optimal actuator locations when we maximize the degree of controllability/observability using H_2 norm [150] and (iii) measures of modal and spatial observability using H_2 norm are equivalent to the measure of modal and spatial controllability using H_2 norm [148] . To implement state feedback control law on a 'smart structure', modal displacements and modal velocities of the modes to be controlled are estimated from output of the sensor. The error vector between estimated and actual modal displacement is given by [158]:

$$\left\{e\left(t\right)\right\} = \left[B_n\right]^{-1}\left[B_r\right]\left\{\eta_r\left(t\right)\right\} \tag{2.54}$$

where B_n is the matrix having first *n* observed modes, B_r is the matrix having r residue modes and $\eta_r(t)$ are the residue modal vectors. Square of the norm of error vector (2.54) is given by [158]:

$$\|e(t)\|^2 = \{e(t)\}^T \{e(t)\} = \{\eta_r(t)\}^T [B_e] \{\eta_r(t)\} \tag{2.55}$$

$[B_e] = [B_r]^T \left([B_n]^{-1}\right)^T [B_n]^{-1} [B_r]$ is a symmetric positive definite matrix. Then, degree of observability can be increased by finding optimal sensor locations using the criterion [158]:

$$\|e(t)\|^2 \le \lambda_{\max}([B_e]) \{\eta_r(t)\}^T \{\eta_r(t)\} \tag{2.56}$$

where $\lambda_{\max}([B_e])$ is the maximum eigenvalue of $[B_e]$.

2.3.6 *Minimizing Spillover Effects*

Many times, a smart flexible structure is discretized into finite number of elements for vibration analysis and control. It is sufficient to account for low frequency dynamical behaviour in most practical situations. While implementing the control law, the model is reduced to include only first few low frequency modes of interest. Only first few low frequency modes are considered in state observer. However state feedback control law based on a reduced model may excite the residual modes. These residual modes appear in sensor output but are not included in the control design. This closed loop interaction with low damping of the residual modes results into spillover instability [159, 160]. If subscript '*c'* refers to controlled modes and subscript '*r*' refers to residual modes then the open loop system is described as [160]:

$$\begin{aligned}\{\dot{s}_c\} &= [A_c]\{s_c\} + [B_c]V_{act} \\ \{\dot{s}_r\} &= [A_r]\{s_r\} + [B_r]V_{act} \\ \{y\} &= [C_c]\{s_c\} + [C_r]\{s_r\}\end{aligned} \tag{2.57}$$

Assuming a perfect knowledge of the controlled modes, full state observer is [160]:

$$\{\dot{\hat{s}}_c\} = [A_c]\{\hat{s}_c\} + [B_c]V_{act} + [L_c](\{y\} - [C_c]\{\hat{s}_c\}) \tag{2.58}$$

where $\hat{s}_c$ is the estimated value of $\{s_c\}$ and $[L_c]$ is the observer gain matrix. The state feedback control law is [160]:

$$V_{act} = -k_c \hat{s}_c \tag{2.59}$$

If $\{s_c\}$ and $\{s_r\}$ are the state variables and $\{e_c\} = \{s_c\} - \{\hat{s}_c\}$, then the interaction between control system and the residual modes is given by [160]:

$$\begin{bmatrix} \dot{s}_c \\ \dot{e}_c \\ \dot{s}_r \end{bmatrix} = \begin{bmatrix} A_c - B_c k_c & B_c k_c & 0 \\ 0 & A_c - L_c C_c & -L_c C_r \\ -B_r k_c & B_r k_c & A_r \end{bmatrix} \begin{bmatrix} s_c \\ e_c \\ s_r \end{bmatrix} \tag{2.60}$$

$[B_r]k_c$ and $[L_c][C_r]$ terms are the result of sensor output being contaminated by residual modes via the term $[C_r]\{s_r\}$ (observation spillover) and the feedback control exciting the residual modes via the term $[B_r]V_{act}$ (control spillover). As a result, the eigen values of the system shift away from their decoupled locations as assumed in control law. If the stability margin of the residual modes is small, even a small shift in eigen values would make them unstable. This is known as spillover instability. These spillover effects can reduce the performance and stability of the controller [161]. However, spillover effects can be reduced if sensors and actuators are placed over a ‘smart structure’ in such a way that effects of residual modes are minimal. Actuators so placed would control desired

modes with minimal control spillover and sensors so placed would sense desired modes with minimal observation spillover. To minimize the spillover effects, performance index (2.38) can be modified as [132]:

$$J = \left(\sum_{j=1}^{2n} \lambda_j \right) \sqrt[2n]{\prod_{j=1}^{2n} \left(\lambda_j \right)} - \gamma \left(\sum_{j=2n_c+1}^{2(n_c+n_r)} \lambda_j \right) \sqrt[2n_r]{\prod_{j=2n_c+1}^{2(n_c+n_r)} \left(\lambda_j \right)} \tag{2.61}$$

where n_c and n_r are the number of the controlled modes and residual modes respectively and γ is the weighting constant which can be selected by the designer. Maximization of this performance index would maximize eigenvalues corresponding to the modes to be controlled and minimize eigenvalues corresponding to the modes to be ignored. This results in reduction of spillover effects [162]. When this criterion is used to control first three modes of a composite cantilevered plate instrumented with two piezoelectric sensors and two piezoelectric actuators, optimal locations are: (i) one sensor at one end of the cantilevered edge (ii) both actuators exactly below first sensor & placed adjacent to each other and (iii) second sensor at second end of the cantilevered edge [162]. To ensure maximum utilization of control energy with minimum spillover effects, criterion (2.34) can be modified as [130]:

$$Z = tr\left[\left(F_r F^{-1} \right)^T \left(F_r F^{-1} \right) \right] \tag{2.62}$$

In this way, significant vibration control can be achieved with only little spillover effect. When criterion (2.56) is used to maximize the degree of observability, spillover effects can be greatly minimized if we minimize the maximum eigen value of $[B_e]$ [158]. Spillover effects can also be addressed by imposing a constraint in criterion (2.46). High

frequency residual modes can be considered for which spatial controllability can be defined as [148]:

$$S_r(r_1) = \left(\frac{1}{\beta_r} \sqrt{\sum_{i=J+1}^{\bar{J}} f_i(r_1)} \right) \times 100\% \tag{2.63}$$

where $\bar{J}$ corresponds to the highest frequency mode that is considered for the spillover reduction and $\beta_r = \max \sum_{i=J+1}^{\bar{J}} f_i(r_1)$. Therefore spillover effects can be reduced by imposing the constraint [148, 153]:

$$S_r(r_1) \le c \tag{2.64}$$

along with the criterion (2.46) where '*c*' is the upper allowable level for spatial controllability for spillover reduction. Criteria (2.40) and (2.52) increase the degree of 'modal controllability' and 'modal observability' respectively but without considering residual modes. These criteria can be modified to include residual modes. New criterion thus obtained for good controllability with minimal spill-over effects is [134]:

$$\begin{aligned} J = \max. & \left\{ (G_c)_{11}, (G_c)_{22}, ..., (G_c)_{n_c n_c} \right\} \\ \& \min. & \left\{ \left(G_c^r\right)_{11}, \left(G_c^r\right)_{22}, ..., \left(G_c^r\right)_{n_r n_r} \right\} \end{aligned} \tag{2.65}$$

and for good observability with minimal spill-over effects is [134]:

$$\begin{aligned} J = \max. & \left\{ (G_o)_{11}, (G_o)_{22}, ..., (G_o)_{n_c n_c} \right\} \\ \& \min. & \left\{ \left(G_o^r\right)_{11}, \left(G_o^r\right)_{22}, ..., \left(G_o^r\right)_{n_r n_r} \right\} \end{aligned} \tag{2.66}$$

where $\left(G_c^r\right)_{ii}$ and $\left(G_o^r\right)_{ii}$ are the eigen values corresponding to residual modes.

Optimal locations obtained for surface bonded piezoelectric sensor and actuator patches using above mentioned criteria are summarized in Table 2.1 and Table 2.2 in case

Criterion	Boundary Condition	Modes to be Controlled	Sensor and Actuator Locations
Maximizing modal forces/ moments	Cantilevered	First Second	actuators must be placed near root one actuator at distance less than 0.216 times beam length driven 180° out of phase with second actuator at distance greater than 0.216 times beam length bonded to opposite side
Maximizing deflection of the host structure	Cantilevered	First Second or higher	optimal length of collocated actuator pair is equal to the length of the beam collocated actuator pair is where opposite edges of actuator correspond to points of equal curvature of beam mode
Minimizing the control efforts	Cantilevered	First	actuators must be placed near root
Maximizing energy dissipated	Cantilevered	First four	actuator at 0.059 times beam length & sensor at 0.067 times beam length for velocity feedback control actuator at 0.042 times beam length & sensor at 0.223 times beam length for state feedback control collocated sensor-actuator pair at 0.125 times beam length for velocity feedback control
	Cantilevered	First four	collocated sensor-actuator pair near beam root for velocity feedback control collocated sensor-actuator pair at beam root for state feedback control
	Cantilevered	First four	collocated sensor-actuator pair at 0.153 times beam length from beam root for velocity feedback control (when one pair is used) first collocated sensor-actuator pair at 0.15 times beam length and second at 0.71 times beam length from beam root for velocity feedback control (when two pairs are used) first collocated sensor-actuator pair at 0.158, second at 0.359 and third at 0.828 times beam length from beam root for velocity feedback control (when three pairs are used)

Criterion	Boundary Condition	Modes to be Controlled	Sensor and Actuator Locations
Maximizing degree of controllability	Cantilevered	First	collocated actuator pair at root
		First two	collocated actuator pair at 0.56 times beam length from root
		First three	collocated actuator pair at 0.7 times beam length from root
	Cantilevered at one end and propped at another	First	collocated actuator pair at 0.3 times beam length from root
		First two	collocated actuator pair at 0.73 times beam length from root
		First three	collocated actuator pair at 0.53 times beam length from root
	Simply Supported	First	collocated actuator pair at mid-span
		First two	collocated actuator pair at 0.3 times beam length from any end
		First three	collocated actuator pair at 0.27 or 0.5 or 0.73 times beam length from left end
Optimal value of LQR performance index	Cantilevered	First	actuator is placed at root, one sensor is placed at a distance of 0.37 times beam length and second at 0.66 times beam length from the root
Maximizing degree of modal controllability	Cantilevered	First	actuator at root
		Second	actuator at root
		Third	actuator at 0.735 times beam length from beam root
		Fourth	actuator at 0.829 times beam length from beam root

Table 2.1: Optimal locations of surface bonded piezoelectric sensor and actuator patches on a smart beam structure

Criterion	Boundary Condition	Modes to be Controlled	Sensor and Actuator Locations
Maximizing modal forces/ moments applied by actuator	Cantilevered	First	two actuators adjacent to each other at mid point of the cantilevered edge
		Second	two actuators at extreme corners of the cantilevered edge
		Third	one actuator at 0.25 times length of cantilevered edge on the cantilevered edge and second actuator at 0.75 times length of cantilevered edge on the cantilevered edge
Maximizing deflection of the host structure	Cantilevered	First	actuator close to the middle of cantilevered edge
		Second & Third	actuators near the corner of the cantilevered edge
		Fourth & Fifth	actuators at anti-nodes
	Cantilevered	First	collocated sensor-actuator pair must be located near the centre line along the cantilevered edge
		Second	one edge of the collocated sensor-actuator pair is on free edge of the plate and other edge is on the cantilevered edge of the plate
		First & Second	one collocated sensor-actuator pair is placed at the centre line along the cantilevered edge and other is placed adjacent to it along the cantilevered edge
	Simply Supported	First five	actuators at anti-nodes of modes of interest
Minimizing the control efforts	Cantilevered	First & Third	actuators should cover areas of high strain
		Second & Fourth	optimal distribution of piezoelectric actuator layer is asymmetric
Optimal value of LQR performance index	Cantilevered	First six	five collocated sensor-actuator pairs at maximum modal strain energies of first two modes, two at maximum modal strain energies of fourth mode and three around the centre of the plate
Expected value of LQR performance index	Cantilevered (Plate shaped wing)	First torsion mode	two actuators at leading and trailing edge of the root, one at the edge of the tip and one at the mid cord of the out board region

Criterion	Boundary Condition	Modes to be Controlled	Sensor and Actuator Locations
Maximizing degree of controllability	Cantilevered	First five	two actuators at extreme corners of cantilevered edge and two adjacent to each other near centre of the plate
	Simply Supported	First	actuator at middle of the plate
		First four	actuators between nodal lines
Maximizing degree of observability & minimizing spillover effects	Cantilevered	First three	one sensor at one end of cantilevered edge, two actuators exactly below this sensor placed adjacent to each other & another sensor at other cantilevered end

Table 2.2: Optimal locations of surface bonded piezoelectric sensor and actuator patches on a smart plate structure

of beam and plate structures. After this literature survey on optimal placement of piezoelectric sensors and actuators, we conclude that according to all criteria: (i) to control the first mode of a cantilevered beam, optimal placement of actuators is near the root of the beam and (ii) to control the higher modes of a cantilevered beam, optimal placement of actuators is away from the root of the beam. Also according to all criteria, in case of a cantilevered plate: (i) optimal placement of actuator is close to the mid-point of cantilevered edge for control of the first mode (ii) optimal placement of actuators is at the corners of cantilevered edge for control of second mode and (iii) optimal placement of actuators is in between the mid point and corners of the cantilevered edge for control of higher modes. According to all criteria in case of simply supported plates, the optimal actuator placements are either (i) at locations where average strains in '*x*' and '*y*' directions are maximum or (ii) at anti-nodes. Actuators should not be placed at nodes. It

is also observed that: (i) optimal placements of piezoelectric sensors and actuators on a 'smart structure' depend upon the optimization criterion and boundary conditions and (ii) optimal locations obtained for each criterion can not be predicted using intuitive method. Placement of sensors and actuators based upon intuitive method can result in poor performance or even failure of AVC scheme [92]. It is therefore recommended that the placement of sensors and actuators on a 'smart structure' should be according to a suitable criterion.

2.4 Techniques to Write Equations of Motion of a 'Smart Structure'

A 'smart structure' is prepared by bonding piezoelectric patches over the host structure by employing finite bonding layer of glue. It is essential to understand the electromechanical interaction between the piezoelectric patch and the host structure. A simple model of two dimensional structure instrumented with piezoelectric patches can be developed by considering electromechanical coupling of piezoelectric patches but without considering mass and stiffness of piezoelectric patches [163-164]. When piezoelectric patch is instrumented on a structure, the dynamics of the structure change due to considerable mass and stiffness of the piezoelectric patch. Static and dynamic analytical models of surface bonded as well as embedded piezoelectric actuators can be obtained by considering the stiffness but ignoring the mass of piezoelectric patch [7]. A refined model can be developed by taking into consideration mass as well as stiffness of piezoelectric patch [18]. If mass and stiffness of piezoelectric patch is ignored then fundamental natural frequency of a beam structure would be wrong by as much as 18% even for open circuit conditions [165]. Natural frequencies shift by as much as 14% if a 'smart structure' is in a closed circuit. This happens due to induction of so called

'generalized stiffness' which is a function of structural mode shapes, piezoelectric patch location and piezoelectric constants [46, 166]. Inertial effect of the piezoelectric patch can be modelled by a grid of lumped masses and stiffness effect by arrays of springs oriented in direction parallel to edges of piezoelectric patch [167]. Models of two dimensional smart plate structures considering mass and stiffness of piezoelectric patches predict accurate dynamics of the 'smart structure' [136, 168]. Therefore, inclusion of inertia and stiffness effects of piezoelectric patches in mathematical modeling is important to capture the structural dynamics. Equilibrium relations, Hamilton's principle, finite element model, modal testing etc. are used to find the equations of motion of the 'smart structure'. Let us discuss these ways one by one.

2.4.1 *Equilibrium Relations*

Equilibrium relations (2.67)-(2.69) can be solved to obtain strains and stresses in the piezoelectric, host and bonding layer [169]:

$$\frac{\partial \sigma_{xx}}{\partial x} + \frac{\partial \sigma_{yx}}{\partial y} + \frac{\partial \sigma_{zx}}{\partial z} + f_x = \rho \ddot{u} \tag{2.67}$$

$$\frac{\partial \sigma_{xy}}{\partial x} + \frac{\partial \sigma_{yy}}{\partial y} + \frac{\partial \sigma_{yz}}{\partial z} + f_y = \rho \ddot{v}" \tag{2.68}$$

$$\frac{\partial \sigma_{xz}}{\partial x} + \frac{\partial \sigma_{yz}}{\partial y} + \frac{\partial \sigma_{zz}}{\partial z} + f_z = \rho \ddot{w} \tag{2.69}$$

where σ_{ij} are normal stresses in j^{th} direction in the plane perpendicular to i^{th} direction, f_i is force vector in i^{th} direction, ρ is density and $u, v", w$ are the displacements along x, y and z-axes. These strains and stresses involve hyperbolic trigonometric functions and depend upon strains at the boundaries of piezoelectric actuator and on voltage applied on the piezoelectric actuator. For a perfectly bonded actuator, bonding layer is assumed to be

infinitely stiff. Under this idealized assumption, strains do not involve trigonometric hyperbolic functions and the strains are transferred between the piezoelectric and structures at concentrated points at the ends of piezoelectric. These strains (2.70) and moments (2.71) are obtained as a sum of two factors: first depending upon strains in the host at the boundaries of piezoelectric patch and the second upon the voltage applied across the piezoelectric actuator [7].

$$\varepsilon_s = \varepsilon_p = \frac{\Psi}{\Psi+\Omega}\left[\frac{\varepsilon_s^{s+}+\varepsilon_s^{s-}}{2}+\frac{\varepsilon_s^{s+}-\varepsilon_s^{s-}}{2}\bar{x}\right]+\frac{\Omega}{\Psi+\Omega}\left(\frac{d_{31}V_{act}}{t_p}\right) \tag{2.70}$$

$$M = R_s t_s^2 b_s\left[\frac{1}{\Psi+\Omega}\left(\frac{\varepsilon_s^{s+}+\varepsilon_s^{s-}}{2}+\frac{\varepsilon_s^{s+}-\varepsilon_s^{s-}}{2}\bar{x}\right)-\frac{1}{\Psi+\Omega}\left(\frac{d_{31}V_{act}}{t_p}\right)\right] \tag{2.71}$$

where $\Psi = \frac{Y_s t_s}{Y_p t_p}$, t_s is base structure thickness, t_p is piezoelectric thickness, Ω is a constant depending upon the assumed beam strain distributions ratio of the beam, ε^{s+} is strain value at the left end, ε^{s-} is strain value at the right end and $\bar{x}$ represents the piezoelectric location. Similarly, equilibrium equations can be solved to obtain strains as well as moments in case of embedded actuators in bending as well as shear mode.

Equilibrium equations can be solved by assuming a solution and finding unknowns of the assumed solution. A 'stress function' $f_1(x,z)$ and an 'electric displacement function' $f_2(x,z)$ can be introduced such that equilibrium relations are satisfied. These functions vary quadratically through the length and their constants can be obtained by using strain compatibility equation (2.72) and electric compatibility equation (2.73).

$$\frac{\partial^2 \varepsilon_x}{\partial z^2} + \frac{\partial^2 \varepsilon_z}{\partial x^2} - \frac{\partial^2 \gamma_{xz}}{\partial x \partial z} = 0 \tag{2.72}$$

$$\frac{\partial E_x}{\partial z} - \frac{\partial E_z}{\partial x} = 0 \tag{2.73}$$

where γ_{xz} is shear strain vector in z^{th} direction in the plane perpendicular to i^{th} direction. In this way stress, strain and electric displacement variations through the thickness and length of a piezoelectric patch can be found [170]. Resultant force acting on a piezoelectric patch can be obtained by integrating stress defined by piezoelectric constitutive equations. Using this resultant force, equations of motion can be obtained [171]. Equilibrium equations can be integrated to get equations of motion involving forces and moments. These forces and moments can be obtained by integrating constitutive equations of piezoelectric as well as of the host structure [172].

2.4.2 *Hamilton's Principle*

Principle of virtual work or Hamilton's principle given by equation (2.74), is a powerful tool to model dynamic systems [173].

$$\delta \int_{t_1}^{t_2} L dt = 0 \tag{2.74}$$

where $L = T - U + W$ is known as Lagrangian of the system. User of this tool has to visualize the dynamic system and then write expression for total kinetic energy (T), total potential energy (U) and total work done (W) at a particular instant of time. Assumed shape functions given by equations (2.75)-(2.77), for flexural and longitudinal motion can be used in kinetic and potential energy expressions [136].

$$u(x, y, z) = \{\psi(x, y)\}^T \{h(t)\} \tag{2.75}$$

$$v(x, y, z) = \{\zeta(x, y)\}^T \{f(t)\} \tag{2.76}$$

$$w(x,y,z) = \{\phi(x,y)\}^T \{g(t)\} \tag{2.77}$$

where ψ, ζ, ϕ are assumed displacement shapes and h, f, g are generalized coordinates in x, y and z-directions. These expressions when substituted in Hamilton's principle give equations of motion of the dynamic system. Typically, a piezoelectric patch may be acted upon by body force, surface traction, point force and surface charge. These all quantities would do some work on the piezoelectric patch. Their work contributions can be added along with total kinetic energy and potential energy of the piezoelectric patch and finally substituted into Hamilton's principle to obtain dynamic equations of motion. Application of variations w.r.t. displacement variable gives equation of motion of 'smart structure' and w.r.t. electric potential gives equation of piezoelectric sensor and actuator [174-176]. If the structure is rotating about an axis, then kinetic energy term 'T' of the Lagrangian functional would also have rotational kinetic energy term of the whole structure [177]. Stresses due to rotations contribute to potential energy term 'U' and angular velocity will contribute to the kinetic energy term 'T'. The equation of motion can be then derived using Lagrange's equation (2.78):

$$\frac{d}{dt}\left(\frac{\partial T}{\partial \dot{q}}\right) - \left(\frac{\partial T}{\partial q}\right) + \frac{\partial U}{\partial q} = Q \tag{2.78}$$

where q and Q are the generalized coordinate and the generalized force respectively. The equation of motion (2.79) so obtained has two extra stiffness matrices: geometric matrix (K_G) and rotational matrix (K_R). Both of these matrices are proportional to the square of the angular velocity [151].

$$[M]\{\ddot{x}\} + [C]\{\dot{x}\} + [K + K_G + K_R]\{x\} = \{F\} \tag{2.79}$$

In case of thermo-electro-mechanical loading, effect of initial stress caused by thermoelectric loading would be considered in potential energy term (2.80) of the Lagrangian [24, 178].

$$U = b\int_0^l \int_{-t/2}^{t/2} \left(\sigma_x \varepsilon_x + \frac{\pi^2}{12} \tau_{xz} \gamma_{xz} + \chi - D_x E_x - D_z E_z \right) dz dx \qquad (2.80)$$

where l is length, b is width, t is thickness of piezoelectric actuator, τ_{ij} is shear stress vector in j^{th} direction in the plane perpendicular to i^{th} direction, the term $\chi = \frac{1}{2}\sigma_x^0 \left(\frac{\partial w}{\partial x} \right)^2$ shows the effect of initial stress 'σ_x^0' that is caused by thermoelectric loading before dynamic deformation takes place and w is the displacements along z-axis.

2.4.3 *Finite Element Technique*

Finite element technique is most widely used tool for the design and analysis of smart structures. In the equations of motion of a 'smart structure', there are two variables namely: displacement and electric potential. A finite element formulation can be constructed and these two variables can be interpolated in terms of nodal values of the element. A three dimensional tetrahedral element (Figure 2.3a) is the most basic geometric form in modeling arbitrary continuum and can be used to model an arbitrary shaped piezoelectric patch [179]. When such thick solid elements are used to model very thin continua, they produce models which are stiffer than actual ones. To overcome this problem, hexahedral solid elements (Figure 2.3b) with three additional internal degrees of freedom can be used [180-181]. Such 3D elements with nodal electric potential dofs when used to model the host structure, increase size of the problem and computational efforts. Therefore, two dimensional 4-noded quadrilateral element (Figure 2.3c) based

upon 'Classical Plate Theory' with 12-mechanical and 1-electric degrees of freedom per element can be used to model a 'smart structure'. These elements overcome excessive stiffness problem and reduce problem size as well as computational efforts [45].

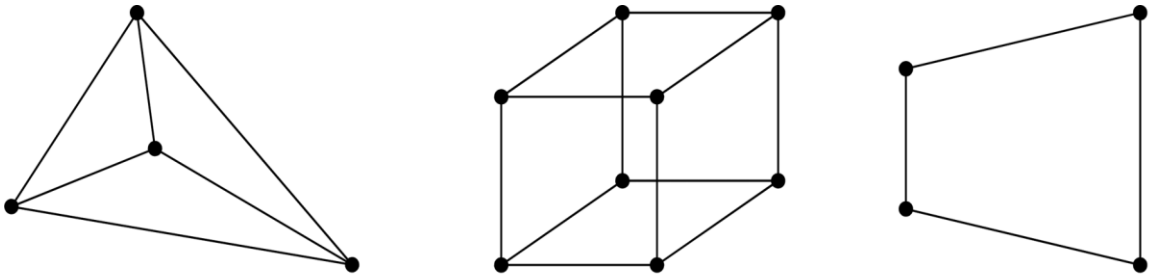

Figure 2.3: Finite element shapes to model a 'smart structure'

However, to capture the dynamics well, three dimensional piezoelectric finite elements are preferred over two dimensional ones [182]. But when these elements are applied to thin plate and shell structures, displacements for a given mesh are much smaller than numerically predicted and stresses are largely inaccurate. This happens due to locking of mesh. When structure is subjected to pure bending then 3D elements applied to thin structures give false shear stress and hence false shear strains in the thickness direction. These false shear strains absorb energy and some of the energy that should go into bending is lost. Therefore, such elements become too stiff in bending and the resulting deformation is smaller than actually it should be. In finite element literature, this phenomenon is known as 'shear locking' [183]. When curved structures bend, the vertical edges of element are oblique and can activate thickness/normal strains in thickness direction which lead to 'trapezoidal locking' [184] due to false thickness strains

[185]. 'Thickness locking' is introduced when false plane strain conditions $(\varepsilon_z = 0)$ are predicted instead of expected plane-stress conditions $(\sigma_z = 0)$ if the element is loaded by bending moment.

Various techniques have been developed to overcome locking effects. If we use (i) 20-noded 3-dimensional brick elements to model piezoelectric patch and the neighbourhood (Figure 2.4a) (ii) 9-noded 2-dimensional shell elements to model rest of the host structure (Figure 2.4c) (iii) 13-noded flat transition elements (Figure 2.4b) to connect solid and shell elements and (iv) excessive aspect ratios of solid and transition elements are avoided then, computational efforts as well as locking effects are minimized [186]. Also, dynamics of 'smart structure' is well captured [47].

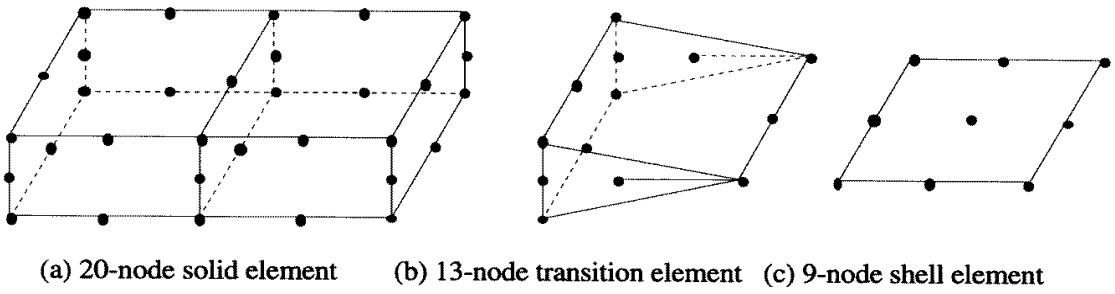

Figure 2.4: A combination of elements to model a smart structure with piezoelectric patches

In case of active constrained layer damping (ACLD), 3-dimensional solid elements to model ACLD area, 2-dimensional shell elements to model host structure and transition elements to connect solid and shell elements is a wise element selection [187]. Piezoelectric finite element models with independently assumed displacement and electric potential are called irreducible finite element models because the field variables

cannot be further reduced. These models are too stiff, susceptible to mesh distortion and locking phenomena. Such models can also be improved if we use mixed/hybrid assumptions. Hybrid tetrahedral finite element with assumed displacement, electric potential and electric displacement can be derived using 'hybrid variational principle' [188]. However, 8-noded hexahedral hybrid piezoelectric finite element with assumed stress, assumed electric displacements and both is more accurate as well as less sensitive to element distortion and aspect ratio. This hybrid piezoelectric finite element is derived using 'general hybrid variational principle' which assumes displacement, stress, strain, electric potential, electric field and electric displacement as independent field variables and the functional is given by:

$$\begin{aligned}\Pi = &\int_{\Omega}\left[H - \begin{Bmatrix}\sigma\\ D\end{Bmatrix}^T\left(\begin{Bmatrix}\varepsilon\\ -E\end{Bmatrix} - \begin{Bmatrix}\nabla_m u\\ \nabla_e \Phi\end{Bmatrix}\right) - f^T u\right]dv \\ &- \int_{S_T}\left(\bar{t}\right)^T u ds - \int_{S_e}\Phi\bar{d}\,ds - \int_{S_u}\left(n_m\sigma\right)^T\left(u-\bar{u}\right)ds - \int_{S_\Phi}\left(n_e D\right)^T\left(\Phi-\bar{\Phi}\right)ds\end{aligned} \tag{2.81}$$

where $H = \frac{1}{2}\begin{Bmatrix}\varepsilon\\ -E\end{Bmatrix}^T\begin{bmatrix}c & e^T\\ e & -\in\end{bmatrix}\begin{Bmatrix}\varepsilon\\ -E\end{Bmatrix}$ is electric enthalpy, ∇_m is differential operator in stress equilibrium equations (2.67)-(2.69), ∇_e is differential operator in charge conservation condition (2.87), Φ is electric potential, n_m & n_e are matrices containing unit outward normal vectors of the respective boundaries and $\bar{t}$, $\bar{d}$ & $\bar{u}$ are prescribed traction, displacement & electric displacement respectively [189]. ANS method [190-191] removes 'shear locking' by interpolating natural transverse shear strains from their samples along the element edges. These sample strains are common to the elements sharing the same edge. In this way, the number of independent shear strains is reduced. ANS method can also be used to remove 'trapezoidal locking' by interpolating natural

thickness strains at the midpoints of element corners [192]. Hybrid stress formulations along with ANS method are used to construct HS-ANS solid shell element which can remove 'shear locking' and 'trapezoidal locking'. 'Thickness locking' can be removed by modifying the generalized stiffness of the laminate host [193]. A more accurate and computationally efficient novel RHEAS element can be used to overcome 'shear locking' and 'thickness locking' [194]. It can be derived by incorporating enhanced assumed strain (EAS) modes [195] and orthogonal interpolation modes [196] in the modified variational principle functional (2.82):

$$\Pi = \frac{1}{2}\begin{Bmatrix} \varepsilon \\ \nabla_e \Phi \end{Bmatrix}^T \begin{bmatrix} c & e^T \\ e & -\in \end{bmatrix} \begin{Bmatrix} \varepsilon \\ \nabla_e \Phi \end{Bmatrix} - \left(\sigma^T + \beta\right)\left(\varepsilon - \nabla_m u_q\right) + \sigma^T \left(\nabla_m u_\lambda\right) + W \tag{2.82}$$

where β is a constant, u_q is conventional displacement field and u_λ is non-conforming displacement field.

For actively controlling a 'smart structure', size of the mathematical model should be as small as possible. Large sized mathematical models can be reduced by employing modal truncation [197], Guyan reduction [198] etc. Another option available for obtaining a small size model is to use spectral finite element. In spectral finite element, displacement function (2.83) is assumed as product of spatial variable and a harmonic function in time.

$$u = U\left(x\right)e^{i\omega t} \tag{2.83}$$

Substitution of these displacement functions into equations of motion of 'smart structure' yields spatial functions (2.84) as summation of harmonic functions in space.

$$U\left(x\right) = a_1 e^{ik_1 x} + a_2 e^{-ik_1 x} + a_3 e^{ik_2 x} + a_4 e^{-ik_2 x} \tag{2.84}$$

where k_1, k_2 are wave numbers of the system and a_i depend upon structural properties. Finite element thus developed exactly captures the physics of the wave propagation and also, very less number of elements are required to model the dynamics of the structure [199].

Thin structures can be analyzed using 'Classical Beam/Plate Theory' wherein shear deformations are ignored. It is adequate for most of the structures where thickness is small as compared to inplane dimensions [200]. However, application of this theory on thicker beams/plates gives wrong results. Higher order displacement field through the thickness is essential to analyze thick beam/plate undergoing shear deformation. So, higher order (3^{rd} order) displacement function equation (2.85) using Reddy's higher order shear deformation theory [201] can be assumed as:

$$u(x,z) = u_0(x) + g_1(z)\frac{\partial w_0(x)}{\partial x} + g_2(z)\psi(x) \tag{2.85}$$

$$w(x,z) = w_0(x) \tag{2.86}$$

where $g_1(z) = -\frac{4z^3}{3h_e^2}$, $g_2(z) = z - \frac{4z^3}{3h_e^2}$, h_e is the thickness of the finite element, u_0 and w_0 are the displacements of a point in the mid-plane along *x* and *z*-axes and ψ represents the shear effect. According to Gauss's law (2.87) [202], divergence of electric displacement for a piezoelectric material is zero i.e. electric displacement should be constant throughout the thickness since there is no free charge inside a piezoelectric material.

$$\vec{\nabla}.\vec{D} = 0 \tag{2.87}$$

Electric displacement is a function of strains and electric field. For a thick piezoelectric material undergoing shear deformation, strains through the thickness are non-uniform as given by equations (2.85) and (2.86). So, electric field through the thickness cannot be assumed constant because such assumption would make electric displacement variable through the thickness and Gauss's law would be violated. It is essential for thick structures to take higher order through the thickness variation of electric field:

$$\phi_i\left(x,\tilde{z}_i\right)= f_{1i}\left(\tilde{z}_i\right)E_{ti}(x)+ f_{2i}\left(\tilde{z}_i\right)E_{bi}(x)+ f_{3i}\left(\tilde{z}_i\right)V_i(x) \tag{2.88}$$

where f_{1i}, f_{2i} and f_{3i} are third order functions in terms of $\tilde{z}_i=\left(\frac{z-z_{0i}}{h_i}+\frac{1}{2}\right)$ and h_i . z_{oi} and h_i are mid-plane position and thickness of the i^{th} layer [203]. Piezoelectrically actuated forces can be estimated efficiently if in-plane strains through the thickness of 'smart structure' are modeled properly. In-plane strains through the thickness can be modelled by layer-wise displacement theory [204]. In layer-wise displacement theory, the structure is assumed to be made up of finite layers. Displacement fields u,v and w given by equations (2.89)-(2.91) at any point in the volume of the structure are linear combination of values of displacement at the nodes of the finite layers.

$$u(x,y,z,t)=\sum_{j=1}^{N}U^J(x,y,t)\Phi^J(z) \tag{2.89}$$

$$v(x,y,z,t)=\sum_{j=1}^{N}V^J(x,y,t)\Phi^J(z) \tag{2.90}$$

$$w(x,y,z,t)=W(x,y,t) \tag{2.91}$$

where U^J and V^J are undetermined coefficients, Φ^J is the Lagrangian interpolation function through the thickness and N is the number of degrees of freedom for the in-

plane displacement along the thickness. To model a composite beam, a two node beam element can be taken with four mechanical and 3*m* degrees of freedom per node where '*m*' is the number of piezoelectric layers in an element [205-206]. Developments in piezoelectric finite elements are well tabulated with special reference to element shape, assumptions made, beam/plate theory etc. [207].

2.4.4 *Modal Testing*

Many times, mathematical model of the 'smart structure' is required in state space form (2.22) to apply a suitable control law. State space model of the system consists of natural frequencies, damping ratios, normalized mode shapes and modal actuation force per unit actuator voltage. All these constants can be obtained by manipulating frequency response functions (FRF) of the 'smart structure' i.e. by performing modal test on the 'smart structure'. If '*x*' is a vector of surface displacements in physical coordinates then for an applied force '*f*' at a spatial position '*l*' and a response measurement at spatial position '*k*', the FRF equation in physical coordinates is:

$$\frac{x_k}{f_i} = \sum_{i=1}^{n}\left[\frac{\Phi_{ki}\Phi_{li}}{a_i\left(s-\lambda_i\right)} + \frac{\Phi_{ki}^{*}\Phi_{li}^{*}}{a_i^{*}\left(s-\lambda_i^{*}\right)}\right] = \sum_{i=1}^{n}\left[\frac{A_i^{k,l}}{\left(s-\lambda_i\right)} + \frac{A_i^{k,l*}}{\left(s-\lambda_i^{*}\right)}\right] \qquad (2.92)$$

where Φ_{ki} is complex modal matrix of eigen vectors, λ_i is the i^{th} complex eigen value of the structure, * refers to the complex conjugate, *n* is the number of modes and pole residue $A_l^{k,l} = \dfrac{\Phi_{ki}}{\Phi_{li}a_i}$. Natural frequencies and damping ratios can be obtained by curve fitting the actual transfer function. Normalized mode shapes and modal actuation forces can be obtained by comparison of numerators of theoretical and experimental transfer functions. FRF equation of a structure gives the response measurement at a spatial

position w.r.t. applied force at another spatial position. It is possible to convert the FRF so that voltage sensed by a piezoelectric sensor is available in response to voltage applied on a piezoelectric actuator. This way, pole residue modal model becomes compatible with broadly available modal analysis algorithms. Existing curve-fit software can be used to estimate system poles, residues and electromechanical coupling matrix [208].

2.5 Techniques to Control Structural Vibrations

Applying suitable modeling techniques as discussed in section 2.4, final equation of the motion of 'smart piezo structure' is obtained as:

$$[M]\{\ddot{x}\}+[C]\{\dot{x}\}+[K]\{x\}=\{F\} \tag{2.93}$$

Equation (2.93) presents a coupled system of equations. Analysis of such a system would become easier if these coupled equations are converted into uncoupled equations. In that case, single degree of freedom system tools can be used to analyze the actual multi degree of freedom system. The process of analyzing multi degree of freedom system using single degree of freedom system tools is known as 'modal analysis'. Using transformation (2.1), coupled equations of motion are converted into uncoupled ones. Uncoupled equations of motion are used to control the desired vibration modes using appropriate control law. In order to control the response of a system using modern control theories, we need to convert uncoupled equations of motion into a state-space model (2.22). To implement control laws, modal vectors are required which cannot be measured by a single sensor patch. However, modal vectors can be estimated using an observer/estimator. A computer program which estimates/observes state vector is called a state estimator/observer. It is constructed using matrices $[A]$, $[B]$ and $[C]$ of the 'state space model' [141]. Kalman [197] and Luenberger [209] observers can be used.

Once we have obtained: (i) the equation of motion (ii) matrices $[A]$, $[B]$, $[C]$ and (iii) modal vectors of 'smart piezo structure', we can control its vibration response using a suitable control technique. Depending upon the nature of 'smart piezo structure', many control techniques have been used by researchers in AVC viz. Independent Modal Space Control [210-211], Modified Independent Modal Space Control [18], Efficient Modal Control [212], Negative Velocity Feedback Control [213-214] , Output Feedback [215], Optimal Control [60, 159, 216], Positive Position Feedback Control [217], Pole Placement Technique [218-219], Lyapunov Functional Control [174, 220], LMS algorithm [221], Sliding Mode Control [222-223], Neural Networks [224-225], Fuzzy Logic Control [37], μ-synthesis Control [226], H_2/ H_∞ Control [227-228] etc. Out of these control techniques, optimal control has been chiefly used in AVC. It provides a simple and powerful tool for designing multivariable systems and controls several modes of the structure. It requires sufficiently accurate model of the system and an observer to estimate the states of the system. Robust and adaptive controllers like fuzzy logic, neural networks, sliding mode, H_∞ etc. are used to control the structural vibrations of smart piezo complex structures where accurate mathematical models are difficult to obtain.

2.6 Software to Implement Active Vibration Control Scheme

To implement the state-of-the-art discussed in previous sections, researcher and engineers need appropriate software to carry out simulations and experiments. Simulation analysis of a mathematical model derived using appropriate modeling technique and control law can be carried out by writing computer code in MATLAB [216], MATHEMATICA [175], VAPAS [229], DYNADID2D [209] etc. Commercial finite element packages such as ANSYS/Multiphysics [70, 230-233], ABAQUS [189-190] ,

MSC/NASTRAN [234] , COSAR [235] etc. are also available to model 'smart piezo structure'. Control action simulations can be carried out in ANSYS [231-232], MATLAB/Simulink [159], MATLAB/Control System Toolbox [236], SCILAB [209, 237] etc. To implement AVC control algorithm experimentally, LabVIEW [197, 216, 232] can be used.

2.7 Inferences from the Literature Review

In sections 2.1 to 2.6, broad literature review on all the aspects of active vibration control of smart structures using piezoelectric sensors and actuators has been presented. This literature review narrates how the field has progressed and from this the research directions in this field can be identified. Following inferences are made from this literature survey:

1. Uptil now, active vibration control has been applied on very simple smart piezo structures.

2. Smart piezo structures would be ultimately used in real life environment where thermal, hygro and other non-linear effects are present. Piezoelectric materials are highly sensitive to these effects. Electromechanical interaction of piezoelectric sensors and actuators in real life environment has not been effectively incorporated in active vibration control schemes. Mathematical models robust to these effects are almost absent in the literature. Moreover, experimental implementation of active vibration control schemes under the influence of these real life environmental effects is very less in the literature.

3. Placement of piezoelectric sensors and actuators on a 'smart structure' should be decided by optimizing a criterion depending upon the shape, size and boundary conditions of 'smart structure' and the end application. Optimal placement of sensors can

be found by maximizing the degree of observability. Optimal placement of actuators can be found either by maximizing modal forces/moments applied by piezoelectric actuators or by maximizing deflection of the host structure or by minimizing control effort/maximizing energy dissipated or by maximizing the degree of controllability. Optimal placement of both sensors and actuators can be found by minimizing the spillover effects. Optimal locations strongly depend upon boundary conditions therefore the boundary conditions must be properly understood. Optimal locations of piezoelectric sensors and actuators can be found by either selecting a single criterion or a combination of more than one criterion. Most of the work is targeted on simple beam and plate structures. Studies on optimal piezoelectric sensor and actuator placement on real life complex structures is absent in the literature.

4. Most of the research in smart piezo structures is concentrated on mathematical modeling of these structures. Finite element modeling technique has been the favourite among all to find the equations of motion. However, most of the techniques to mathematically model a 'smart piezo structure' are suitable only for simple structures and not for complex real life structures. It is difficult to practically extend these techniques to model real life structures where lots of complexities including unforeseen boundary conditions are present. Very less work is available on online system identification of smart structures.

5. Piezoelectric coefficients and permittivity change with change in temperature. This **fact** has been ignored by all the works on active vibration control of smart piezo structures.

It is obvious from this literature review that research in smart piezo structures should be directed in such a way so that active vibration control technique serves the mankind in coming years.

2.8 Scope of the Present Work

Present work is an attempt to extend active vibration control technique to real life environment, at least in part. Real life structures have to work under actual environmental conditions where temperature, hygro and other non-linear effects keep on changing. Among these, temperature effect is the most prominent in environment which affects the performance of a 'smart piezo structure' significantly. So far, researchers have studied the effects of temperature variations to induce structural vibrations in smart piezo structures. Change in piezoelectric properties with temperature has been ignored. As discussed in sub-section 2.2.1, piezoelectric strain and permittivity coefficients are temperature sensitive. Sensing and actuation behaviour of piezoelectric materials depend upon these coefficients. However, temperature dependence of piezoelectric strain and permittivity coefficients has not been incorporated in active vibration control design so far. This may be due to the fact that there are no reliable analytical relationships in the literature for temperature dependence of piezoelectric strain and permittivity coefficients. If temperature dependence of piezoelectric strain and permittivity coefficients is not included in piezoelectric constitutive equations then: (i) vibration response of the 'smart structure' would be wrongly estimated by sensor (ii) actuator response would also be wrongly estimated (iii) controller would apply wrong control voltages on actuator and (iv) performance of AVC would not be maintained and it can even fail if ambient temperatures are substantially away from 'reference temperature'. Such temperature

variations would be frequently encountered in real life situations where AVC is to be used in near future. Existing schemes will not maintain active vibration control performance if 'ambient temperature' is other than 'reference temperature' of the piezoelectric material. These schemes are doomed to fail at ambient temperatures significantly different than 'reference temperature'. Therefore, to fill this gap in the literature, present work proposes a new active vibration control scheme for smart piezo structures which is robust to temperature variations. Proposed scheme has been made robust to temperature variations by incorporating temperature variations of piezoelectric strain and permittivity coefficients into existing active vibration control design. The scheme has been analytically derived and experimentally verified for a smart piezo plate structure.

2.9 Research Plan and Thesis Organization

In the present work, PZT-5H piezoceramic patches have been used as sensors and actuators for active vibration control of a smart plate. Temperature dependence of 'd_{31}' and '$\in_{33}$' coefficients is included in piezoelectric constitutive equations from the experimental characterization of PZT-5H [78]. Curve fit technique is used to include the temperature variation of 'd_{31}' and '$\in_{33}$' in these augmented constitutive equations. d-form augmented piezoelectric constitutive equations are converted into e-form. Using e-form constitutive equations, a finite element model of smart two dimensional plate instrumented with piezoelectric patches is derived. Coupled equations of motion are uncoupled using modal analysis. Equations of motion are written in state space form. Modal vectors are estimated using Kalman observer. First mode of smart cantilevered plate is actively controlled using negative first modal velocity feedback law at various

ambient temperatures. Simulation results are presented using MATLAB software. Active vibration control is shown robust to temperature variations. Finally, proposed AVC scheme is experimentally verified. Execution of the research plan has been systematically reported in the present thesis. A brief summary of the thesis is as under:

Chapter I begins with an introduction to the world of smart structures. Their uses and the role of piezoelectric sensors and actuators in smart piezo structures is discussed. Basic introduction to piezoelectricity is followed by an introduction to the active vibration control 'state-of-the-art'. In **Chapter II,** broad literature review of active vibration control 'state-of-the-art' using piezoelectric sensors and actuators is presented. Scope of the present work and the research plan is also discussed. In **Chapter III,** mathematical model of a plate structure instrumented with piezoelectric sensor and actuator patches is derived using finite element method and Hamilton's principle. Equations of motion are written in state space form. Mathematical model is validated in **Chapter IV** using a computer program written in MATLAB. A negative velocity feedback control law which takes into account temperature dependence of piezoelectric stress coefficients 'e_{31}' and permittivity '$\in_{33}$' is derived for first modal active vibration control of cantilevered smart piezo plate. Robustness of the proposed control law with respect to temperature variations is proved using simulation results. **Chapter V** is dedicated to experimental work. Real time first modal active vibration control of cantilevered smart plate instrumented with a collocated sensor-actuator pair is achieved at elevated temperatures successfully. It is observed that existing control law fails to maintain the active vibration control performance at elevated temperatures. However, experimental results show that the new scheme proposed in present research work has

better active vibration control performance at elevated temperatures. **Chapter VI** summarizes the conclusions of the present work and gives important directions for future work in the field of active vibration control of smart piezo structures.

2.10 Contribution of Present Thesis

Piezoelectric materials are ultimate choice as sensors and actuators in smart structures. But performance of piezoelectric materials is sensitive to temperature. So far, researchers have ignored the influence of temperature on piezoelectric coefficients and permittivity. Present thesis fills this gap in the literature. In this thesis, a new scheme for active vibration control of a 'smart piezo structure' at ambient temperatures other than the 'reference temperature' of piezoelectric material is proposed. The proposed scheme includes the temperature dependence of piezoelectric strain/stress coefficients and the permittivity. The beauty of the present work is that the whole new scheme is analytically derived and experimentally verified. Excellent experimental results have been obtained. This contribution can help active vibration control and the 'smart piezo structure' technology to work in real life environment.

CHAPTER III

MATHEMATICAL MODELING OF SMART PIEZO PLATE

In the making of a ‘smart structure’, mathematical modeling is an important phase. Performance of a ‘smart structure’ depends upon the accuracy of its mathematical model. Physical phenomena happening inside and outside the ‘smart structure’ is properly understood and incorporated in the mathematical model. Also, boundary conditions of the ‘smart structure’ are to be properly understood and considered in the mathematical model. In the present work, a cantilevered plate structure instrumented with piezoelectric sensors and actuators is considered. Finite element method is used to model the smart piezo plate structure. Equation of motion is found using Hamilton’s principle. Equation of motion so obtained, consists of several modes of vibration. However, only first few modes have significant contribution to the structural vibrations. Therefore, the coupled equation of motion consisting of several modes of vibration is decoupled using ‘modal analysis’. Modal equations corresponding to the modes of interest are retained and remaining modal equations are truncated. Modal equations so retained are written in state space form. This form of mathematical model is used to control the response of ‘smart piezo structure’ using an appropriate digital control law. In the following sections, equations of motion of a cantilevered smart piezo plate structure are obtained in state space form using finite element method, Hamilton’s principle and ‘modal analysis’.

3.1 Finite Element Model

Finite element method (FEM) is a numerical technique for finding approximate solutions of partial differential as well as of integral equations. Therefore, it is well suited

for finding the equations of motion of simple and complex structures. When applied practically, this technique is known as finite element analysis (FEA). In this technique, the structure is divided into identical finite elements forming a grid called mesh having a well defined system of points called nodes. Nodes are assigned to certain locations of the finite element depending upon anticipated stress levels and have fixed degrees of freedom. Shape of the finite element is carefully designed in accordance with the shape of the main structure. The finite element mesh contains all the material and structural properties. The structural problem is thus reduced into one finite element and interpolated in terms of the nodes of finite element. Equation of motion of one finite element is found using Hamilton's principle. Equation of motion of the entire structure is found by assembling all the finite elements of the structure. Boundary conditions of the structure need to be considered very carefully. This technique is suited for structural and vibrational analysis of a structure against random vibrations, shock and impact.

Before finding the equations of motion of a 'smart piezo structure', we have to choose appropriate piezoelectric constitutive equations. In following sub-sections, suitable piezoelectric constitutive equations are suggested. Available *d*-form piezoelectric constitutive equations are converted into *e*-form and finally, coupled equations of motion are derived using finite element technique.

3.1.1 *Piezoelectric Constitutive Equations*

As discussed in sub-section 2.2.1, constitutive equations being used to model 'smart piezo structure' working at ambient temperatures other than 'reference temperature' address thermal strain and pyroelectric effects only. In these constitutive equations, the changes in elastic, piezoelectric and dielectric properties of 'smart piezo structure' with

temperature are ignored. Piezoelectric stress (e_{31}, e_{33}, e_{15}) and permittivity $(\in_{33})$ coefficients are measured at 'reference temperature' only and are assumed not to vary away from 'reference temperature'. In other words, piezoelectric strain/stress coefficients and permittivity are assumed constant at all temperatures. However, experimental characterization of piezoceramic PZT-5H (as shown in Figure 3.1) reveals that: (i) magnitude of piezoelectric strain coefficient (d_{31}) increases linearly with temperature and (ii) permittivity $(\in_{33})$ increases non-linearly with temperature [78]. Constitutive equations which treat piezoelectric strain/stress and permittivity coefficients independent of temperature can not capture the smart structural dynamics accurately at ambient temperatures. Therefore, temperature dependence of piezoelectric strain/stress and permittivity coefficients should be used in piezoelectric constitutive equations. Accurate analytical relationships giving temperature dependence of these coefficients are not available. However, temperature dependence of these coefficients can be found using experimental characterization of piezoceramic material being used as transducer. Using experimental values of 'd_{31}' and '$\in_{33}$' coefficients at different ambient temperatures, augmented constitutive equations are [78]:

$$\varepsilon_{ij} = s_{ijkl}^{E,T}\sigma_{kl} + d_{nij}^{T}E_n + \bar{d}_{nij}E_n\Delta T + \alpha_{ij}^{E}\Delta T \tag{3.1}$$

$$D_n = d_{nij}^{T}\sigma_{ij} + \bar{d}_{nij}\sigma_{ij}\Delta T + \in_{nm}^{\sigma,T} E_m + \bar{\in}_{nm}E_m\Delta T + p_n^{\sigma}\Delta T \tag{3.2}$$

Augmented constitutive equations (2.5) and (2.6) are in *d*-form. We have to convert these *d*-form constitutive equations into *e*-form. Since $\sigma_{ij} = c_{ijkl}\varepsilon_{kl}$ and $d_{nij}c_{ijkl} = e_{nkl}$ [6], equation (2.6) can be written as:

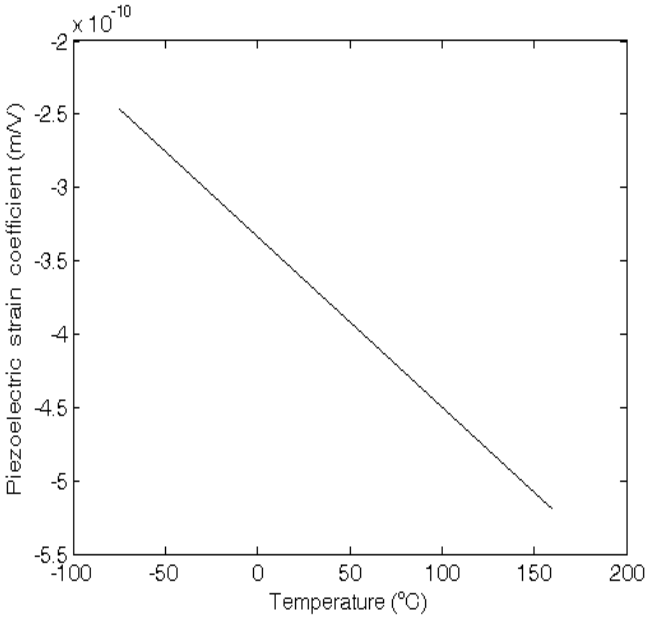

Figure 3.1a: Temperature dependence of strain coefficient (d_{31}) of piezoceramic PZT-5H

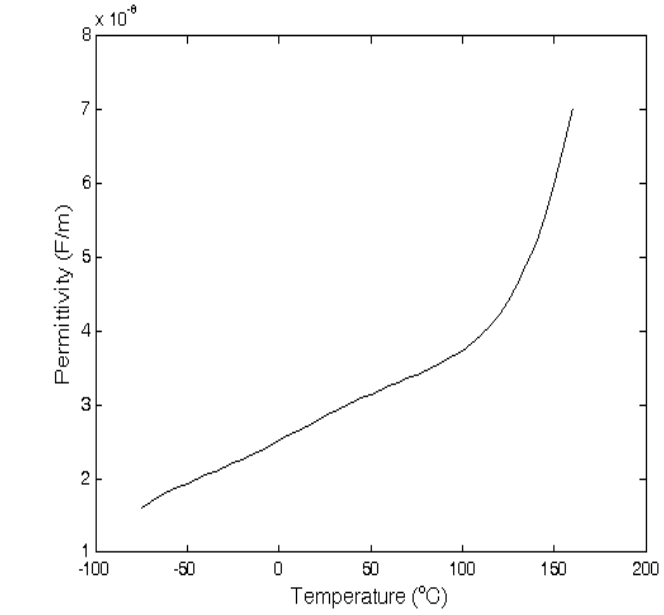

Figure 3.1b: Temperature dependence of permittivity $(\in_{33})$ of piezoceramic PZT-5H

$$D_n = \left(d_{nij}^T + \bar{d}_{nij}\Delta T\right)c_{ijkl}\varepsilon_{kl} + \left(\in_{nm}^{\sigma,T} + \bar{\in}_{nm}\Delta T\right)E_m + p_n^{\sigma}\Delta T$$
$$= \left(d_{nij}^T c_{ijkl} + \bar{d}_{nij}c_{ijkl}\Delta T\right)\varepsilon_{kl} + \left(\in_{nm}^{\sigma,T} + \bar{\in}_{nm}\Delta T\right)E_m + p_n^{\sigma}\Delta T$$
$$= \left(e_{nkl}^T + \bar{e}_{nkl}\Delta T\right)\varepsilon_{kl} + \left(\in_{nm}^{\sigma,T} + \bar{\in}_{nm}\Delta T\right)E_m + p_n^{\sigma}\Delta T$$

where 'n' and 'm' vary from 1 to 3. 'ij' and 'kl' vary from 1 to 6. Writing 'μ' in place of 'kl':

$$D_n = \left(e_{n\mu}^T + \bar{e}_{n\mu}\Delta T\right)\varepsilon_{\mu} + \left(\in_{nm}^{\sigma,T} + \bar{\in}_{nm}\Delta T\right)E_m + p_n^{\sigma}\Delta T$$
$$= e_{n\mu}^T\varepsilon_{\mu} + \bar{e}_{n\mu}\varepsilon_{\mu}\Delta T + \in_{nm}^{\sigma,T} E_m + \bar{\in}_{nm}E_m\Delta T + p_n^{\sigma}\Delta T$$

Expanding above equation in terms of its elements and on dropping the superscripts for convenience we get:

$$D_1 = \left(e_{11}\varepsilon_1 + e_{12}\varepsilon_2 + ... + e_{16}\varepsilon_6\right) + \left(\overline{e_{11}}\varepsilon_1 + \overline{e_{12}}\varepsilon_2 + ... + \overline{e_{16}}\varepsilon_6\right)\Delta T$$
$$+ \left(\in_{11} E_1 + \in_{12} E_2 + \in_{13} E_3\right) + \left(\overline{\in_{11}}E_1 + \overline{\in_{12}}E_2 + \overline{\in_{13}}E_3\right)\Delta T + p_1\Delta T$$

$$D_2 = \left(e_{21}\varepsilon_1 + e_{22}\varepsilon_2 + ... + e_{26}\varepsilon_6\right) + \left(\overline{e_{21}}\varepsilon_1 + \overline{e_{22}}\varepsilon_2 + ... + \overline{e_{26}}\varepsilon_6\right)\Delta T$$
$$+ \left(\in_{21} E_1 + \in_{22} E_2 + \in_{23} E_3\right) + \left(\overline{\in_{21}}E_1 + \overline{\in_{22}}E_2 + \overline{\in_{23}}E_3\right)\Delta T + p_2\Delta T$$

$$D_3 = \left(e_{31}\varepsilon_1 + e_{32}\varepsilon_2 + ... + e_{36}\varepsilon_6\right) + \left(\overline{e_{31}}\varepsilon_1 + \overline{e_{32}}\varepsilon_2 + ... + \overline{e_{36}}\varepsilon_6\right)\Delta T$$
$$+ \left(\in_{31} E_1 + \in_{32} E_2 + \in_{33} E_3\right) + \left(\overline{\in_{31}}E_1 + \overline{\in_{32}}E_2 + \overline{\in_{33}}E_3\right)\Delta T + p_3\Delta T$$

In matrix form, these equations are written as:

$$\begin{Bmatrix} D_1 \\ D_2 \\ D_3 \end{Bmatrix} = \begin{bmatrix} e_{11} & e_{12} & e_{13} & e_{14} & e_{15} & e_{16} \\ e_{21} & e_{22} & e_{23} & e_{24} & e_{25} & e_{26} \\ e_{31} & e_{32} & e_{33} & e_{34} & e_{35} & e_{36} \end{bmatrix} \begin{Bmatrix} \varepsilon_1 & \varepsilon_2 & \varepsilon_3 & \varepsilon_4 & \varepsilon_5 & \varepsilon_6 \end{Bmatrix}^T$$
$$+ \begin{bmatrix} \overline{e_{11}} & \overline{e_{12}} & \overline{e_{13}} & \overline{e_{14}} & \overline{e_{15}} & \overline{e_{16}} \\ \overline{e_{21}} & \overline{e_{22}} & \overline{e_{23}} & \overline{e_{24}} & \overline{e_{25}} & \overline{e_{26}} \\ \overline{e_{31}} & \overline{e_{32}} & \overline{e_{33}} & \overline{e_{34}} & \overline{e_{35}} & \overline{e_{36}} \end{bmatrix} \begin{Bmatrix} \varepsilon_1 & \varepsilon_2 & \varepsilon_3 & \varepsilon_4 & \varepsilon_5 & \varepsilon_6 \end{Bmatrix}^T \Delta T$$

$$+\begin{bmatrix} \in_{11} & \in_{12} & \in_{13} \\ \in_{21} & \in_{22} & \in_{23} \\ \in_{31} & \in_{32} & \in_{33} \end{bmatrix}\begin{Bmatrix} E_1 \\ E_1 \\ E_1 \end{Bmatrix}+\begin{bmatrix} \overline{\in_{11}} & \overline{\in_{12}} & \overline{\in_{13}} \\ \overline{\in_{21}} & \overline{\in_{22}} & \overline{\in_{23}} \\ \overline{\in_{31}} & \overline{\in_{32}} & \overline{\in_{33}} \end{bmatrix}\begin{Bmatrix} E_1 \\ E_1 \\ E_1 \end{Bmatrix}\Delta T+\begin{Bmatrix} p_1 \\ p_2 \\ p_3 \end{Bmatrix}\Delta T$$

This equation can be represented as:

$$\begin{aligned}\{D\}_{3x1} &= \left(\left[e^T\right]_{3x6}+\left[\bar{e}\right]_{3x6}\Delta T\right)\{\varepsilon\}_{6x1} \\ &+\left(\left[\in^T\right]_{3x3}+\left[\bar{\in}\right]_{3x3}\Delta T\right)\{E\}_{3x1}+\left\{p^\sigma\right\}_{3x1}\Delta T\end{aligned} \tag{3.3}$$

This is the *e*-form of augmented constitutive equation (2.6). After rearranging the terms, equation (2.5) can be written as:

$$s_{ijkl}^{E,T}\sigma_{kl}=\varepsilon_{ij}-\left(d_{nij}^T+\bar{d}_{nij}\Delta T\right)E_n-\alpha_{ij}^E\Delta T$$

$$\sigma_{kl}=\left(s_{ijkl}^{E,T}\right)^{-1}\varepsilon_{ij}-\left(s_{ijkl}^{E,T}\right)^{-1}\left(d_{nij}^T+\bar{d}_{nij}\Delta T\right)E_n-\left(s_{ijkl}^{E,T}\right)^{-1}\alpha_{ij}^E\Delta T$$

where 'n' varies from 1 to 3 and 'ij' & 'kl' vary from 1 to 6. Substituting $\left(s_{ijkl}^{E,T}\right)^{-1}=c_{ijkl}$ [6] in the above equation we get:

$$\begin{aligned}\sigma_{kl} &= c_{ijkl}\varepsilon_{ij}-c_{ijkl}\left(d_{nij}^T+\bar{d}_{nij}\Delta T\right)E_n-c_{ijkl}\alpha_{ij}^E\Delta T \\ &= c_{ijkl}\varepsilon_{ij}-\left(d_{nij}^T c_{ijkl}+\bar{d}_{nij}c_{ijkl}\Delta T\right)E_n-c_{ijkl}\alpha_{ij}^E\Delta T \\ &= c_{ijkl}\varepsilon_{ij}-\left(e_{nkl}^T+\bar{e}_{nkl}\Delta T\right)E_n-c_{ijkl}\alpha_{ij}^E\Delta T\end{aligned}$$

On writing 'λ' in place of 'ij' and 'μ' in place of 'kl':

$$\sigma_\mu=c_{\lambda\mu}\varepsilon_\lambda-\left(e_{n\mu}^T+\bar{e}_{n\mu}\Delta T\right)E_n-c_{\lambda\mu}\alpha_\lambda^E\Delta T$$

Expanding above equation in terms of its elements and dropping the superscripts for convenience, we get:

$$\begin{aligned}\sigma_1 &= \left(c_{11}\varepsilon_1+c_{21}\varepsilon_2+.....+c_{61}\varepsilon_6\right)-\left(e_{11}E_1+e_{21}E_2+e_{31}E_3\right) \\ &-\left(\overline{e_{11}}E_1+\overline{e_{21}}E_2+\overline{e_{31}}E_3\right)\Delta T-(c_{11}\alpha_1+c_{21}\alpha_2.....+c_{61}\alpha_6)\Delta T\end{aligned}$$

$$\sigma_2 = \left(c_{12}\varepsilon_1 + c_{22}\varepsilon_2 + ... + c_{62}\varepsilon_6\right) - \left(e_{12}E_1 + e_{22}E_2 + e_{32}E_3\right)$$
$$-\left(\overline{e_{12}}E_1 + \overline{e_{22}}E_2 + \overline{e_{32}}E_3\right)\Delta T - (c_{12}\alpha_1 + c_{22}\alpha_2 ..... + c_{62}\alpha_6)\Delta T$$

……..

$$\sigma_6 = \left(c_{16}\varepsilon_1 + c_{26}\varepsilon_2 + ... + c_{66}\varepsilon_6\right) - \left(e_{16}E_1 + e_{26}E_2 + e_{36}E_3\right)$$
$$-\left(\overline{e_{16}}E_1 + \overline{e_{26}}E_2 + \overline{e_{36}}E_3\right)\Delta T - (c_{16}\alpha_1 + c_{26}\alpha_2 ..... + c_{66}\alpha_6)\Delta T$$

In matrix form, above equations become:

$$\begin{Bmatrix}\sigma_1\\ \sigma_2\\ \sigma_3\\ \sigma_4\\ \sigma_5\\ \sigma_6\end{Bmatrix} = \begin{bmatrix} c_{11} & c_{21} & c_{31} & c_{41} & c_{51} & c_{61}\\ c_{12} & c_{22} & c_{32} & c_{42} & c_{52} & c_{62}\\ c_{13} & c_{23} & c_{33} & c_{43} & c_{53} & c_{63}\\ c_{14} & c_{24} & c_{34} & c_{44} & c_{54} & c_{64}\\ c_{15} & c_{25} & c_{35} & c_{45} & c_{55} & c_{65}\\ c_{16} & c_{26} & c_{36} & c_{46} & c_{56} & c_{66}\end{bmatrix}\begin{Bmatrix}\varepsilon_1\\ \varepsilon_2\\ \varepsilon_3\\ \varepsilon_4\\ \varepsilon_5\\ \varepsilon_6\end{Bmatrix} - \begin{bmatrix} e_{11} & e_{21} & e_{31}\\ e_{12} & e_{22} & e_{32}\\ e_{13} & e_{23} & e_{33}\\ e_{14} & e_{24} & e_{34}\\ e_{15} & e_{25} & e_{35}\\ e_{16} & e_{26} & e_{36}\end{bmatrix}\begin{Bmatrix}E_1\\ E_2\\ E_3\end{Bmatrix}$$
$$-\begin{bmatrix} \overline{e_{11}} & \overline{e_{21}} & \overline{e_{31}}\\ \overline{e_{12}} & \overline{e_{22}} & \overline{e_{32}}\\ \overline{e_{13}} & \overline{e_{23}} & \overline{e_{33}}\\ \overline{e_{14}} & \overline{e_{24}} & \overline{e_{34}}\\ \overline{e_{15}} & \overline{e_{25}} & \overline{e_{35}}\\ \overline{e_{16}} & \overline{e_{26}} & \overline{e_{36}}\end{bmatrix}\begin{Bmatrix}E_1\\ E_2\\ E_3\end{Bmatrix}\Delta T - \begin{bmatrix} c_{11} & c_{21} & c_{31} & c_{41} & c_{51} & c_{61}\\ c_{12} & c_{22} & c_{32} & c_{42} & c_{52} & c_{62}\\ c_{13} & c_{23} & c_{33} & c_{43} & c_{53} & c_{63}\\ c_{14} & c_{24} & c_{34} & c_{44} & c_{54} & c_{64}\\ c_{15} & c_{25} & c_{35} & c_{45} & c_{55} & c_{65}\\ c_{16} & c_{26} & c_{36} & c_{46} & c_{56} & c_{66}\end{bmatrix}\begin{Bmatrix}\alpha_1\\ \alpha_2\\ \alpha_3\\ \alpha_4\\ \alpha_5\\ \alpha_6\end{Bmatrix}\Delta T$$

This equation can be represented as:

$$\{\sigma\}_{6x1} = [c]_{6x6}\left(\{\varepsilon\}_{6x1} - \{\alpha^E\}_{6x1}\Delta T\right) - \left(\left[e^T\right]_{6x3}^T + \left[\bar{e}\right]_{6x3}^T \Delta T\right)\{E\}_{3x1} \qquad (3.4)$$

This is the *e*-form of augmented constitutive equation (2.5). Now, *e*-form augmented constitutive equations are:

$$\{D\} = \left(\left[e^T\right] + \left[\bar{e}\right]\Delta T\right)\{\varepsilon\} + \left(\left[\in^T\right] + \left[\bar{\in}\right]\Delta T\right)\{E\} + \{p^\sigma\}\Delta T \qquad (3.3)$$

$$\{\sigma\} = [c]\left(\{\varepsilon\} - \{\alpha^E\}\Delta T\right) - \left(\left[e^T\right]^T + \left[\bar{e}\right]^T \Delta T\right)\{E\} \tag{3.4}$$

where $\left[e^T\right]$ and $\left[\in^T\right]$ are the matrices of piezoelectric stress and permittivity coefficients respectively at 'reference temperature'. $\left[\bar{e}\right]$ and $\left[\bar{\in}\right]$ matrices represent change per unit temperature in piezoelectric stress and permittivity coefficients respectively. These two equations represent direct and inverse piezoelectric effects respectively. From equations (3.3) and (3.4), it can be observed when 'ambient temperature' is other than 'reference temperature', e_{31} and $\in_{33}$ coefficients are:

$$\begin{aligned} e_{31} &= e_{31}^T + \overline{e_{31}}\Delta T \\ \in_{33} &= \in_{33}^T + \overline{\in_{33}}\Delta T \end{aligned} \tag{3.5}$$

where e_{31}^T and $\in_{33}^T$ are 'piezoelectric stress coefficient' and 'permittivity' respectively at 'reference temperature' of 25°C. At 'reference temperature', ΔT=0 and

$$\begin{aligned} e_{31} &= e_{31}^T \\ \in_{33} &= \in_{33}^T \end{aligned} \tag{3.6}$$

e_{31} Coefficients are calculated from d_{31} coefficients using the relation [6]:

$$[e] = [d][c] \tag{3.7}$$

For piezoceramic PZT-5H sensor and actuator, e_{31} and $\in_{33}$ coefficients are obtained from experimental data [78] at ambient temperatures ranging from -75°C to 160°C. Low voltages are generated across sensor as compared to actuators where high voltages are applied to control the response of 'smart piezo structure'. Therefore, e_{31} coefficients given in Table 3.1 for PZT-5H actuator are measured at large electric field. These are 1.5 times greater than those of PZT-5H sensor which are measured at low electric field [78].

Ambient Temperature $(^{\circ}C)$	**Piezoelectric strain coefficient** (d_{31}) (m/V)	**Permittivity** $(\in_{33})$ (F/m)
–75	-2.47×10^{-10}	1.6×10^{-8}
–25	-3.05×10^{-10}	2.21×10^{-8}
25	-3.63×10^{-10}	2.84×10^{-8}
75	-4.21×10^{-10}	3.41×10^{-8}
100	-4.50×10^{-10}	3.74×10^{-8}
120	-4.73×10^{-10}	4.23×10^{-8}
130	-4.85×10^{-10}	4.63×10^{-8}
140	-4.96×10^{-10}	5.19×10^{-8}
150	-5.08×10^{-10}	5.97×10^{-8}
160	-5.20×10^{-10}	7.03×10^{-8}

Table 3.1: **Experimental values of strain coefficient (d_{31}) and permittivity $(\in_{33})$ for piezoceramic PZT-5H actuator at different ambient temperatures**

Actual values of e_{31} and $\in_{33}$ coefficients at ambient temperatures away from reference temperature are included in augmented constitutive equations (3.3) and (3.4) using curve fit method. Following curve fits are obtained for e_{31} and $\in_{33}$:

$$e_{31} = e_{31}^{T} - 0.1044\Delta T \tag{3.8}$$

$$\in_{33} = \in_{33}^{T} + 14.63\Delta T - 0.0252\Delta T^{2} - (5.92\times10^{-4})\Delta T^{3} + (4.35\times10^{-6})\Delta T^{4} + (7.19\times10^{-8})\Delta T^{5} \tag{3.9}$$

Clearly, e_{31} varies linearly with temperature whereas variation of $\in_{33}$ with temperature is of fifth order.

3.1.2 *Finite Element Analysis of Smart Piezo Plate Structure*

Now, we derive finite element model of a cantilevered smart piezo plate using 4-noded plane finite elements and Kirchoff's classical plate theory. Consider a flexible elastic isotropic plate structure (Figure 3.2a). A piezoelectric sensor-actuator pair polarized in thickness direction is bonded at opposite faces to the plate. The top and bottom surface of each piezoelectric is covered by electrodes. At the piezo location, structure is composite in thickness direction with two piezoelectric and one elastic isotropic layer. The plate structure is divided into discrete finite elements (Figure 3.2c). The geometry of one finite element is shown in Figure 3.3. 'ζ' & 'η' are the natural coordinates of finite element and they are related to global coordinates (x, y) as:

$$\zeta = \frac{x}{a} \text{ and } \eta = \frac{y}{b} \tag{3.10}$$

Each finite element has 4-nodes and each node has three degrees of freedom: one translational (w) and two rotational (θ_x and θ_y). If $\{u_e\}$ is the displacement vector of an element then displacement in z-direction can be interpolated as:

$$w = [N]_{1x12} \{u_e\}_{12\times 1} \tag{3.11}$$

where $[N]_{1x12}$ is Hermite's interpolation function [173]. Ignoring shear deformations in the plate and using Kirchhoff's classical plate theory [238], the strains developing in the plate can be written as:

$$\{\varepsilon\} = \begin{Bmatrix} \partial u / \partial x \\ \partial v'' / \partial y \\ \partial v'' / \partial x + \partial u / \partial y \end{Bmatrix}$$

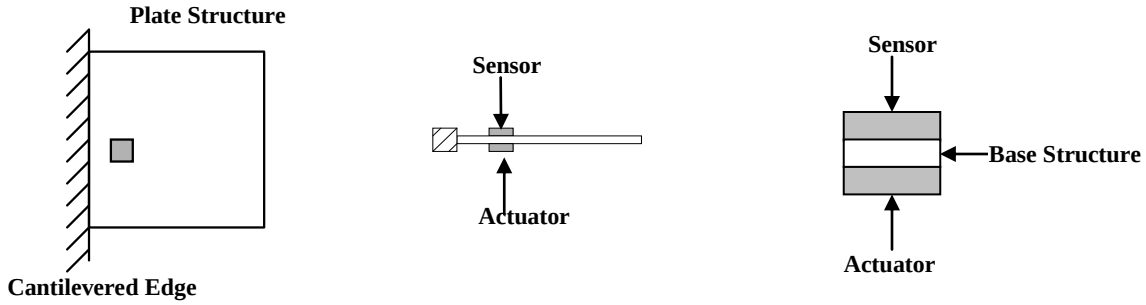

(a) Top View **(b) Side View** **(c) Plate Finite Element**

Figure 3.2: Top and side views of cantilevered plate instrumented with one collocated piezoelectric sensor-actuator pair (Figure (a) and Figure (b)) and, plate finite element (Figure (c))

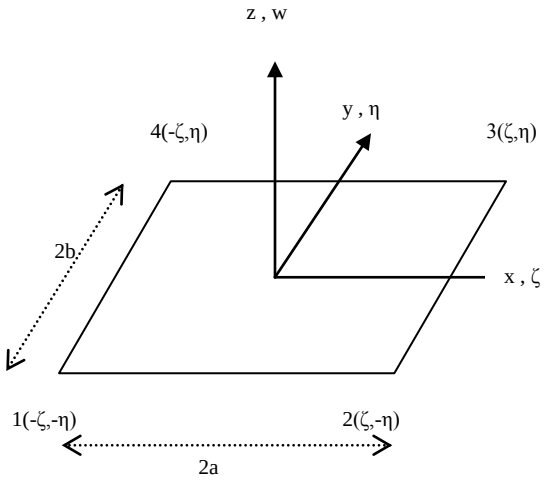

Figure 3.3: **Geometry of a 2-D rectangular thin finite element**

where $u = -z\dfrac{\partial w}{\partial x}$ and $v'' = -z\dfrac{\partial w}{\partial y}$. On substituting values of u and v'' we get:

$$\{\varepsilon\} = \begin{Bmatrix} -z\,\partial^2/\partial x^2 \\ -z\,\partial^2/\partial y^2 \\ -2z\,\partial^2/\partial x\partial y \end{Bmatrix} w = z \begin{Bmatrix} -z\,\partial^2/\partial x^2 \\ -z\,\partial^2/\partial y^2 \\ -2z\,\partial^2/\partial x\partial y \end{Bmatrix}_{3x1} \quad [N]_{1x12}\{u_e\}_{12x1}$$

If we take $[B_u]_{3x12} = \begin{Bmatrix} -z\,\partial^2/\partial x^2 \\ -z\,\partial^2/\partial y^2 \\ -2z\,\partial^2/\partial x\partial y \end{Bmatrix}_{3x1} [N]_{1x12}$, we have:

$$\{\varepsilon\}_{3x1} = z[B_u]_{3x12}\{u_e\}_{12x1} \tag{3.12}$$

Piezoceramic PZT-5H being used as sensor and actuator is polarized in +ve z-direction. Also, electric field vector is the divergence of potential difference. Therefore:

$$\{E\}_{3x1} = -\{\nabla\}_{3x1} v = -\begin{Bmatrix} 0 \\ 0 \\ 1/d \end{Bmatrix} v = -\{B_v\} v \quad \text{where,} \quad \{B_v\}_{3x1} = \begin{Bmatrix} 0 \\ 0 \\ 1/d \end{Bmatrix}_{3x1} . \tag{3.13}$$

where 'v' is the voltage across piezoelectric patch of thickness 'd'. If ρ is the density, A is the area, f^e is external force and q is the charge on a finite element then:

Kinetic energy of one finite element:

$$T_e = \frac{1}{2}\int_S \rho_s \dot{w}^2 d\tau + \frac{1}{2}\int_P \rho_P \dot{w}^2 d\tau \tag{3.14}$$

Potential energy of one finite element:

$$V_e = \frac{1}{2}\int_S \{\varepsilon\}^T \{\sigma\} d\tau + \frac{1}{2}\int_P \{\varepsilon\}^T \{\sigma\} d\tau \tag{3.15}$$

Electric energy stored in one finite element:

$$W_{elect} = \frac{1}{2}\int_P \{E\}^T \{D\} d\tau \tag{3.16}$$

External surface traction or point force can act on a 'smart structure'. These forces would do work on the 'smart structure' and as a result energy stored per element is:

$$W_{ext(I)} = \int_{A_S} \{w\}^T \left\{ f_S^e \right\} dA_S \tag{3.17}$$

Work required to apply external charge on the surface of a piezoelectric is:

$$W_{ext(II)} = -\int_{A_P} qvdA_P \tag{3.18}$$

Now, Lagrangian for one finite element of 'smart structure' can be obtained as:

$$L = T_e - V_e + (W_{elect} + W_{ext(I)} + W_{ext(II)}) \tag{3.19}$$

On substituting the values of T_e , V_e , W_{elect}, $W_{ext(I)}$ and $W_{ext(II)}$ from finite element relations (3.14)-(3.18)), the Lagrangian becomes:

$$L = \left(\frac{1}{2}\int_S \rho_s \dot{w}^2 d\tau + \frac{1}{2}\int_P \rho_P \dot{w}^2 d\tau \right) - \left(\frac{1}{2}\int_S \{\varepsilon\}^T \{\sigma\} d\tau + \frac{1}{2}\int_P \{\varepsilon\}^T \{\sigma\} d\tau \right)$$
$$+ \left(\frac{1}{2}\int_P \{E\}^T \{D\} d\tau + \int_{A_S} \{w\}^T \left\{ f_S^e \right\} dA_S - \int_{A_P} qvdA_P \right)$$

On substituting the values of w, $\{\varepsilon\}$ and $\{E\}$ from eqns. (3.11)-(3.13), the Lagrangian:

$$L = \left(\frac{1}{2}\int_S \rho_s \left(\{\dot{u}_e\}^T [N]^T [N] \{\dot{u}_e\} \right) d\tau + \frac{1}{2}\int_P \rho_P \left(\{\dot{u}_e\}^T [N]^T [N] \{\dot{u}_e\} \right) d\tau \right)$$
$$- \left(\frac{1}{2}\int_S \left(z[B_u]\{u_e\} \right)^T \{\sigma\} d\tau + \frac{1}{2}\int_P \left(z[B_u]\{u_e\} \right)^T \{\sigma\} d\tau \right)$$
$$+ \left(\frac{1}{2}\int_P \left(-\{B_v\} v \right)^T \{D\} d\tau + \int_{A_S} \left([N]\{u_e\} \right)^T \left\{ f_S^e \right\} dA_S - \int_{A_P} qvdA_P \right)$$

$$
\begin{aligned}
&= \left(\frac{1}{2}\int_S \rho_s \left(\{\dot{u}_e\}^T [N]^T [N] \{\dot{u}_e\} \right) d\tau + \frac{1}{2}\int_P \rho_P \left(\{\dot{u}_e\}^T [N]^T [N] \{\dot{u}_e\} \right) d\tau \right) \\
&- \left(\frac{1}{2}\int_S z \{u_e\}^T [B_u]^T \{\sigma\} d\tau + \frac{1}{2}\int_P z \{u_e\}^T [B_u]^T \{\sigma\} d\tau \right) \\
&+ \left(-\frac{1}{2}\int_P v \{B_v\}^T \{D\} d\tau + \int_{A_S} \{u_e\}^T [N]^T \left\{ f_S^e \right\} dA_S - \int_{A_P} qv dA_P \right)
\end{aligned} \tag{3.20}
$$

Values of $\{D\}$ and $\{\sigma\}$ when substituted from the augmented constitutive equations (3.3) and (3.4) into equation (3.20) give:

$$
\begin{aligned}
L = &\left(\frac{1}{2}\int_S \rho_s \left(\{\dot{u}_e\}^T [N]^T [N] \{\dot{u}_e\} \right) d\tau + \frac{1}{2}\int_P \rho_P \left(\{\dot{u}_e\}^T [N]^T [N] \{\dot{u}_e\} \right) d\tau \right) \\
&- \left(\begin{array}{l} \frac{1}{2}\int_S z \{u_e\}^T [B_u]^T \left([c_S] \left(\{\varepsilon\} - \{\alpha_S\} \Delta T \right) \right) d\tau \\ + \frac{1}{2}\int_P z \{u_e\}^T [B_u]^T \left([c_P] \left(\{\varepsilon\} - \{\alpha_P\} \Delta T \right) - \left(\left[e^T \right]^T + \left[\bar{e} \right]^T \Delta T \right) \{E\} \right) d\tau \end{array} \right) \\
&+ \left(\begin{array}{l} -\frac{1}{2}\int_P v \{B_v\}^T \left(\left(\left[e^T \right] + \left[\bar{e} \right] \Delta T \right) \{\varepsilon\} + \left(\left[\in^T \right] + \left[\bar{\in} \right] \Delta T \right) \{E\} + \Delta T \{p\} \right) d\tau \\ + \int_{A_S} \{u_e\}^T [N]^T \left\{ f_S^e \right\} dA_S - \int_{A_P} qv dA_P \end{array} \right)
\end{aligned} \tag{3.21}
$$

On substituting $\{\varepsilon\}$ and $\{E\}$ from equations (3.12) and (3.13) into equation (3.21), the Lagrangian becomes:

$$
\begin{aligned}
L = &\left(\frac{1}{2}\int_S \rho_s \left(\{\dot{u}_e\}^T [N]^T [N] \{\dot{u}_e\} \right) d\tau + \frac{1}{2}\int_P \rho_P \left(\{\dot{u}_e\}^T [N]^T [N] \{\dot{u}_e\} \right) d\tau \right) \\
&- \left(\frac{1}{2}\int_S z \{u_e\}^T [B_u]^T \left([c_S] \left(z [B_u] \{u_e\} - \{\alpha_S\} \Delta T \right) \right) d\tau \right) \\
&- \frac{1}{2}\int_P z \{u_e\}^T [B_u]^T \left([c_P] \left(z [B_u] \{u_e\} - \{\alpha_P\} \Delta T \right) - \left(\left[e^T \right]^T + \left[\bar{e} \right]^T \Delta T \right) \left(- \{B_v\} v \right) \right) d\tau \\
&- \frac{1}{2}\int_P v \{B_v\}^T \left(\left(\left[e^T \right] + \left[\bar{e} \right] \Delta T \right) \left(z [B_u] \{u_e\} \right) + \left(\left[\in^T \right] + \left[\bar{\in} \right] \Delta T \right) \left(- \{B_v\} v \right) + \Delta T \{p\} \right) d\tau
\end{aligned}
$$

$$+\int_{A_S}\{u_e\}^T[N]^T\left\{f_S^e\right\}dA_S-\int_{A_P}qvdA_P$$

Which on further simplification becomes:

$$\begin{aligned}L=&\frac{1}{2}\int_S\left(\rho_s\{\dot{u}_e\}^T[N]^T[N]\{\dot{u}_e\}\right)d\tau+\frac{1}{2}\int_P\left(\rho_P\{\dot{u}_e\}^T[N]^T[N]\{\dot{u}_e\}\right)d\tau\\&-\frac{1}{2}\int_S\left(z^2\{u_e\}^T[B_u]^T[c_S][B_u]\{u_e\}-z\{u_e\}^T[B_u]^T[c_S]\{\alpha_S\}\Delta T\right)d\tau\\&-\frac{1}{2}\int_P\begin{pmatrix}z^2\{u_e\}^T[B_u]^T[c_P][B_u]\{u_e\}-z\{u_e\}^T[B_u]^T[c_P]\{\alpha_P\}\Delta T\\+zv\{u_e\}^T[B_u]^T\left[e^T\right]^T\{B_v\}+zv\{u_e\}^T[B_u]^T\left[\bar{e}\right]^T\{B_v\}\Delta T\end{pmatrix}d\tau\\&-\frac{1}{2}\int_P\begin{pmatrix}vz\{B_v\}^T\left[e^T\right][B_u]\{u_e\}+vz\{B_v\}^T\left[\bar{e}\right][B_u]\{u_e\}\Delta T\\-v^2\{B_v\}^T\left[\in^T\right]\{B_v\}-v^2\{B_v\}^T\left[\bar{\in}\right]\{B_v\}\Delta T+v\{B_v\}^T\{p\}\Delta T\end{pmatrix}d\tau\\&+\int_{A_S}\{u_e\}^T[N]^T\left\{f_S^e\right\}dA_S-\int_{A_P}qvdA_P\end{aligned}\tag{3.22}$$

3.1.3 *Finding Equations of Motion Using Hamilton's Principle*

Hamilton's principle is an important tool to find the equation of motion of a mechanical system. It states that the motion of the system between time intervals from 't_1' to 't_2' is such that the line integral $I=\int_{t_1}^{t_2}Ldt$ has a stationary value for the correct path of the motion. Mathematically,

$$\delta I=\delta\int_{t_1}^{t_2}Ldt=0\tag{3.23}$$

Therefore, the equation of motion of finite element in discussion can be derived using Hamilton's principle. The value of Lagrangian 'L', when substituted from equation (3.22) into Hamilton's principle (3.23) gives:

$$\begin{aligned}\delta\int_{t_1}^{t_2} L dt = \delta\int_{t_1}^{t_2}\Bigg[& \frac{1}{2}\int_S\left(\rho_s\{\dot{u}_e\}^T[N]^T[N]\{\dot{u}_e\}\right)d\tau+\frac{1}{2}\int_P\left(\rho_P\{\dot{u}_e\}^T[N]^T[N]\{\dot{u}_e\}\right)d\tau \\ & -\frac{1}{2}\int_S\left(z^2\{u_e\}^T[B_u]^T[c_S][B_u]\{u_e\}-z\{u_e\}^T[B_u]^T[c_S]\{\alpha_S\}\Delta T\right)d\tau \\ & -\frac{1}{2}\int_P\begin{pmatrix} z^2\{u_e\}^T[B_u]^T[c_P][B_u]\{u_e\}-z\{u_e\}^T[B_u]^T[c_P]\{\alpha_P\}\Delta T \\ +zv\{u_e\}^T[B_u]^T\left[e^T\right]^T\{B_v\}+zv\{u_e\}^T[B_u]^T\left[\bar{e}\right]^T\{B_v\}\Delta T\end{pmatrix}d\tau \\ & -\frac{1}{2}\int_P\begin{pmatrix} vz\{B_v\}^T\left[e^T\right][B_u]\{u_e\}+vz\{B_v\}^T\left[\bar{e}\right][B_u]\{u_e\}\Delta T \\ -v^2\{B_v\}^T\left[\in^T\right]\{B_v\}-v^2\{B_v\}^T\left[\bar{\in}\right]\{B_v\}\Delta T+v\{B_v\}^T\{p\}\Delta T\end{pmatrix}d\tau \\ & +\int_{A_S}\{u_e\}^T[N]^T\left\{f_S^e\right\}dA_S-\int_{A_P}qvdA_P\Bigg]dt \\ = & \,0\end{aligned} \tag{3.24}$$

Above equation, contains two variables namely $\{u_e\}$ and 'v'. To solve this, we have to take variations w.r.t. both the variables one by one. First, taking variation w.r.t. $\{u_e\}$ we get:

$$\begin{aligned}\delta\int_{t_1}^{t_2} L dt = \int_{t_1}^{t_2}\Bigg[& \frac{1}{2}\int_S\left(\rho_s\{\delta\dot{u}_e\}^T[N]^T[N]\{\dot{u}_e\}\right)d\tau+\frac{1}{2}\int_S\left(\rho_s\{\dot{u}_e\}^T[N]^T[N]\{\delta\dot{u}_e\}\right)d\tau \\ & +\frac{1}{2}\int_P\left(\rho_P\{\delta\dot{u}_e\}^T[N]^T[N]\{\dot{u}_e\}\right)d\tau+\frac{1}{2}\int_P\left(\rho_P\{\dot{u}_e\}^T[N]^T[N]\{\delta\dot{u}_e\}\right)d\tau \\ & -\frac{1}{2}\int_S\begin{pmatrix} z^2\{\delta u_e\}^T[B_u]^T[c_S][B_u]\{u_e\}+z^2\{u_e\}^T[B_u]^T[c_S][B_u]\{\delta u_e\} \\ -z\{\delta u_e\}^T[B_u]^T[c_S]\{\alpha_S\}\Delta T\end{pmatrix}d\tau \\ & -\frac{1}{2}\int_P\begin{pmatrix} z^2\{\delta u_e\}^T[B_u]^T[c_P][B_u]\{u_e\}+z^2\{u_e\}^T[B_u]^T[c_P][B_u]\{\delta u_e\} \\ -z\{\delta u_e\}^T[B_u]^T[c_P]\{\alpha_P\}\Delta T\end{pmatrix}d\tau \\ & -\frac{1}{2}\int_P\left(zv\{\delta u_e\}^T[B_u]^T\left[e^T\right]^T\{B_v\}+zv\{\delta u_e\}^T[B_u]^T\left[\bar{e}\right]^T\{B_v\}\Delta T\right)d\tau \\ & -\frac{1}{2}\int_P\left(vz\{B_v\}^T\left[e^T\right][B_u]\{\delta u_e\}+vz\{B_v\}^T\left[\bar{e}\right][B_u]\{\delta u_e\}\Delta T\right)d\tau\end{aligned}$$

$$+\int_{A_S}\{\delta u_e\}^T[N]^T\left\{f_S^e\right\}dA_S\Bigg]dt$$
$$=0$$

Since $[c_S]$ and $[c_P]$ are symmetric, so after re-arranging the terms we get:

$$\begin{aligned}\delta\int_{t_1}^{t_2}Ldt=\int_{t_1}^{t_2}\Bigg[&\frac{1}{2}\int_S\left(\rho_s\{\delta\dot{u}_e\}^T[N]^T[N]\{\dot{u}_e\}\right)d\tau+\frac{1}{2}\int_S\left(\rho_s\{\delta\dot{u}_e\}^T[N]^T[N]\{\dot{u}_e\}\right)d\tau\\&+\frac{1}{2}\int_P\left(\rho_P\{\delta\dot{u}_e\}^T[N]^T[N]\{\dot{u}_e\}\right)d\tau+\frac{1}{2}\int_P\left(\rho_P\{\delta\dot{u}_e\}^T[N]^T[N]\{\dot{u}_e\}\right)d\tau\\&-\frac{1}{2}\int_S\begin{pmatrix}z^2\{\delta u_e\}^T[B_u]^T[c_S][B_u]\{u_e\}+z^2\{\delta u_e\}^T[B_u]^T[c_S][B_u]\{u_e\}\\-z\{\delta u_e\}^T[B_u]^T[c_S]\{\alpha_S\}\Delta T\end{pmatrix}d\tau\\&-\frac{1}{2}\int_P\begin{pmatrix}z^2\{\delta u_e\}^T[B_u]^T[c_P][B_u]\{u_e\}+z^2\{\delta u_e\}^T[B_u]^T[c_P][B_u]\{u_e\}\\-z\{\delta u_e\}^T[B_u]^T[c_P]\{\alpha_P\}\Delta T\end{pmatrix}d\tau\\&-\frac{1}{2}\int_P\left(zv\{\delta u_e\}^T[B_u]^T\left[e^T\right]^T\{B_v\}+zv\{\delta u_e\}^T[B_u]^T\left[\bar{e}\right]^T\{B_v\}\Delta T\right)d\tau\\&-\frac{1}{2}\int_P\left(vz\{\delta u_e\}^T[B_u]^T\left[e^T\right]^T\{B_v\}+vz\{\delta u_e\}^T[B_u]^T\left[\bar{e}\right]^T\{B_v\}\Delta T\right)d\tau\\&+\int_{A_S}\{\delta u_e\}^T[N]^T\left\{f_S^e\right\}dA_S\Bigg]dt\\=0&\end{aligned}$$

Adding like terms:

$$\begin{aligned}\delta\int_{t_1}^{t_2}Ldt=\int_{t_1}^{t_2}\Bigg[&\int_S\left(\rho_s\{\delta\dot{u}_e\}^T[N]^T[N]\{\dot{u}_e\}\right)d\tau\\&+\int_P\left(\rho_P\{\delta\dot{u}_e\}^T[N]^T[N]\{\dot{u}_e\}\right)d\tau\\&-\int_S\left(z^2\{\delta u_e\}^T[B_u]^T[c_S][B_u]\{u_e\}-\frac{z}{2}\{\delta u_e\}^T[B_u]^T[c_S]\{\alpha_S\}\Delta T\right)d\tau\\&-\int_P\left(z^2\{\delta u_e\}^T[B_u]^T[c_P][B_u]\{u_e\}-\frac{z}{2}\{\delta u_e\}^T[B_u]^T[c_P]\{\alpha_P\}\Delta T\right)d\tau\end{aligned}$$

$$-\int_P \left(zv\{\delta u_e\}^T [B_u]^T \left[e^T\right]^T \{B_v\} + zv\{\delta u_e\}^T [B_u]^T \left[\bar{e}\right]^T \{B_v\} \Delta T \right) d\tau$$

$$+ \int_{A_S} \{\delta u_e\}^T [N]^T \left\{ f_S^e \right\} dA_S \Bigg] dt$$

$$= 0$$

Integrating first two terms w.r.t. time by parts, above equation becomes:

$$\delta \int_{t_1}^{t_2} L dt = \int_S \left(\rho_s \{\delta u_e\}^T [N]^T [N] \{\dot{u}_e\} \right) \Big|_{t_1}^{t_2} d\tau - \int_{t_1}^{t_2} \int_S \left(\rho_s \{\delta u_e\}^T [N]^T [N] \{\ddot{u}_e\} \right) d\tau dt$$

$$+ \int_P \left(\rho_P \{\delta u_e\}^T [N]^T [N] \{\dot{u}_e\} \right) \Big|_{t_1}^{t_2} d\tau - \int_{t_1}^{t_2} \int_P \left(\rho_P \{\delta u_e\}^T [N]^T [N] \{\ddot{u}_e\} \right) d\tau dt$$

$$+ \int_{t_1}^{t_2} \Bigg[-\int_S \left(z^2 \{\delta u_e\}^T [B_u]^T [c_S][B_u]\{u_e\} - \frac{z}{2} \{\delta u_e\}^T [B_u]^T [c_S]\{\alpha_S\} \Delta T \right) d\tau$$

$$-\int_P \left(z^2 \{\delta u_e\}^T [B_u]^T [c_P][B_u]\{u_e\} - \frac{z}{2} \{\delta u_e\}^T [B_u]^T [c_P]\{\alpha_P\} \Delta T \right) d\tau$$

$$-\int_P \left(zv\{\delta u_e\}^T [B_u]^T \left[e^T\right]^T \{B_v\} + zv\{\delta u_e\}^T [B_u]^T \left[\bar{e}\right]^T \{B_v\} \Delta T \right) d\tau$$

$$+ \int_{A_S} \{\delta u_e\}^T [N]^T \left\{ f_S^e \right\} dA_S \Bigg] dt$$

$$= 0$$

Since first and third terms in the above equation have same values at 't_1' and 't_2', so they vanish. Therefore, above equation becomes:

$$\delta \int_{t_1}^{t_2} L dt = \int_{t_1}^{t_2} \Bigg[-\int_S \left(\rho_s \{\delta u_e\}^T [N]^T [N] \{\ddot{u}_e\} \right) d\tau - \int_P \left(\rho_P \{\delta u_e\}^T [N]^T [N] \{\ddot{u}_e\} \right) d\tau$$

$$-\int_S \left(z^2 \{\delta u_e\}^T [B_u]^T [c_S][B_u]\{u_e\} - \frac{z}{2} \{\delta u_e\}^T [B_u]^T [c_S]\{\alpha_S\} \Delta T \right) d\tau$$

$$-\int_P \left(z^2 \{\delta u_e\}^T [B_u]^T [c_P][B_u]\{u_e\} - \frac{z}{2} \{\delta u_e\}^T [B_u]^T [c_P]\{\alpha_P\} \Delta T \right) d\tau$$

$$-\int_P \left(zv\{\delta u_e\}^T [B_u]^T \left[e^T\right]^T \{B_v\} + zv\{\delta u_e\}^T [B_u]^T \left[\bar{e}\right]^T \{B_v\} \Delta T \right) d\tau$$

$$+\int_{A_S}\{\delta u_e\}^T[N]^T\left\{f_S^e\right\}dA_S\Bigg]dt$$
$$=0$$

Each term on right hand side has $\{\delta u_e\}^T$ in common. Taking $\{\delta u_e\}^T$ outside, we get:

$$\delta\int_{t_1}^{t_2}Ldt=\{\delta u_e\}^T\int_{t_1}^{t_2}\Bigg[-\int_S\left(\rho_s[N]^T[N]\{\ddot{u}_e\}\right)d\tau-\int_P\left(\rho_P[N]^T[N]\{\ddot{u}_e\}\right)d\tau$$
$$-\int_S\left(z^2[B_u]^T[c_S][B_u]\{u_e\}-\frac{z}{2}[B_u]^T[c_S]\{\alpha_S\}\Delta T\right)d\tau$$
$$-\int_P\left(z^2[B_u]^T[c_P][B_u]\{u_e\}-\frac{z}{2}[B_u]^T[c_P]\{\alpha_P\}\Delta T\right)d\tau$$
$$-\int_P\left(zv[B_u]^T\left[e^T\right]^T\{B_v\}+zv[B_u]^T\left[\bar{e}\right]^T\{B_v\}\Delta T\right)d\tau+\int_{A_S}[N]^T\left\{f_S^e\right\}dA_S\Bigg]dt$$
$$=0$$

In order to satisfy above equality, the terms inside the square bracket should vanish i.e.

$$-\int_S\left(\rho_s[N]^T[N]\{\ddot{u}_e\}\right)d\tau-\int_P\left(\rho_P[N]^T[N]\{\ddot{u}_e\}\right)d\tau-\int_S z^2[B_u]^T[c_S][B_u]\{u_e\}d\tau$$
$$+\frac{1}{2}\int_S z[B_u]^T[c_S]\{\alpha_S\}\Delta Td\tau-\int_P z^2[B_u]^T[c_P][B_u]\{u_e\}d\tau+\frac{1}{2}\int_P z[B_u]^T[c_P]\{\alpha_P\}\Delta Td\tau$$
$$-\int_P zv[B_u]^T\left[e^T\right]^T\{B_v\}d\tau-\int_P zv[B_u]^T\left[\bar{e}\right]^T\{B_v\}\Delta Td\tau+\int_{A_S}[N]^T\left\{f_S^e\right\}dA_S=0$$

After rearranging the terms, above equation can be written as:

$$\left(\int_S\rho_s[N]^T[N]d\tau+\int_P\rho_P[N]^T[N]d\tau\right)\{\ddot{u}_e\}$$
$$+\left(\int_S z^2[B_u]^T[c_S][B_u]d\tau+\int_P z^2[B_u]^T[c_P][B_u]d\tau\right)\{u_e\}$$
$$+\left(\int_P z[B_u]^T\left[e^T\right]^T\{B_v\}d\tau+\int_P z[B_u]^T\left[\bar{e}\right]^T\{B_v\}\Delta Td\tau\right)v$$

$$= \int_{A_S} [N]^T \left\{ f_S^e \right\} dA_S + \frac{1}{2}\int_S z[B_u]^T [c_S]\{\alpha_S\}\Delta T d\tau + \frac{1}{2}\int_P z[B_u]^T [c_P]\{\alpha_P\}\Delta T d\tau$$

or

$$\left(\left[m_S^e\right]+\left[m_P^e\right]\right)\{\ddot{u}_e\}+\left(\left[k_S^e\right]+\left[k_P^e\right]\right)\{u_e\}+\left(\left[k_{uv}^e\right]+\left[\bar{k}_{uv}\right]\right)v=\left\{F_S^e\right\}+\left\{F_{T,S}^e\right\}+\left\{F_{T,P}^e\right\} \quad (3.25)$$

where;

$\left[m_S^e\right]=\int_S \rho_S [N]^T [N] d\tau$ is host structural element mass matrix,

$\left[m_P^e\right]=\int_P \rho_P [N]^T [N] d\tau$ is piezoelectric element mass matrix,

$\left[k_S^e\right]=\int_S z^2 [B_u]^T [c_S][B_u] d\tau$ is host structural element stiffness matrix,

$\left[k_P^e\right]=\int_P z^2 [B_u]^T [c_P][B_u] d\tau$ is piezoelectric element stiffness matrix,

$\left[k_{uv}^e\right]=\left[k_{vu}^e\right]^T=\int_P z\{B_u\}^T \left[e^T\right][B_v] d\tau$ is electromechanical interaction matrix,

$\left[\bar{k}_{uv}^e\right]_{1x12}=\left[\bar{k}_{vu}^e\right]_{1x12}^T=\int_P z\{B_u\}^T \left[\bar{e}\right][B_v]\Delta T d\tau$ is change in electromechanical interaction matrix when 'ambient temperature' is other than 'reference temperature',

$\left\{F_S^e\right\}_{12x3} = \int_{A_S} [N]^T \left\{ f_S^e \right\} dA_S$ is external force acting on the surface of finite element of 'smart structure',

$\left\{F_{T,S}^e\right\}_{12x1} = \frac{1}{2}\int_S z[B_u]^T [c_S]\{\alpha_S\}\Delta T d\tau$ is the force on element due to thermal expansion of the host structure and

$\left\{F^e_{T,P}\right\}_{12x1} = \frac{1}{2}\int_P z\left[B_u\right]^T\left[c_P\right]\left\{\alpha_P\right\}\Delta T d\tau$ is the force on element due to thermal expansion of piezoelectric.

Now, taking variation of equation (3.24) w.r.t. 'v' we get:

$$\begin{aligned}\delta\int_{t_1}^{t_2} L dt = \int_{t_1}^{t_2}\Bigg[& -\frac{1}{2}\int_P\Big(z(\delta v)\{u_e\}^T\left[B_u\right]^T\left[e^T\right]^T\{B_v\} + z(\delta v)\{u_e\}^T\left[B_u\right]^T\left[\bar{e}\right]^T\{B_v\}\Delta T\Big)d\tau \\ & -\frac{1}{2}\int_P\begin{pmatrix} z(\delta v)\{B_v\}^T\left[e^T\right]\left[B_u\right]\{u_e\} + z(\delta v)\{B_v\}^T\left[\bar{e}\right]\left[B_u\right]\{u_e\}\Delta T \\ -2v(\delta v)\{B_v\}^T\left[\in^T\right]\{B_v\} - 2v(\delta v)\{B_v\}^T\left[\bar{\in}\right]\{B_v\}\Delta T \\ +(\delta v)\{B_v\}^T\{p\}\Delta T\end{pmatrix}d\tau \\ & -\int_{A_P}(\delta v)qdA_P\Bigg]dt \\ = 0\end{aligned}$$

Each term on right hand side has 'δv' in common. Taking 'δv' outside and rearranging the terms, we get:

$$\begin{aligned}\delta\int_{t_1}^{t_2} L dt = \delta v\int_{t_1}^{t_2}\Bigg[& -\frac{1}{2}\int_P\Big(z\{B_v\}^T\left[e^T\right]\left[B_u\right]\{u_e\} + z\{B_v\}^T\left[\bar{e}\right]\left[B_u\right]\{u_e\}\Delta T\Big)d\tau \\ & -\frac{1}{2}\int_P\begin{pmatrix} z\{B_v\}^T\left[e^T\right]\left[B_u\right]\{u_e\} + z\{B_v\}^T\left[\bar{e}\right]\left[B_u\right]\{u_e\}\Delta T \\ -2v\{B_v\}^T\left[\in^T\right]\{B_v\} - 2v\{B_v\}^T\left[\bar{\in}\right]\{B_v\}\Delta T \\ +\{B_v\}^T\{p\}\Delta T\end{pmatrix}d\tau \\ & -\int_{A_P} qdA_P\Bigg]dt \\ = 0\end{aligned}$$

Adding like terms, we get:

$$\delta\int_{t_1}^{t_2} L dt = \delta v\int_{t_1}^{t_2}\Bigg[-\int_P\Big(z\{B_v\}^T\left[e^T\right]\left[B_u\right]\{u_e\} + z\{B_v\}^T\left[\bar{e}\right]\left[B_u\right]\{u_e\}\Delta T\Big)d\tau$$

$$+\int_P \left(v\{B_v\}^T \left[\in^T\right]\{B_v\} + v\{B_v\}^T \left[\bar{\in}\right]\{B_v\}\Delta T - \frac{1}{2}\{B_v\}^T \{p\}\Delta T \right) d\tau$$
$$- \int_{A_P} qdA_P \Bigg] dt$$
$$= 0$$

In order to satisfy above equality, the terms inside the square bracket on right hand side should vanish i.e.

$$-\int_P \left(z\{B_v\}^T \left[e^T\right][B_u]\{u_e\} + z\{B_v\}^T \left[\bar{e}\right][B_u]\{u_e\}\Delta T \right) d\tau$$
$$+\int_P \left(v\{B_v\}^T \left[\in^T\right]\{B_v\} + v\{B_v\}^T \left[\bar{\in}\right]\{B_v\}\Delta T - \frac{1}{2}\{B_v\}^T \{p\}\Delta T \right) d\tau - \int_{A_P} qdA_P = 0$$

On further simplification:

$$-\int_P \left(z\{B_v\}^T \left[e^T\right][B_u] + z\{B_v\}^T \left[\bar{e}\right][B_u]\Delta T \right)\{u_e\} d\tau$$
$$+\int_P \left(\{B_v\}^T \left[\in^T\right]\{B_v\} + \{B_v\}^T \left[\bar{\in}\right]\{B_v\}\Delta T \right) v d\tau - \frac{1}{2}\int_P \{B_v\}^T \{p\}\Delta T d\tau = \int_{A_P} qdA_P$$

Above equation can be written as:

$$-\left(\left[k_{vu}^e\right] + \left[\bar{k}_{vu}^e\right] \right)\{u_e\} + \left(\left[k_{vv}\right] + \left[\bar{k}_{vv}^e\right] \right) v - Q_{pyro}^e = Q_{ext}^e$$

After re-arranging the terms we get:

$$v = \left(\left[k_{vv}^e\right] + \left[\bar{k}_{vv}^e\right] \right)_{1x1}^{-1} \left(Q_{ext}^e + Q_{pyro}^e + \left(\left[k_{vu}^e\right] + \left[\bar{k}_{vu}^e\right] \right)\{u_e\} \right) \qquad (3.26)$$

where;

$\left[k_{vv}^e\right] = \int_P \{B_v\}^T \left[\in^T\right]\{B_v\} d\tau$ is the capacitance of piezoelectric sensor patch,

$\left[\bar{k}_{vv}^{e}\right]=\int_{P}\{B_v\}^{T}\left[\bar{\in}\right]\{B_v\}\Delta T d\tau$ is change in the capacitance of piezoelectric sensor patch when 'ambient temperature' is other than 'reference temperature',

$Q_{ext}^{e}=\int_{A_P} qdA_P$ is external charge applied on piezoelectric surface and

$Q_{pyro}^{e}=\frac{1}{2}\int_{P}\{p\}^{T}\{B_v\}\Delta T d\tau$ is the charge developed on piezoelectric patch due to 'pyroelectric effect'.

Equation (3.26) gives total voltage generated across piezoceramic PZT-5H patch as a result of: (i) static voltage due to 'thermal strain effect' (ii) static voltage due to 'pyroelectric effect' (iii) dynamic voltage due to structural vibrations and (iv) external charge applied. On substituting the value of 'v' into equation (3.25) we get:

$$\left(\left[m_S^e\right]+\left[m_P^e\right]\right)\{\ddot{u}_e\}+\left(\left[k_S^e\right]+\left[k_P^e\right]\right)\{u_e\}$$
$$+\left(\left[k_{uv}^e\right]+\left[\bar{k}_{uv}^e\right]\right)\left(\left[k_{vv}^e\right]+\left[\bar{k}_{vv}^e\right]\right)_{1x1}^{-1}\left(Q_{ext}^e+Q_{pyro}^e+\left(\left[k_{vu}^e\right]+\left[\bar{k}_{vu}^e\right]\right)\{u_e\}\right)$$
$$=\left\{F_S^e\right\}+\left\{F_{T,S}^e\right\}+\left\{F_{T,P}^e\right\}$$

After rearranging the terms:

$$\left(\left[m_S^e\right]+\left[m_P^e\right]\right)\{\ddot{u}_e\}$$
$$+\left(\left[k_S^e\right]+\left[k_P^e\right]+\left(\left[k_{uv}^e\right]+\left[\bar{k}_{uv}^e\right]\right)\left(\left[k_{vv}^e\right]+\left[\bar{k}_{vv}^e\right]\right)^{-1}\left(\left[k_{vu}^e\right]+\left[\bar{k}_{vu}^e\right]\right)\right)\{u_e\}$$
$$=\left\{F_S^e\right\}+\left\{F_{T,S}^e\right\}+\left\{F_{T,P}^e\right\}-\left(\left[k_{uv}^e\right]+\left[\bar{k}_{uv}^e\right]\right)\left(\left[k_{vv}^e\right]+\left[\bar{k}_{vv}^e\right]\right)^{-1}\left(Q_{ext}^e+Q_{pyro}^e\right)$$

or

$$\left[M_e\right]_{12x12}\{\ddot{u}_e\}+\left[K_e\right]_{12x12}\{u_e\}=\{F_e\}_{12x1} \tag{3.27}$$

where;

$\left[M_e\right]_{12x12} = \left[m_S^e\right] + \left[m_P^e\right]$ is elemental mass matrix,

$\left(\left[k_{vv}^e\right] + \left[\bar{k}_{vv}^e\right]\right) = Z_{sensor}$ is capacitance of sensor patch at ambient temperature,

$\left[K_e\right]_{12x12} = \left[k_S^e\right] + \left[k_P^e\right] + \left(\left[k_{uv}^e\right] + \left[\bar{k}_{uv}^e\right]\right)\left(\left[k_{vu}^e\right] + \left[\bar{k}_{vu}^e\right]\right)Z_{sensor}^{-1}$ is elemental total stiffness matrix,

$\left\{F_e\right\}_{12x1} = \left\{F_S^e\right\} + \left\{F_{T,S}^e\right\} + \left\{F_{T,P}^e\right\} + \left\{F_{E,P}^e\right\}$ is the total force acting on finite element and

$\left\{F_{E,P}^e\right\} = -\left(\left[k_{uv}^e\right] + \left[\bar{k}_{uv}^e\right]\right)\left(Q_{ext}^e + Q_{pyro}^e\right)Z_{sensor}^{-1}$ is the electric force component acting on one finite element. Equation (3.27) is the equation of motion of one finite element of the smart piezo plate structure as shown in Figure 3.2c. Electric force on a piezoelectric patch is due to 'thermal strain effect', 'pyroelectric effect' and external charges. We can also observe that the stiffness of finite element increases as a result of electromechanical interaction between the host structure and the piezoelectric patches. This is known as 'generalized stiffness'. In this case, generalized stiffness:

$$K_{generalized} = \left(\left[k_{uv}^e\right] + \left[\bar{k}_{uv}^e\right]\right)\left(\left[k_{vu}^e\right] + \left[\bar{k}_{vu}^e\right]\right)Z_{sensor}^{-1}$$

Now, the smart plate is divided into similar 64 finite elements forming eighty one nodes as shown in Figure 3.4. By assembly procedure, the global equation of motion of the smart plate structure is obtained as:

$$\left[M\right]_{243x243}\left\{\ddot{x}\right\}_{243x1} + \left[K\right]_{243x243}\left\{x\right\}_{243x1} = \left\{F\right\}_{243x1} \tag{3.28}$$

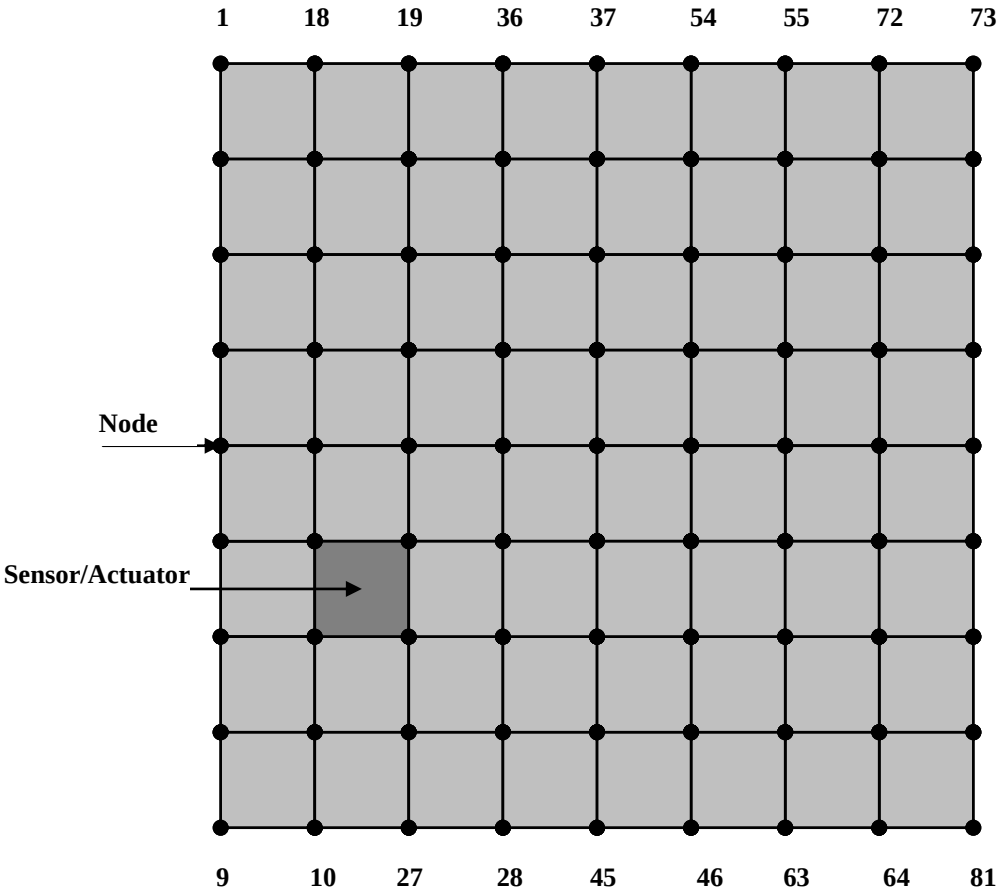

Figure 3.4: Smart piezo plate structure divided into 64 finite elements with 81 nodes.

In the presence of viscous damping, motion of 'smart piezo structure' will be resisted by a force whose magnitude is proportional to that of the velocity but in opposite direction. So, the final equation of motion of smart piezo plate structure becomes:

$$[M]_{243x243}\{\ddot{x}\}_{243x1}+[C']_{243x243}\{\dot{x}\}_{243x1}+[K]_{243x243}\{x\}_{243x1}=\{F\}_{243x243} \tag{3.29}$$

This is the equation of motion of a two dimensional smart cantilevered plate instrumented with one collocated PZT-5H sensor-actuator pair. In the finite element model of plate, there are 81 nodes each having three degrees of freedom. Therefore, the mass, damping and stiffness matrices are of order 243x243. For a smart plate cantilevered along one edge, above equation reduces to:

$$[M]_{216x216}\{\ddot{x}\}_{216x1}+[C']_{216x216}\{\dot{x}\}_{216x1}+[K]_{216x216}\{x\}_{216x1}=\{F\}_{216x216} \quad (3.30)$$

This is the equation of motion of a two dimensional cantilevered smart plate instrumented with one collocated piezoelectric sensor-actuator pair. Total force $\{F\}$ acting on smart cantilevered piezo plate structure has three components: (i) mechanical force component $\{F_S\}$ (ii) thermal force component $\{F_{T,S}\}\&\{F_{T,P}\}$ and (iii) electric force component $\{F_{E,P}\}$. Mechanical and thermal force components can influence the equilibrium position of 'smart structure'. Electric force component enhances system damping and therefore can suppress smart structural vibrations. It is termed as 'control force'. For PZT-5H polarized in positive z-direction:

$$[e]=\begin{bmatrix}0&0&0\\0&0&0\\e_{31}&e_{31}&0\end{bmatrix},\ [\in]=\begin{bmatrix}\in_{11}&0&0\\0&\in_{11}&0\\0&0&\in_{33}\end{bmatrix}\text{ and }\{p\}=\begin{Bmatrix}0\\0\\p_z\end{Bmatrix}. \quad (3.31)$$

For piezoelectric and host structure, elasticity matrices and thermal expansion vectors are:

$$[c]=\frac{Y}{\left(1-v'^2\right)}\begin{bmatrix}1&v'&0\\v'&1&0\\0&0&\frac{1-v'}{2}\end{bmatrix}\text{ and }\{\alpha\}=\begin{Bmatrix}\alpha_x\\\alpha_y\\0\end{Bmatrix}. \quad (3.32)$$

where v' is the Poisson's ratio.

3.2 Modal Analysis

Equation (1.30) represents a system of coupled equations. Analysis of such a system would become easier if these coupled equations are converted into uncoupled equations. In that case single degree of freedom system tools can be used to analyze the actual multi

degree of freedom system. The process of analyzing multi degree of freedom system using single degree of freedom system tools is known as 'modal analysis'. To do so, we use the transformation:

$$\{x\}_{nx1} = [U]_{nxm}\{\eta\}_{mx1} \tag{3.33}$$

To decouple the damping matrix, we consider damping as a linear combination of the mass and stiffness matrices:

$$[C']_{216x216} = \alpha[M]_{216x216} + \beta[K]_{216x216} \tag{3.34}$$

This type of damping is known as Rayleigh or proportional damping. 'α' and 'β' are known as Rayleigh mass and stiffness damping coefficients respectively. Restricting the analysis to first three modes only:

$$\{x\}_{216x1} = [U]_{216x3}\{\eta\}_{3x1} \tag{3.35}$$

On substituting equation (3.35) into equation (3.30):

$$[M][U]\{\ddot{\eta}\} + [C'][U]\{\dot{\eta}\} + [K][U]\{\eta\} = \{F\} \tag{3.36}$$

Pre-multiplying throughout by $[U]^T$:

$$[U]^T[M][U]\{\ddot{\eta}\} + [U]^T[C'][U]\{\dot{\eta}\} + [U]^T[K][U]\{\eta\} = [U]^T\{F\}$$

which on simplification gives the uncoupled equations of motion as:

$$\ddot{\eta}_1 + c_1'\dot{\eta}_1 + \omega_1^2\eta_1 = f_1 \tag{3.37}$$

$$\ddot{\eta}_2 + c_2'\dot{\eta}_2 + \omega_2^2\eta_2 = f_2 \tag{3.38}$$

$$\ddot{\eta}_3 + c_3'\dot{\eta}_3 + \omega_3^2\eta_3 = f_3 \tag{3.39}$$

where modal force vector $\{f\}_{3x1} = [U]^T_{3x216}\{F\}_{216x1}$, ω_m is 'modal frequency', modal damping $c_m^{'} = 2\zeta_m\omega_m = \alpha + \beta\omega_m^2$ and modal damping ratio:

$$\zeta_m = \frac{\alpha}{2\omega_m} + \frac{\omega_m}{2}\beta \tag{3.40}$$

Equations (3.37)-(3.39) are the uncoupled equations of motion in modal form which represents the motion of first three modes of smart piezo plate structure. Total force $\{F\}$ acting on smart cantilevered piezo plate structure given by equation (3.27) is:

$$\{F\} = \{F_S\} + \{F_{T,S}\} + \{F_{T,P}\} + \{F_{E,P}\} \tag{3.41}$$

Let total external surface force acting on the 'smart piezo structure' is zero i.e. $\{F_S\} = 0$. Also, force on smart plate due to thermal expansion of host i.e. $\{F_{T,S}\} = 0$. On substituting $\{F_{T,P}\} = F_{piezothermo}$ (say) and $\{F_{E,P}\}$ from equation into equation (3.41) we get modal force vector:

$$\{f\}_{3x1} = [U]^T\{F\} = [U]^T\left\{F_{piezothermo} - \left(\left[k_{uv}^e\right] + \left[\bar{k}_{uv}^e\right]\right)\left(Q_{ext}^e + Q_{pyro}^e\right)Z_{sensor}^{-1}\right\} \tag{3.42}$$

where $Q_{ext} = Z_{act}V_{ext}$ is the total external charge applied on piezo-actuator surface, $Z_{act} = \frac{(\in_{33}^T + \bar{\in}_{33}\Delta T)A}{d}$ is the capacitance of piezoelectric actuator and 'V_{ext}' is the external voltage applied on it. Component of modal force $\{f\}$ which depends upon external voltage (V_{ext}) applied on the piezo-actuator is termed as 'control force'. Therefore, control force;

$$\{f_c\} = -[U]^T\left(\left[k_{uv}^e\right] + \left[\bar{k}_{uv}^e\right]\right)Z_{sensor}^{-1}Z_{act}V_{ext} \tag{3.43}$$

3.3 State Space Model of the Cantilevered Smart Piezo Plate Structure

To control the response of a 'smart structure' using modern control theories, we need to write the uncoupled modal equations of motion in state space form. A state space model represents a system in the form of first order differential equations. The variables are called 'state variables' (say $\{s\}$) and a set of values of these state variables at any time 't' is called 'state of the system' at time 't' [141]. The state of the system at any time 't' is represented by the state equation:

$$\{\dot{s}\} = [A]\{s\} + [B]\{u\} \tag{3.44}$$

It relates the first derivative $\{\dot{s}\}$ of the state variables with variable themselves and the input $\{u\}$. Matrix $[A]$ is known as 'system state matrix' and matrix $[B]$ is known as the 'control matrix'. The output of the system is a function of $\{s\}$ and is given by:

$$\{y\} = [C]\{s\} \tag{3.45}$$

where [C] is the 'output matrix'. Equations (3.44) and (3.45) form state space model of the system. In order to control the vibration response of smart piezo plate structure, we have to convert modal equations (3.37)-(3.39) into a state-space model. Let,

$$\dot{\eta}_1 = x_1 \quad , \quad \dot{\eta}_2 = x_2 \quad \text{and} \quad \dot{\eta}_3 = x_3$$

$$\text{or} \quad \dot{\eta}_1 - x_1 = 0 \ , \ \dot{\eta}_2 - x_2 = 0 \quad \text{and} \quad \dot{\eta}_3 - x_3 = 0 \tag{3.46}$$

Using eq.(3.46), equations (3.37)-(3.39) can be written as:

$$\dot{x}_1 + c_1^{'} x_1 + w_1^2 \eta_1 = f_1 \tag{3.47}$$

$$\dot{x}_2 + c_2^{'} x_2 + w_2^2 \eta_2 = f_2 \tag{3.48}$$

$$\dot{x}_3 + c_3^{'} x_3 + w_3^2 \eta_3 = f_3 \tag{3.49}$$

In matrix form, equations (3.46)-(3.49) are written as:

$$\begin{bmatrix} 0 & 0 & 0 & +1 & 0 & 0 \\ 0 & 0 & 0 & 0 & +1 & 0 \\ 0 & 0 & 0 & 0 & 0 & +1 \\ 1 & 0 & 0 & 0 & 0 & 0 \\ 0 & 1 & 0 & 0 & 0 & 0 \\ 0 & 0 & 1 & 0 & 0 & 0 \end{bmatrix}_{6x6} \begin{Bmatrix} \dot{\eta}_1 \\ \dot{\eta}_2 \\ \dot{\eta}_3 \\ \dot{x}_1 \\ \dot{x}_2 \\ \dot{x}_3 \end{Bmatrix}_{6x1} + \begin{bmatrix} w_1^2 & 0 & 0 & c_1^{'} & 0 & 0 \\ 0 & w_2^2 & 0 & 0 & c_2^{'} & 0 \\ 0 & 0 & w_3^2 & 0 & 0 & c_3^{'} \\ 0 & 0 & 0 & -1 & 0 & 0 \\ 0 & 0 & 0 & 0 & -1 & 0 \\ 0 & 0 & 0 & 0 & 0 & -1 \end{bmatrix}_{6x6} \begin{Bmatrix} \eta_1 \\ \eta_2 \\ \eta_3 \\ x_1 \\ x_2 \\ x_3 \end{Bmatrix}_{6x1} \tag{3.50}$$

$$= \{ f_1 \quad f_2 \quad f_3 \quad 0 \quad 0 \quad 0 \}^T_{6x1}$$

Sub-matrices $\begin{bmatrix} +1 & 0 & 0 \\ 0 & +1 & 0 \\ 0 & 0 & +1 \end{bmatrix}$, $\begin{bmatrix} w_1^2 & 0 & 0 \\ 0 & w_2^2 & 0 \\ 0 & 0 & w_3^2 \end{bmatrix}$ and $\begin{bmatrix} c_1^{'} & 0 & 0 \\ 0 & c_2^{'} & 0 \\ 0 & 0 & c_3^{'} \end{bmatrix}$ appearing in equation (3.50) are the modal mass $\left(=[U]^T [M][U]\right)$, modal stiffness $\left(=[U]^T [K][U]\right)$ and modal damping $\left(=[U]^T [C'][U]\right)$ matrices respectively. Let,

$$\{s\}_{6x1} = \begin{Bmatrix} \eta_1 \\ \eta_2 \\ \eta_3 \\ x_1 \\ x_2 \\ x_3 \end{Bmatrix}_{6x1} \quad , [m']_{6x6} = \begin{bmatrix} 0 & 0 & 0 & +1 & 0 & 0 \\ 0 & 0 & 0 & 0 & +1 & 0 \\ 0 & 0 & 0 & 0 & 0 & +1 \\ 1 & 0 & 0 & 0 & 0 & 0 \\ 0 & 1 & 0 & 0 & 0 & 0 \\ 0 & 0 & 1 & 0 & 0 & 0 \end{bmatrix}_{6x6} ,$$

$$[k']_{6x6} = \begin{bmatrix} w_1^2 & 0 & 0 & c_1^{'} & 0 & 0 \\ 0 & w_2^2 & 0 & 0 & c_2^{'} & 0 \\ 0 & 0 & w_3^2 & 0 & 0 & c_3^{'} \\ 0 & 0 & 0 & -1 & 0 & 0 \\ 0 & 0 & 0 & 0 & -1 & 0 \\ 0 & 0 & 0 & 0 & 0 & -1 \end{bmatrix}_{6x6} \tag{3.51}$$

Now, equation (3.50) can be written as:

$$\{\dot{s}\} = -[m']^{-1}[k']\{s\} + [m']^{-1}\{f_1 \quad f_2 \quad f_3 \quad 0 \quad 0 \quad 0\}^T \qquad (3.52)$$

Now putting $\{f_1 \quad f_2 \quad f_3\}^T = \{f\}_{3x1}$ and $-[m']^{-1}_{6x6}[k']_{6x6} = [A]_{6x6}$, above equation becomes:

$$\{\dot{s}\} = [A]_{6x6}\{s\}_{6x1} + [m']^{-1}_{6x6}\{\{f\}_{3x1} \quad 0 \quad 0 \quad 0\}^T_{6x1} \qquad (3.53)$$

On substituting $\{f\}_{3x1}$ from equation (3.42), above equation becomes:

$$\{\dot{s}\}_{6x1} = [A]_{6x6}\{s\}_{6x1} + [m']^{-1}_{6x6}\begin{Bmatrix} [U]^T\{F_{piezothermo} - \{F_m\}(Z_{act}V_{ext} + Q_{pyro})\} \\ 0 \\ 0 \\ 0 \end{Bmatrix}_{6x1}$$

where $\{F_m\}_{216x1} = \left(\left[k^e_{uv}\right] + \left[\bar{k}^e_{uv}\right]\right)Z^{-1}_{sensor}$. Now take,

$$[B]_{6x1} = [m']^{-1}_{6x6}\begin{Bmatrix} -[U]^T_{3x216}\{F_m\}_{216x1}Z_{act} \\ 0 \\ 0 \\ 0 \end{Bmatrix}_{6x1} \quad \text{and}$$

$$[G]_{6x1} = [m']^{-1}_{6x6}\begin{Bmatrix} \left([U]^T_{3x216}\{F_{piezothermo}\}_{216x1} - [U]^T_{3x216}\{F_m\}_{216x1}Q_{pyro}\right)_{3x1} \\ 0 \\ 0 \\ 0 \end{Bmatrix}_{6x1} \qquad (3.54)$$

Using notations given in equation (3.54), equation (3.53) becomes:

$$\{\dot{s}\}_{6x1} = [A]_{6x6}\{s\}_{6x1} + [B]_{6x1}V_{ext} + [G]_{6x1} \qquad (3.55)$$

This is the state equation of state space model . On substituting Q_{ext} equal to zero in equation (3.26), the voltage generated in piezoelectric sensor as a result of strains developing on the host structure is obtained as:

$$v_{sensor} = \left(Q_{pyro} + \left(\left[k_{vu}^{e} \right] + \left[\bar{k}_{vu}^{e} \right] \right) \{ u_e \} \right)_{1x1} Z_{sensor}^{-1} \tag{3.56}$$

This gives the output equation of state space model.

Equations (3.55) and (3.56) represent the first three modal equations of motion of a cantilevered smart piezo plate structure in state space form. The vibration response of this 'smart piezo structure' can now be controlled using modern control theories.

CHAPTER IV

ACTIVE VIBRATION CONTROL OF SMART PIEZO PLATE: THEORY AND SIMULATIONS

Vibration analysis of smart piezo plate structure can be done by writing a computer program for the mathematical model derived in previous chapter. In this chapter, theoretical vibration analysis of a cantilevered smart piezo plate has been done using a computer program written in MATLAB. The finite element model is verified by comparing the results with valid mathematical models. A 'negative velocity feedback' control law which is robust to temperature variations, is derived for the first modal active vibration control of a cantilevered smart piezo plate. Modal state vectors are estimated using Kalman state observer. Dependence of various active vibration control parameters on piezoelectric stress coefficients 'e_{31}' and permittivity '$\in_{33}$' is shown. Simulation results prove the robustness of proposed active vibration control law with respect to temperature variations.

4.1 Validation of the Mathematical Model

As derived in previous chapter, coupled equation of motion of a cantilevered smart piezo plate structure divided into 64 elements and 81 nodes is:

$$[M]_{216x216}\{\ddot{x}\}_{216x1}+[C']_{216x216}\{\dot{x}\}_{216x1}+[K]_{216x216}\{x\}_{216x1}=\{F\}_{216x216}$$

In state space form, the first three modal equations of motion are written as:

State equation:
$$\{\dot{s}\}_{6x1}=[A]_{6x6}\{s\}_{6x1}+[B]_{6x1}V_{ext}+[G]_{6x1} \tag{4.1}$$

Output equation:
$$v_{sensor}=\left(Q_{pyro}+\left(\left[k_{vu}^{e}\right]+\left[\bar{k}_{vu}^{e}\right]\right)\{u_e\}\right)_{1x1}Z_{sensor}^{-1} \tag{4.2}$$

A computer program written in MATLAB for this state space model is used to study the vibration behaviour of cantilevered smart piezo plate structure. In the present study, we have considered one PZT-5H piezoceramic sensor and one PZT-5H piezoceramic actuator. Both sensor and actuator are of identical dimensions. Length and breadth of sensor and actuator is equal to that of one finite element of the plate structure. Sensor and actuators are instrumented to the plate structure in collocated fashion at opposite faces of the plate. Position of sensor-actuator pair is near the cantilevered end as shown in Figure 3.4. First five natural frequencies are calculated using the computer program at ambient temperature of 25ºC. These natural frequencies are compared to the mathematical model derived by [37] in Table 4.1.

Mode	**Natural frequencies using present FEM (in Hertz)**	**Natural frequencies using FEM by [37] (in Hertz)**
1^{st}	21.1638	21.1638
2^{nd}	51.2398	51.2398
3^{rd}	123.8088	123.8088
4^{th}	159.3523	159.3523
5^{th}	183.1445	183.1445

Table 4.1: **A comparison of first five natural frequencies obtained using present finite element analysis and the finite element analysis done by [37].**

It can be observed that natural frequencies in both the cases match excellently. It proves the accuracy of mathematical model derived in present work. Resulting smart piezo plate structure is now manually displaced through 2mm vertically. First four modal vibrations and the mode shapes of the cantilevered smart piezo plate structure are shown in Figure 4.1 and Figure 4.2 respectively.

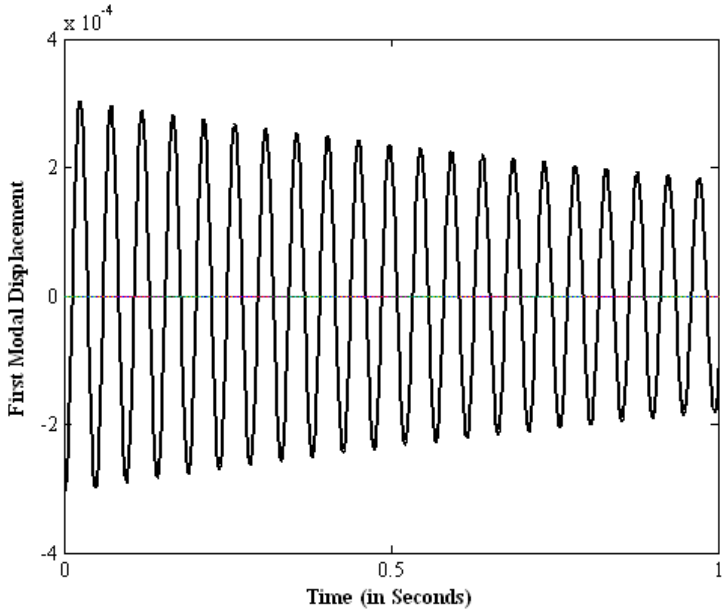

Figure 4.1a: First modal vibrations

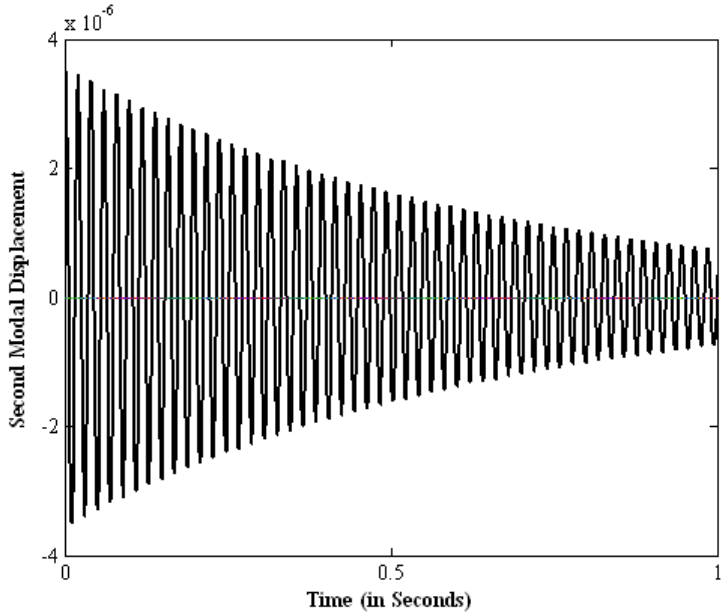

Figure 4.1b: Second modal vibrations

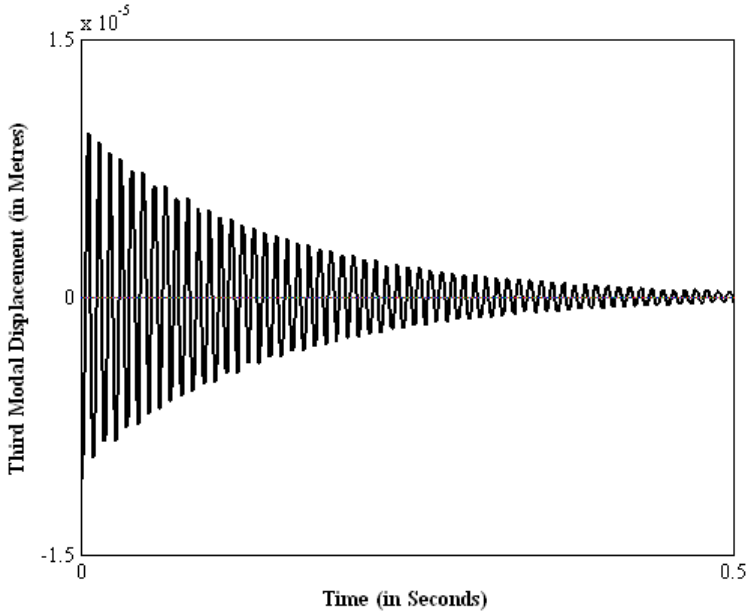

Figure 4.1c: Third modal vibrations

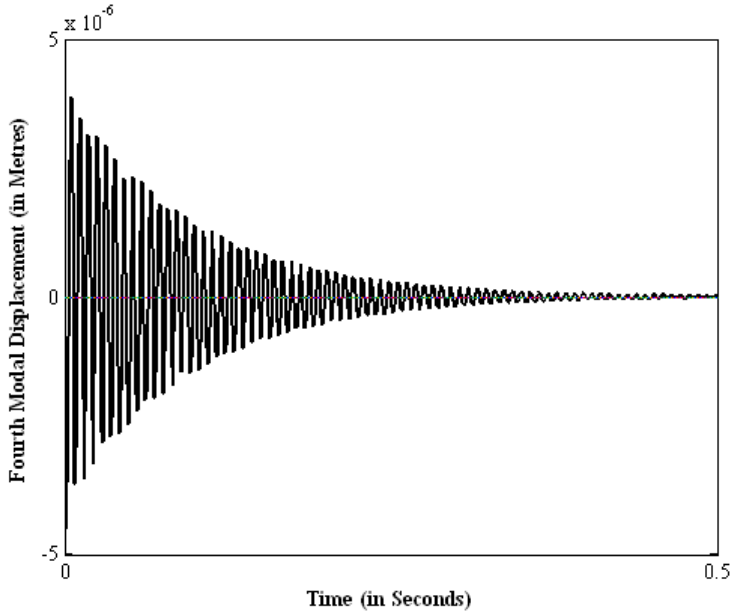

Figure 4.1d: Fourth modal vibrations

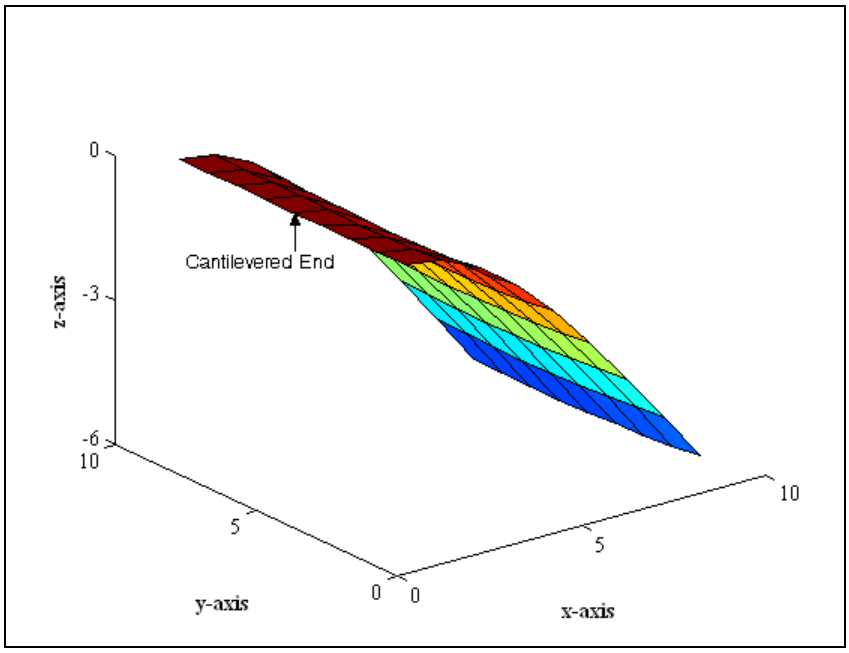

Figure 4.2a: First mode shape

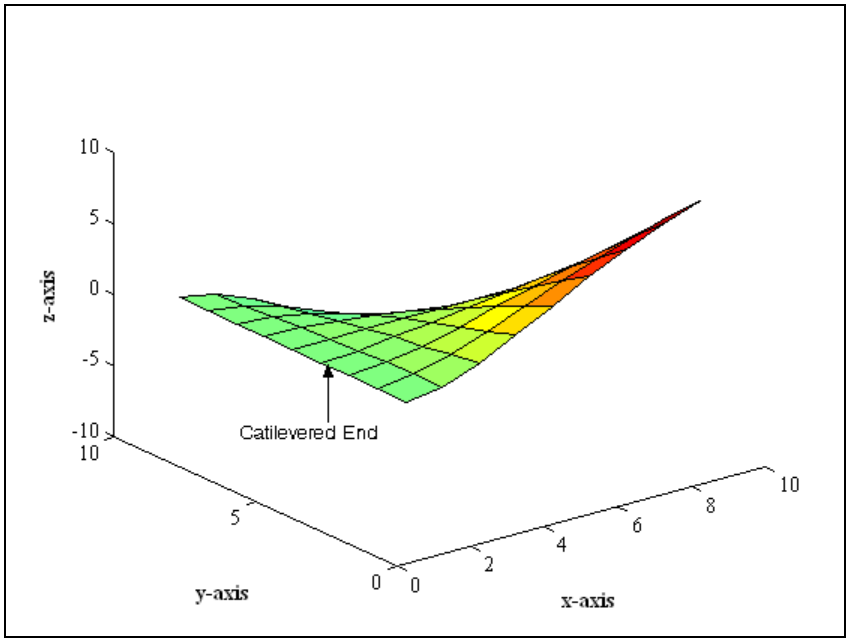

Figure 4.2b: Second mode shape

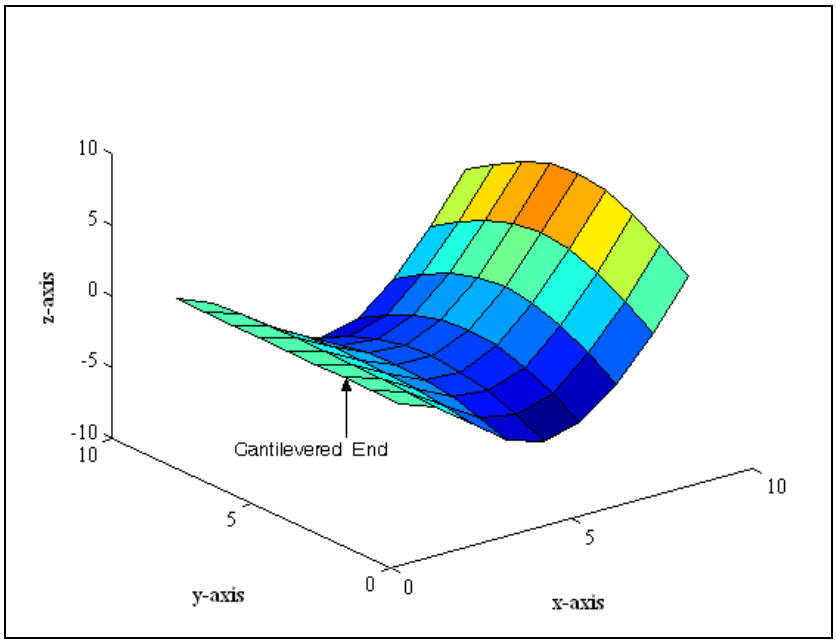

Figure 4.2c: Third mode shape

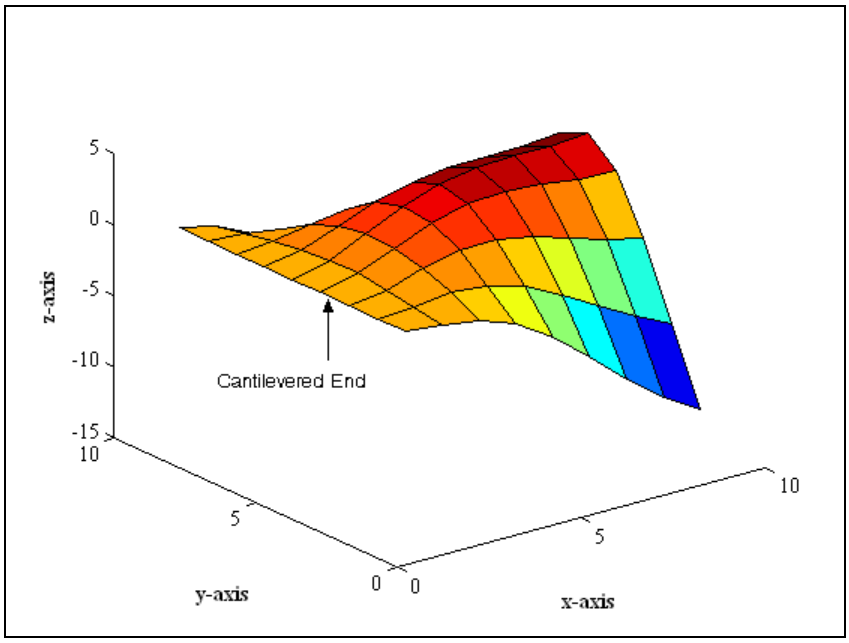

Figure 4.2d: Fourth mode shape

4.2 Active Vibration Control Law

Vibrations of the 'smart piezo structure' can be controlled using a suitable control law. In practice, only the first few vibration modes are of interest. Structural vibrations can be controlled if dominating modes are controlled. This control approach is known as 'modal control' and is commonly used in active vibration control. Uncoupled equations of motion are used to control the desired vibration modes using appropriate control law. External control voltage to be applied on the actuator for controlling the structural vibrations depends upon the sensor signal, number of modes to be controlled and the type of control law to be used. In the present work, we will apply 'negative velocity feedback' control law for controlling the vibrations of cantilevered smart piezo plate structure. Using 'negative velocity feedback' control algorithm, one can control only one vibration mode of the structure. In case of a cantilevered smart piezo plate structure displaced vertically, the vibration response would be dominated by first modal vibrations. In present work, our aim is to control the first modal vibrations of the cantilevered smart piezo plate structure. For controlling the first mode of vibrations, 'negative velocity feedback' control law is [92]:

$$\text{First modal control force} = -k\dot{\eta}_1 \tag{4.3}$$

where 'k' is the gain and '$\dot{\eta}_1$' is the first modal velocity. From equation (3.43), the modal control force is obtained as:

$$\{f_c\} = -[U]^T \left(\left[k_{uv}^e \right] + \left[\bar{k}_{uv}^e \right] \right) Z_{sensor}^{-1} Z_{act} V_{ext} \tag{4.4}$$

When identical PZT-5H sensor and actuator are at same 'ambient temperature':

$$Z_{sensor} = Z_{act}$$

The 'first modal control force' now becomes:

$$\{f_c\}_1 = -\left(\left[U\right]^T\left(\left[k_{uv}^e\right]+\left[\bar{k}_{uv}^e\right]\right)\right)_1 V_{ext} \tag{4.5}$$

Comparing equations (4.3) and (4.5), we get:

$$\left(\left[U\right]^T\left(\left[k_{uv}^e\right]+\left[\bar{k}_{uv}^e\right]\right)\right)_1 V_{ext} = k\dot{\eta}_1$$

which gives:

$$V_{ext} = \frac{k\dot{\eta}_1}{\left(\left[U\right]^T\left(\left[k_{uv}^e\right]+\left[\bar{k}_{uv}^e\right]\right)\right)_1} \tag{4.6}$$

where first modal velocity '$\dot{\eta}_1$' is estimated using Kalman observer. Equation (4.6) calculates the external voltage to be applied on the piezoelectric actuator patch for controlling the first modal vibrations of smart piezo plate structure.

4.3 Estimation of Modal Vectors Using Kalman State Observer

As can be observed from equation (4.6), external voltage to be applied on piezoelectric actuator patch using to negative first modal velocity feedback control law to control the first modal vibrations depends upon first modal velocity '$\dot{\eta}_1$'. First modal velocity cannot be measured by a single sensor patch. However, modal displacements and modal velocities can be estimated using Kalman state observer/estimator. A computer program which estimates/observes full state vector is called a state estimator/observer. Kalman state observer can be constructed using following equations [141]:

$$\{\eta_e\} = \left[A_d\right]\{\eta_e\} + \left[B_d\right]V_{ext} + \left[L\right](v_{sensor} - \left[X\right]\{\eta_e\}) \tag{4.7}$$

$$\{\eta_e\} = \{\eta_e\} + \left[M\right](v_{sensor} - \left[X\right]\{\eta_e\}) \tag{4.8}$$

where $\{\eta_e\}$ is estimated full state vector, matrices $[A_d]$ and $[B_d]$ are the discretized forms of matrices $[A]$ and $[B]$ of the state equation. $[L]$ and $[M]$ are Kalman observer gain matrices. Matrix $[X]$ is obtained from output equation of the state space model.

4.4 Dependence of Various Parameters on Piezoelectric Stress Coefficient (e_{31}) and Permittivity ($\in_{33}$)

Performance of active vibration control technique depends upon: (i) sensor voltage (ii) Kalman state observer (iii) control voltage (iv) control efforts (v) thermal strain effect and (vi) pyroelectric effect. In this section, we will show that all these factors depend upon piezoelectric stress coefficients 'e_{31}' and permittivity '$\in_{33}$'.

4.4.1 *Sensor Voltage*

From equation (3.56), voltage generated across PZT-5H sensor is given by:

$$v_{sensor} = \frac{\left(Q_{pyro} + \left(\left[k_{vu}^{e}\right] + \left[\bar{k}_{vu}^{e}\right]\right)\{u_e\}\right)}{Z_{sensor}} \tag{4.9}$$

After substituting the values of Q_{pyro}, $\left[k_{vu}^{e}\right]$, $\left[\bar{k}_{vu}^{e}\right]$, $\left[k_{vv}^{e}\right]$, $\left[\bar{k}_{vv}^{e}\right]$ and $\{u_e\}$ from equations (3.25), (3.26) and (3.33) into equation (4.9) we get:

$$v_{sensor} = \frac{\left(\frac{1}{2}\int_P \{p\}^T \{B_v\}\Delta T dT + \left(\int_P z\{B_v\}^T \left[e^T\right][B_u]d\tau + \int_P z\{B_v\}^T \left[\bar{e}\right][B_u]\Delta T d\tau\right)[U]\{\eta\}\right)}{\left(\int_P v\{B_v\}^T \left[\in^T\right]\{B_v\}d\tau + \int_P v\{B_v\}^T \left[\bar{\in}\right]\{B_v\}\Delta T d\tau\right)}$$

which gives:

$$v_{sensor}\, \alpha\, \frac{e_{31}}{\in_{33}}\{\eta\} \tag{4.10}$$

Thus, sensor voltage is directly proportional to the product of piezoelectric stress coefficient 'e_{31}' and modal displacement 'η' and inversely proportional to the permittivity '$\in_{33}$'.

4.4.2 *Kalman State Observer*

Matrices $[B],[X],[L]$ and $[M]$ appearing in Kalman state observer equations (4.7) and (4.8) depend upon 'e_{31}' and '$\in_{33}$'. Therefore, modal state vectors would depend upon 'e_{31}' and '$\in_{33}$'. In other words, first modal velocity '$\dot{\eta}_1$' estimated by Kalman observer depends upon 'e_{31}' and '$\in_{33}$'.

4.4.3 *Control Voltage*

The control voltage to be applied on piezoelectric actuator patch in order to control the first modal vibrations of smart piezo plate structure is given by equation (4.6):

$$V_{ext} = \frac{k\dot{\eta}_1}{\left([U]^T\left(\left[k_{uv}^e\right]+\left[\bar{k}_{uv}^e\right]\right)\right)_1}$$

After substituting the values of $\left[k_{uv}^e\right]$ and $\left[\bar{k}_{uv}^e\right]$ from equation (3.25) into above equation we get:

$$V_{ext} = \frac{k\dot{\eta}_1}{\left([U]^T\left(\int_P z\{B_v\}^T\left[e^T\right][B_u]d\tau+\int_P z\{B_v\}^T\left[\bar{e}\right][B_u]\Delta T d\tau\right)\right)_1}$$

This gives:

$$V_{ext}\,\alpha\,\frac{1}{e_{31}}\dot{\eta}_1 \tag{4.11}$$

Therefore, external control voltage to be applied on piezoelectric actuator is directly proportional to modal velocity '$\dot{\eta}_1$' and inversely proportional to piezoelectric stress coefficient 'e_{31}'.

4.4.4 *Control Effort*

Control effort is defined as the total work done by controller on the system to settle down structural vibrations upto a pre-defined limit. It is the electrical power consumed by controller multiplied by time. Power consumption in a 'smart piezo structure' depends upon the admittance of 'smart piezo structure' and external applied voltage. Magnitude of power consumed in a 'smart piezo structure' can be calculated using electro-mechanical impedance method [239] as:

$$\text{Power consumed} = \sqrt{\left[\frac{V_0^2}{2} * \text{Re}(Y)\right]^2 + \left[\frac{V_0^2}{2} * \text{Im}(Y)\right]^2} \tag{4.12}$$

where, 'V_0' is peak control voltage applied to actuator. '$\text{Re}(Y)$' and '$\text{Im}(Y)$' are real and imaginary parts of coupled electromechanical admittance respectively for piezoelectric actuator. '$\text{Re}(Y)$' is proportional to 'e_{31}' and '$\text{Im}(Y)$' is proportional to both 'e_{31}' and '$\in_{33}$'. Using equation (4.12), control effort applied by controller to actively control one cycle of structural vibrations can be calculated as:

$$\text{Control effort} = (\text{Power consumed}) \times (\text{Time Period}) \tag{4.13}$$

Now, total control effort can be calculated by adding control effort to actively control each cycle of structural vibrations up to the desired limit. As power consumed in a 'smart structure' depends upon 'e_{31}' and '$\in_{33}$', therefore 'total control effort' also depends upon 'e_{31}' and '$\in_{33}$' coefficients.

4.4.5 *Thermal Strain Effect*

When 'ambient temperature' is other than 'reference temperature', introduction of thermal stresses as a result of different thermal expansion coefficients of the host structure and piezo electric material causes 'thermal strain effect'. It affects the performance of 'smart piezo structure'. In addition to the dynamic voltage due to structural vibrations, a static voltage is generated across piezoelectric sensor due to 'thermal strain effect'. Active vibration control law is defined to control only structural vibrations. Static sensor voltage as a result of thermal strain is removed before entering into the controller so that it is not wrongly attributed to signal due to structural vibrations. To do so, static sensor voltage due to 'thermal strain effect' is estimated at particular 'ambient temperature' and subsequently removed from the sensor output before the calculation of control voltage so that optimum control efforts are applied on actuator. Static sensor voltage developed on piezoelectric patch depends upon the static strains developed across the sensor as a result of 'thermal strain effect'. Therefore, static sensor voltage due to 'thermal strain effect' can be measured using equation (4.9). This gives static sensor voltage due to thermal strains as:

$$V_{tse} \alpha \frac{e_{31}}{\in_{33}} \tag{4.14}$$

Clearly, static voltage as a result of 'thermal strain effect' is directly proportional to 'e_{31}' and inversely proportional to '$\in_{33}$'. Due to different 'e_{31}' and '$\in_{33}$' coefficients of piezoelectric sensor and actuator patches under closed loop conditions, generation of static voltage as a result of 'thermal strain effect' induces a net static displacement in

smart piezo plate [71]. As a result, 'equilibrium position' of the smart piezo plate also changes under closed loop conditions.

4.4.6 *Pyroelectric Effect*

Since time immemorial, people in India and Ceylon knew that a tourmaline crystal when placed in hot ashes, first attracts and then repels the ashes. That is why this crystal was known as 'Ceylon Magnet' till the middle of 18^{th} century. In 1756, Aepinus noted opposite polarities at the two ends of heated tourmaline crystal. Brewster gave it the name 'pyroelectricity' in 1824. He also observed the 'pyroelectric effect' in Rochelle salt. The first definite theory of pyroelectricity was given by Lord Kelvin who postulated a state of permanent polarization in every pyroelectric crystal. Those crystals having one or more axes, whose ends are unlike, that is to say hemihedral crystals with oblique faces, have the special physical property of giving rise to two electric poles of opposite signs at the extremities of these axes when they are subjected to a change in temperature [1]. Pyroelectricity was discovered much before the discovery of 'piezoelectricity'. Every pyroelectric crystal is also piezoelectric.

The basic characteristic of piezoelectric materials which enable them to be used as sensors and actuators are: direct piezoelectric effect, converse piezoelectric effect and 'pyroelectric effect'. In 'pyroelectric effect', the piezoelectric material responds to changes in temperature by producing an electrical response. Just like 'thermal strain effect', a static voltage is generated across piezoelectric sensor due to 'pyroelectric effect'. If a piezoelectric material is eloctroded and connected to an external circuit which integrates the charge, the pyroelectric coefficient is defined as [67]:

$$p = \frac{\Delta(Q/A)}{\Delta T} = \frac{1}{A}\frac{\Delta Q}{\Delta T}$$

where 'A' is electrode area and ΔQ is the change in total charge due to change in sample temperature ΔT. Charge generated (Q) and voltage (V) are related to the capacitance (Z) as:

$$Q = ZV$$

Therefore, static voltage on piezoelectric sensor and actuator patches as a result of 'pyroelectric effect' is calculated as:

$$\begin{aligned} (V_{pyro})_{sensor} &= \frac{\left(Q_{pyro}\right)_{sensor}}{Z_{sensor}} \\ (V_{pyro})_{act} &= \frac{\left(Q_{pyro}\right)_{act}}{Z_{act}} \end{aligned} \tag{4.15}$$

Simply by inspection of terms appearing in Q_{pyro}, Z_{sensor} and Z_{act} expressions, we find:

$$V_{pyro} \ \alpha \ \frac{1}{\in_{33}}$$

Therefore, static voltage as a result of 'pyroelectric effect' is inversely proportional to '$\in_{33}$'. Negative velocity feedback control law given by equation (4.6) is defined to control only structural vibrations. These structural vibrations generate dynamic voltages across the sensor. We need to manipulate only these dynamic voltages in control law. Therefore while implementing active vibration control scheme practically, static sensor voltage as a result of pyroelectric effects is pre-estimated and removed before entering into the controller so that it is not wrongly attributed to structural vibrations. This would provide accurate information to the controller and optimum control efforts can be applied on actuator. Further, due to different 'e_{31}' and '$\in_{33}$' coefficients of piezoelectric sensor and actuator patches under closed loop conditions, generation of static voltage as a result

of 'pyroelectric effect' induces a net static displacement in smart piezo plate. As a result, 'equilibrium position' of the smart piezo plate changes under closed loop conditions.

4.5 Contribution of the Proposed Temperature Robust Control Scheme

We have seen that: (i) sensor voltage (ii) control voltage (iii) Kalman state observer (iv) control efforts (v) thermal strain effect and (vi) pyroelectric effect all depend upon either piezoelectric stress coefficient 'e_{31}' or the permittivity '$\in_{33}$' or both. At temperatures other than 'reference temperature' of the piezoelectric material, piezoelectric stress coefficient 'e_{31}' and the permittivity '$\in_{33}$' have different values. At such temperatures, 'e_{31}' and '$\in_{33}$' values measured at 'reference temperature' can not be considered. If temperature dependence of 'e_{31}' and '$\in_{33}$' is ignored then: (i) sensor and actuator behaviour can not be accurately estimated (ii) modal state vectors of the 'smart structure' are wrongly estimated by Kalman state observer (iii) static sensor voltages generated as a result of thermal strain and pyroelectric effects are wrongly calculated and (iv) 'equilibrium position' of the 'smart piezo structure' is also wrongly estimated. As a result, the controller applies wrong control voltages on actuator. The active vibration control performance will not be maintained and the scheme fails at temperatures substantially away from 'reference temperature' of the piezoelectric material. Therefore existing active vibration control technique wherein temperature dependence of 'e_{31}' and '$\in_{33}$' is ignored, is non-robust to temperature variations.

In present work, the active vibration control scheme is derived using augmented constitutive equations which take into account temperature dependence of piezoelectric stress coefficient 'e_{31}' and permittivity '$\in_{33}$'. Since temperature dependence of 'e_{31}'

and '$\in_{33}$' is not analytically known so their experimental values measured at ambient temperatures are used via curve fit method. Control law so derived, applies required control voltages on piezoelectric actuator at different ambient temperatures according to the need of 'smart piezo structure'. When augmented piezoelectric constitutive equations are used: (i) sensor and actuator behaviour (ii) modal state vectors of the 'smart structure' measured by Kalman state observer (iii) static sensor voltages generated as a result of thermal strain and pyroelectric effects and (iv) 'equilibrium position' of the 'smart piezo structure' are all accurately estimated at all temperatures. As a result, the controller applies accurate control voltages on the actuator at all temperatures. Active vibration control performance is maintained at each temperature and the scheme therefore becomes robust to temperature variations.

4.6 Results and Discussions

A computer program has been written in MATLAB for the state space model, active vibration control law and Kalman state observer derived in present work. Using this computer code, simulation results on active vibration control of a smart cantilevered plate instrumented with one piezoelectric sensor-actuator pair are presented at different ambient temperatures ranging from -75 to 160°C. A square isotropic steel plate with material properties given in Table 4.2 is considered as host structure. Material properties of isotropic steel plate are constant over the temperature range considered. A square piezoceramic PZT-5H patch with material properties given in Table 4.2 is used as sensor and an identical patch of same material and size is used as an actuator. The plate structure is divided into 64 finite elements, each having dimensions 2cm x 2cm and marked as per

Property	Units	Host Structure	Piezoceramic (PZT-5H)
Length	m	0.16	0.02
Breadth	m	0.16	0.02
Thickness	m	0.0006	0.00106
Density	kgm^{-3}	7800	7500
Young's Modulus	Nm^{-2}	2.07×10^{11}	6.76×10^{10}
Poisson's Ratio	unitless	0.3	0.3
Curie Temperature	^oC	-	190
Reference Temperature	^oC	25	25
Dielectric Constant	unitless	-	3200
Rayleigh Damping Coefficients	rad sec^{-1}	$\alpha = 0.01$	
	sec	$\beta = 0.00016$	

Table 4.2: **Material properties of smart piezo plate.**

plan shown in Figure 4.3. For stable negative velocity feedback control, sensor and actuator are bonded to the host at 'reference temperature' in such a way so as to form a perfect collocated sensor-actuator pair [91] as shown in (Figure 3.2b). The optimal placement of collocated sensor-actuator pair is at location '12' (Figure 4.3) for first mode control of a cantilevered plate [7]. This location is near the cantilevered edge and is the region of high average strains. The smart piezo plate so formed is cantilevered along one edge (Figure 3.2a). It is assumed that temperature of smart piezo plate is same as ambient temperature. In absence of any thermal gradient, dynamic vibrations are not induced. Cantilevered smart plate is now disturbed by giving initial vertical displacement of 2 mm to the free edge opposite to the cantilevered edge at known ambient temperature. This type of disturbance would excite the first vibration mode predominantly. Peak sensor

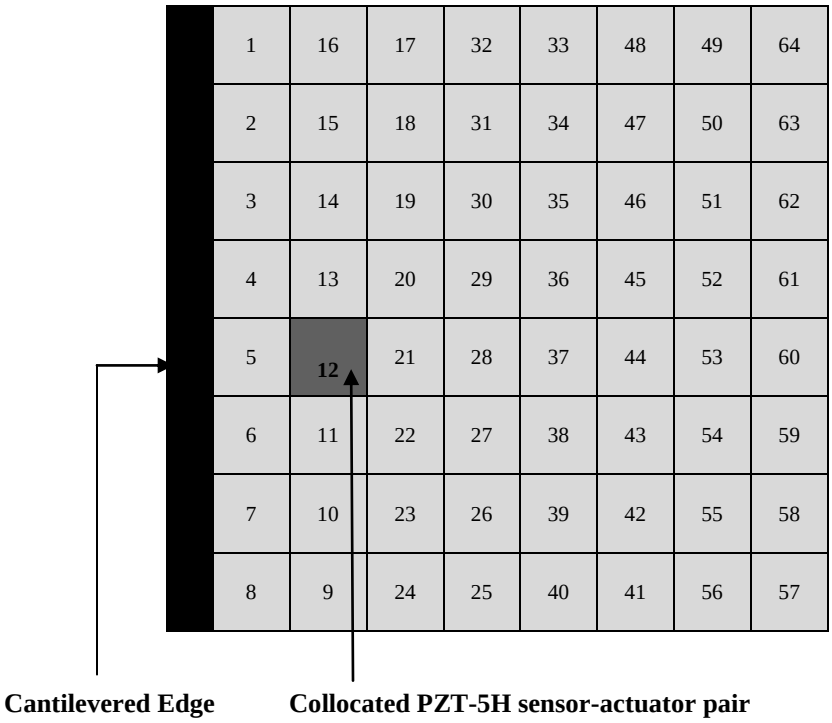

Figure 4.3: Top view of the smart piezo plate structure cantilevered along one edge and instrumented with one optimally placed collocated PZT-5H sensor-actuator pair

voltage, actual and estimated first modal velocity, static sensor voltage and static displacement in equilibrium position are studied and compared at various ambient tempeeratures ranging from -75 to 160°C under two cases: (i) when temperature dependence of 'e_{31}' and '$\in_{33}$' is not included in piezoelectric constitutive equations and (ii) when temperature dependence of 'e_{31}' and '$\in_{33}$' is included in piezoelectric constitutive equations. First modal vibrations so developed, are actively controlled at various ambient temperatures ranging from -75 to 160°C using: (i) existing control law which do not include temperature dependence of 'e_{31}' and '$\in_{33}$' (Non-robust control with respect to temperature) and (ii) temperature robust control law given by equation

(4.6) which do include temperature dependence of 'e_{31}' and '$\in_{33}$' (Robust control with respect to temperature).

4.6.1 *Sensor Output*

Figure 4.4 shows variation of piezoceramic PZT-5H peak sensor voltage with ambient temperature when edge of smart plate opposite to the cantilevered edge is

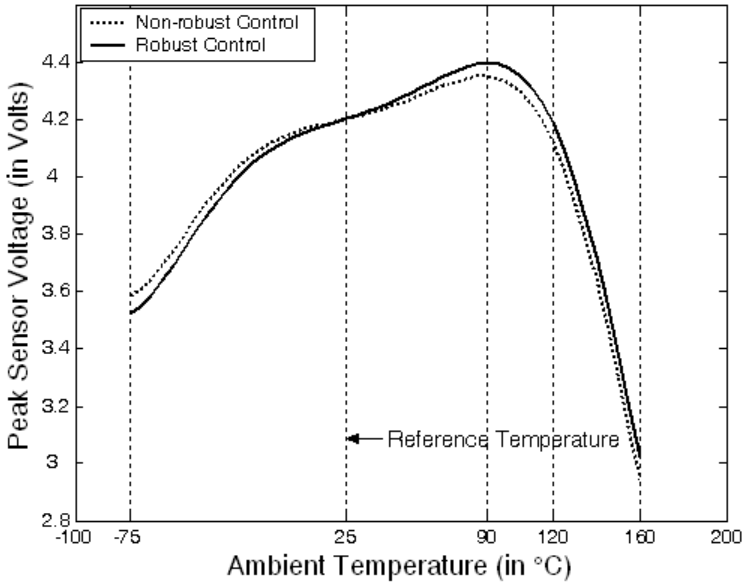

Figure 4.4: A variation of PZT-5H peak sensor voltage with ambient temperature

initially displaced by 2 mm. It is observed that peak sensor voltage increases initially with increase in ambient temperature. After ambient temperature 90ºC, say 'inversion temperature', it decreases with further increase in ambient temperature. This happens because both 'e_{31}' and '$\in_{33}$' increase with ambient temperature (Figure 3.1) and sensor voltage is proportional to $\frac{e_{31}}{\in_{33}}$. Up to 'inversion temperature', 'e_{31}' dominates '$\in_{33}$' and the reverse happens afterwards. Peak sensor voltage decreases sharply after 120ºC as

'$\in_{33}$' increases sharply at such temperatures (Figure 3.1). Below 'reference temperature', peak sensor voltage is less when robust control law is used. However above 'reference temperature', it is higher than that in case of non-robust control law. At 'reference temperature', peak sensor voltage using robust and non-robust control laws is same. This trend has been observed experimentally [75].

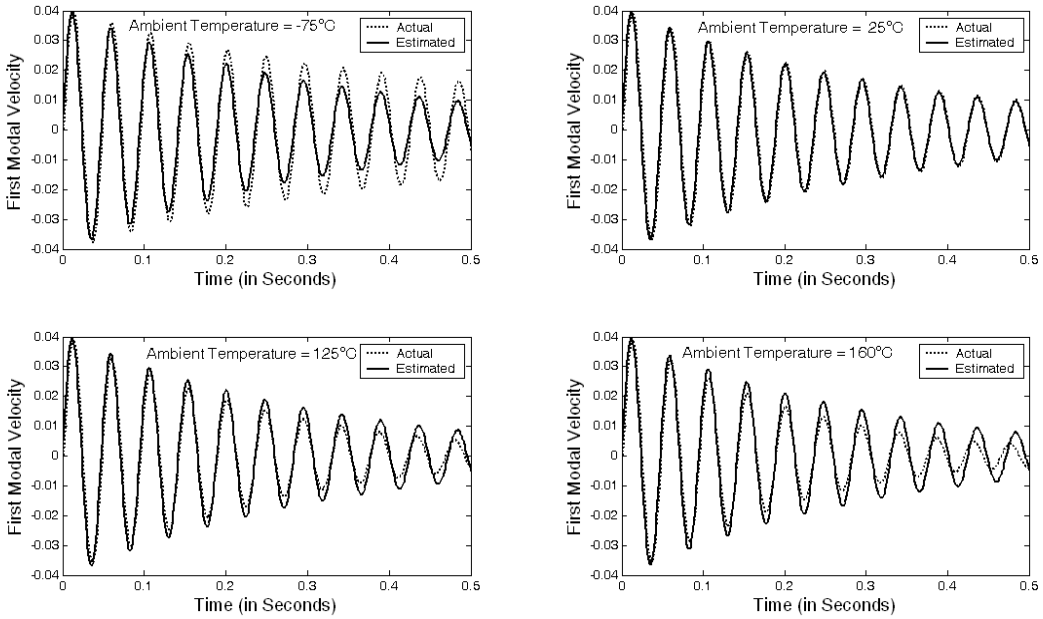

Figure 4.5a: **Plots for actual and estimated first modal velocities with time at different ambient temperatures when temperature dependence of 'e_{31}' and '$\in_{33}$' is not included in piezoelectric constitutive equations**

4.6.2 *Estimator Output*

Figure 4.5a shows time response of first modal velocity estimated by Kalman observer and the actual first modal velocity when temperature dependence of 'e_{31}' and '$\in_{33}$' is not included in piezoelectric constitutive equations. It can be seen when 'ambient temperature' is less than 'reference temperature', estimated first modal velocity is less than actual one. When 'ambient temperature' is more than 'reference temperature',

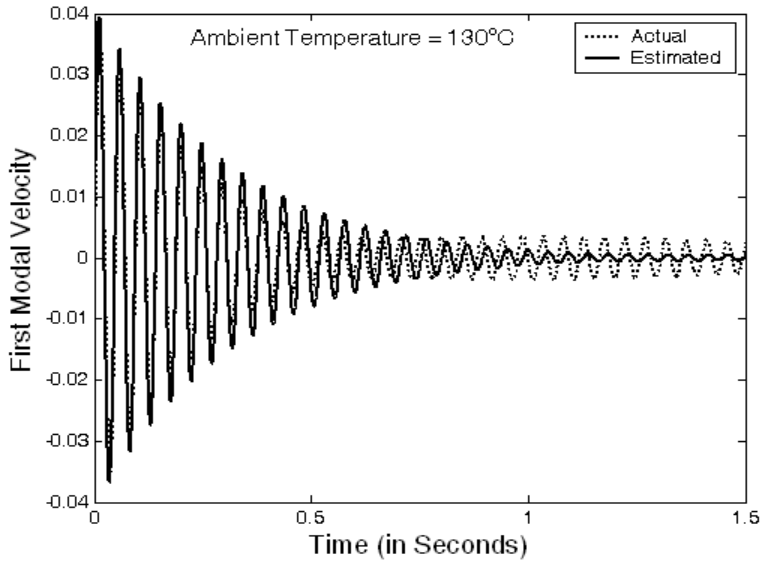

Figure 4.5b: A plot showing excited actual first modal velocity at higher ambient temperature when temperature dependence of 'e_{31}' and '$\in_{33}$' is not included in piezoelectric constitutive equations

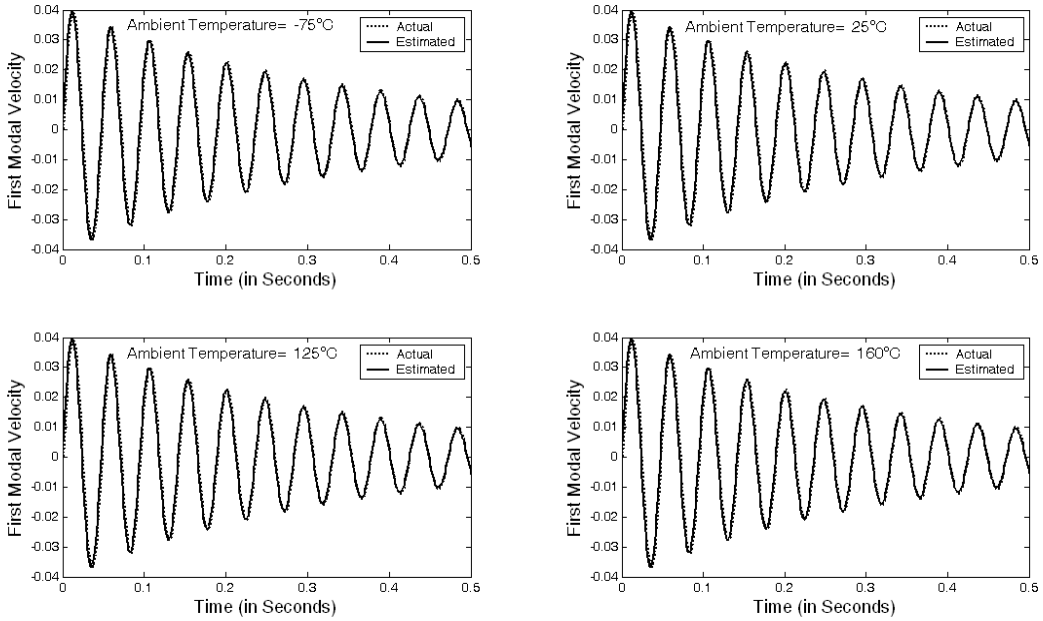

Figure 4.5c: Plots for actual and estimated first modal velocities with time at different ambient temperatures when temperature dependence of 'e_{31}' and '$\in_{33}$' is included in piezoelectric constitutive equations

estimated first modal velocity is more than actual one. More the difference between ambient and reference temperatures, more is the mismatch between estimated and actual signals. However at 'reference temperature', actual and estimated signals are same. When 'ambient temperature' is sufficiently higher than 'reference temperature', a phase difference is also present between estimated and actual signals. As a result, actual first modal velocity gets excited at higher temperatures (Figure 4.5b). Thus, Kalman observer is not able to estimate accurately when ambient temperatures are other than 'reference temperature'. However, when temperature dependence of 'e_{31}' and '$\in_{33}$' is included in piezoelectric constitutive equations, Kalman observer becomes robust to temperature variations and estimates accurately at all ambient temperatures (Figure 4.5c).

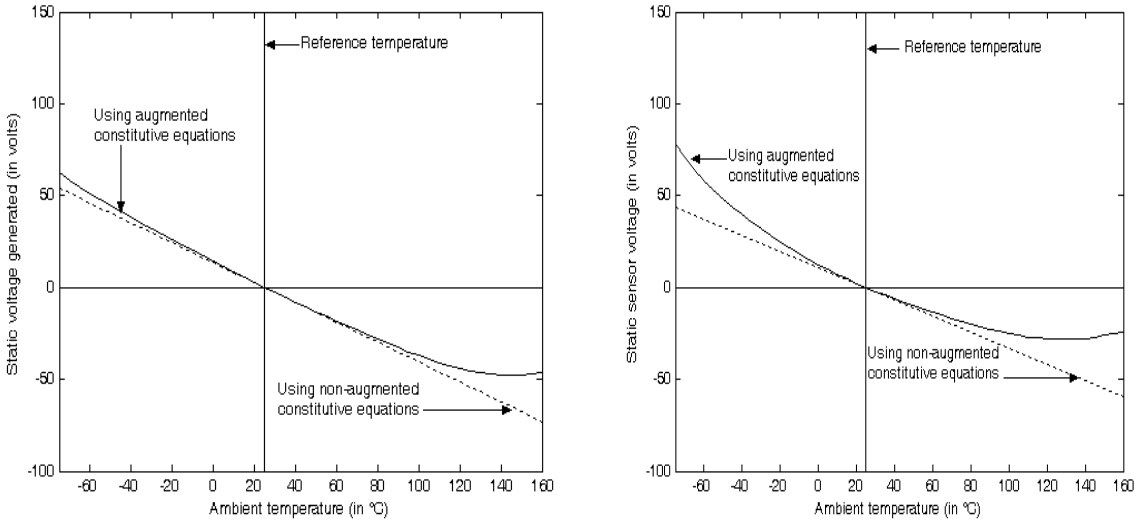

Figure 4.6a and Figure 4.6b: Static sensor voltage vs. 'ambient temperature' due to (a) thermal strain and (b) pyroelectric effects

4.6.3 *Static Sensor Voltage*

When 'ambient temperature' is other than 'reference temperature', a static voltage difference is generated across the electrodes of piezoceramic PZT-5H as a result of

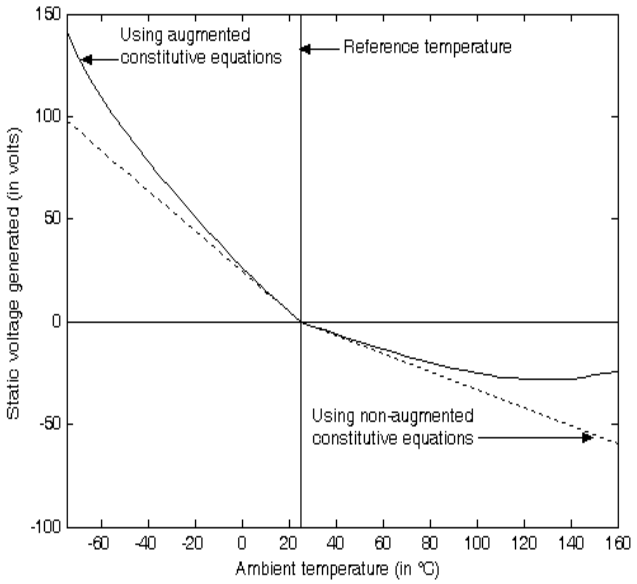

Figure 4.6c: A variation of static voltage generated vs. 'ambient temperature' due to combined thermal strain and pyroelectric effects

'pyroelectric effect'. In addition to this, thermally induced deformations/strains also introduce static voltage difference across PZT-5H. Static voltage so developed causes static deflection in smart piezo plate. Static sensor voltage due thermal strain and pyroelectric effects is compared for augmented and non-augmented constitutive equations in Figure 4.6a and Figure 4.6b. When 'ambient temperature' is less than 'reference temperature', static sensor voltage is always more using augmented constitutive equations. For 'ambient temperature' more than 'reference temperature', static sensor voltage is always less using augmented constitutive equations. Thermal strain effect dominates 'pyroelectric effect' at ambient temperatures higher than 'reference temperature' in both cases. At ambient temperatures less than 'reference temperature', 'pyroelectric effect' dominates 'thermal strain effect' when augmented equations are used. Static sensor voltage, as a result of combined thermal strain and pyroelectric effects is shown in Figure 4.6c. It is linear using non-augmented constitutive

equations and non-linear using augmented constitutive equations. As a result, control voltage would be different in both cases. This difference is significant and cannot be ignored in active structural vibration and precision control.

4.6.4 *Equilibrium Position*

Smart cantilevered plate is disturbed by giving initial vertical displacement of 2 mm to the free edge of plate opposite to cantilevered edge at different 'ambient temperatures'. First modal displacements at 'reference temperature' and at ambient temperature other than 'reference temperature' are compared under closed loop conditions. It is observed that equilibrium position is zero at 'reference temperature' (Figure 4.7a) and it is displaced from zero position when 'ambient temperature' is other than 'reference temperature' (Figure 4.7b and Figure 4.7c). This static displacement in equilibrium position is due to generation of static voltages across PZT-5H piezoceramic patches as a result of thermal strain and pyroelectric effects. Since static voltages so generated depend upon 'e_{31}' and '$\in_{33}$', equilibrium positions at various ambient temperatures would be different in case of non-augmented and augmented constitutive equations (Figure 4.7b and Figure 4.7c). Variation of equilibrium position with ambient temperatures is shown in Figure 4.7d for both the cases. It can be seen that equilibrium positions under these two cases are different. This difference in equilibrium positions is significant and cannot be ignored in active structural vibration and precision control.

4.6.5 *Peak Control Voltage*

Modal vibrations can be controlled by using the modal control law given by equation (4.6). This vibration control technique is known as active vibration control.

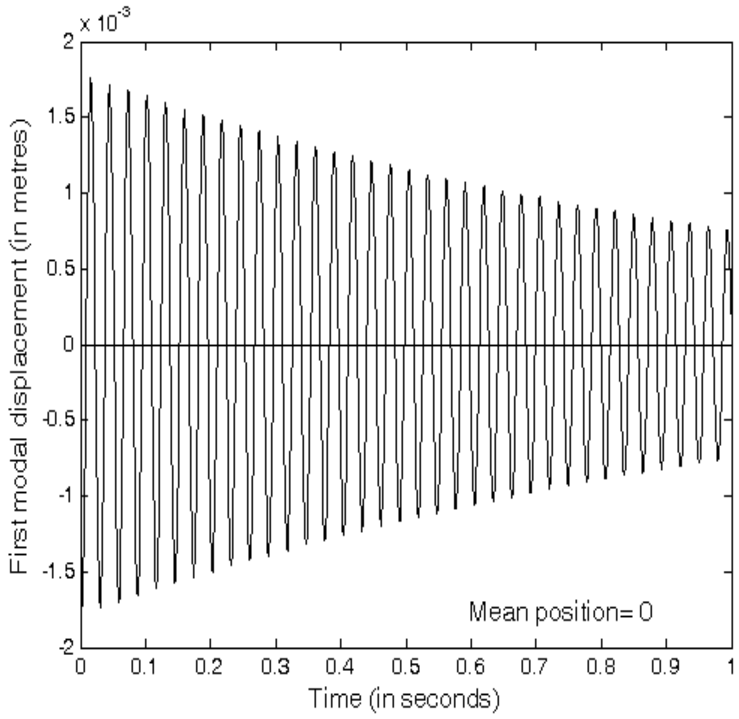

Figure 4.7a: First modal displacement at 'reference temperature'

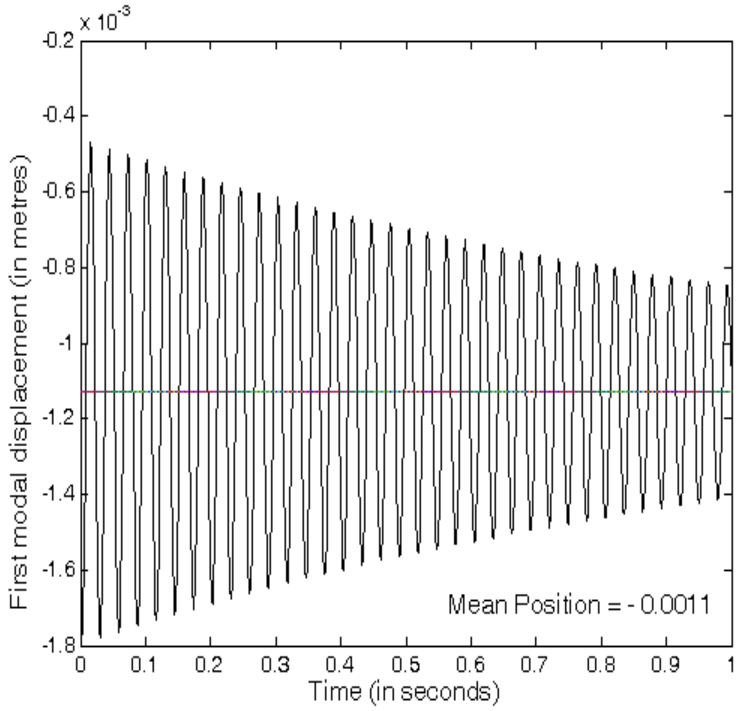

Figure 4.7b: First modal displacement at 'ambient temperature' 90°C using non-augmented constitutive equations

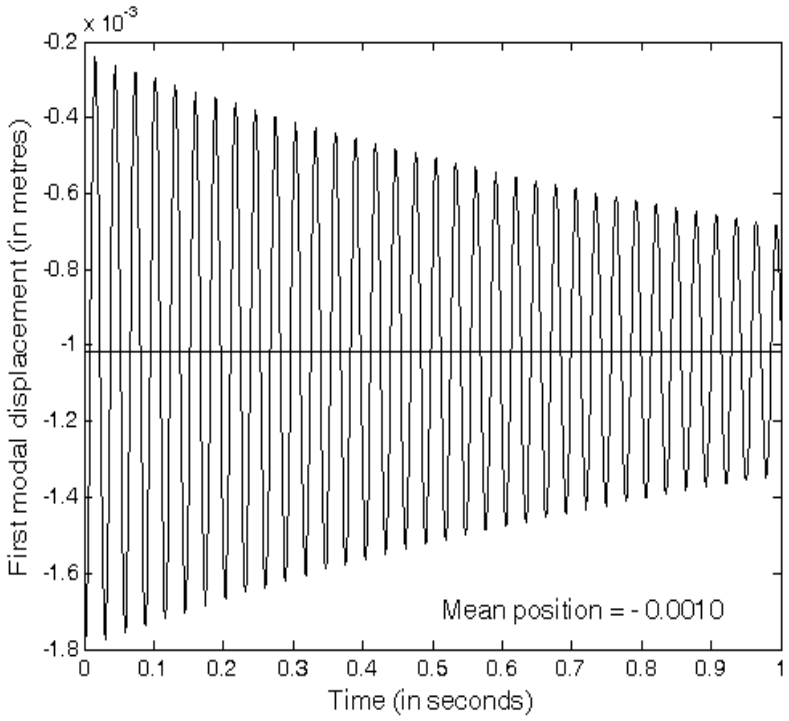

Figure 4.7c: First modal displacement at 'ambient temperature' 90ºC using augmented constitutive equations

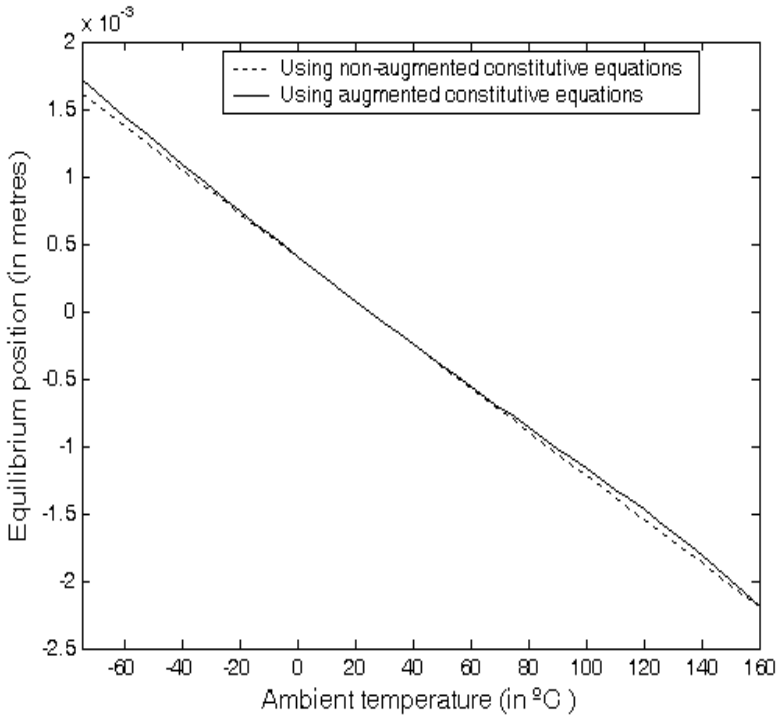

Figure 4.7d: A variation of 'equilibrium position' vs. 'ambient temperature'

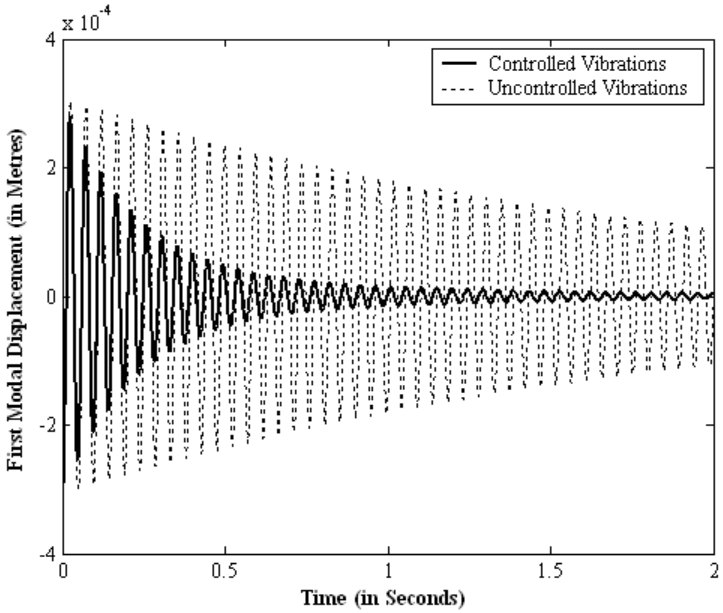

Figure 4.8a: First modal active vibration control of cantilevered smart piezo plate

Figure 4.8a shows the effectiveness of this control scheme wherein first modal vibrations of the smart cantilevered plate have been controlled using modal control law given by equation (4.6). This control law calculates the control voltages to be applied on the actuator. As sensing and actuation by piezoelectric materials depend upon 'e_{31}' and '$\in_{33}$', therefore control voltages to be applied on piezoelectric actuator patch should be different at different temperatures. Figure 4.8b shows a variation of 'peak control voltage' with 'ambient temperature'. It is observed the same peak control voltages are applied to actuator at all ambient temperatures when temperature non-robust control law is used. However, it decreases non-linearly with temperature when temperature robust control law is used. This happens because control voltage is directly proportional to $\frac{1}{e_{31}}\{\dot{\eta}_1\}$ and 'e_{31}' increases with increase in temperature for piezoceramic PZT-5H (Figure 3.1a). In case of temperature non-robust control law, peak control voltage is less

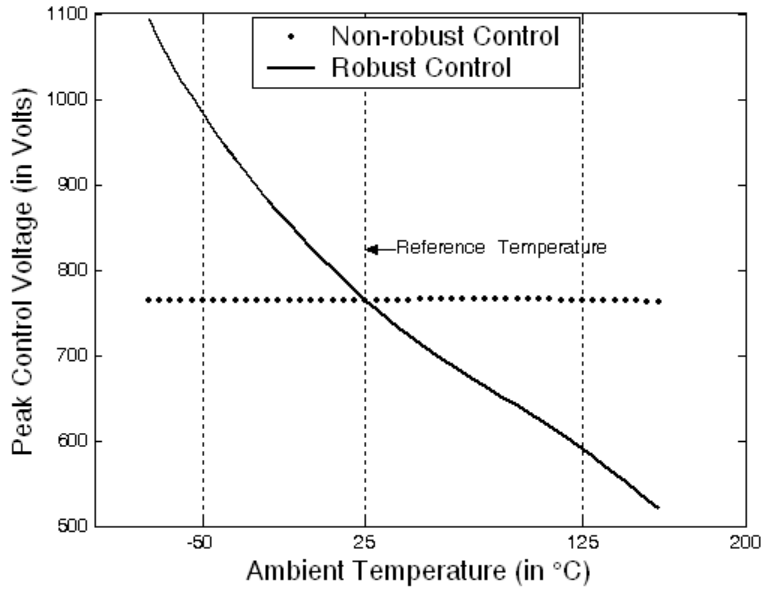

Figure 4.8b: A variation of 'peak control voltage' with 'ambient temperature' using (i) non-robust control and (ii) robust control laws with respect to temperature

at ambient temperatures below 'reference temperature' because $\{\dot{\eta}_1\}$ is under estimated and 'e_{31}' is treated as constant. Peak control voltage is more at ambient temperatures above 'reference temperature' because $\{\dot{\eta}_1\}$ is over estimated at these temperatures and 'e_{31}' is again treated as constant.

4.6.6 *Total Control Effort*

External control effort applied on piezo actuator should be able to cope with the demands of the 'smart piezo structure'. If it is less or more than required then there will be significant deterioration in active vibration control performance. Figure 4.9 shows a variation of 'total control effort' with 'ambient temperature' applied to 'smart piezo structure' in order to settle down first modal displacement up to $1/10^{th}$ of the peak value. It can be observed that 'total control effort' decreases non-linearly with increase in

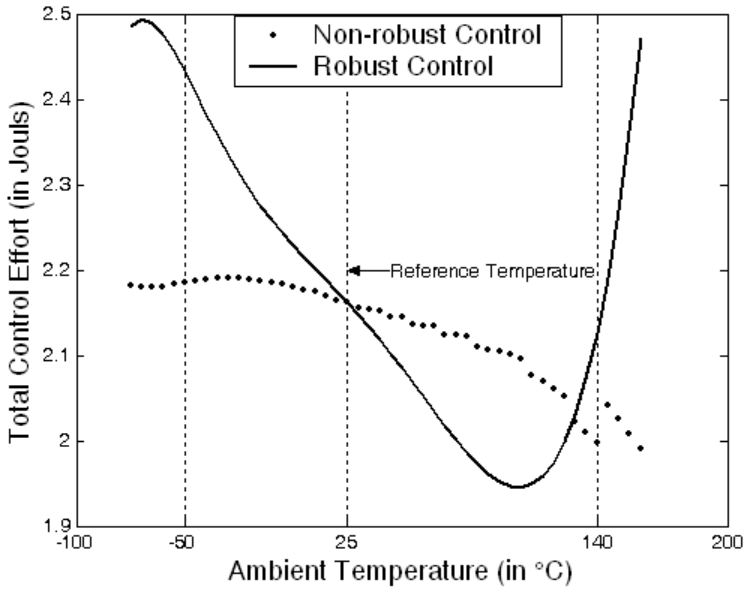

Figure 4.9: A variation of 'total control effort' with 'ambient temperature' using (i) temperature non-robust and (ii) temperature robust control laws

temperature in case of both non-robust and robust control laws. In case of robust control law, it also starts increasing non-linearly after 120ºC. When non-robust control law is used, less control effort is applied at ambient temperatures below 'reference temperature' because $\{\dot{\eta}_1\}$ is under estimated at these temperatures. At ambient temperatures above 'reference temperature', applied control efforts are more because $\{\dot{\eta}_1\}$ is over estimated. A sudden rise in control efforts is also observed after 140ºC. This can be attributed to the fact that actual first modal velocity gets excited at these temperatures. When robust control law is used, accurate control efforts are applied. Control effort applied on piezo actuator is directly proportional to '$\in_{33}$' which increases sharply after 120°C (Figure 3.1b). Therefore, 'total control effort' using robust control law also increases sharply after this temperature. This temperature is an 'optimal temperature' where minimum amount of energy is consumed.

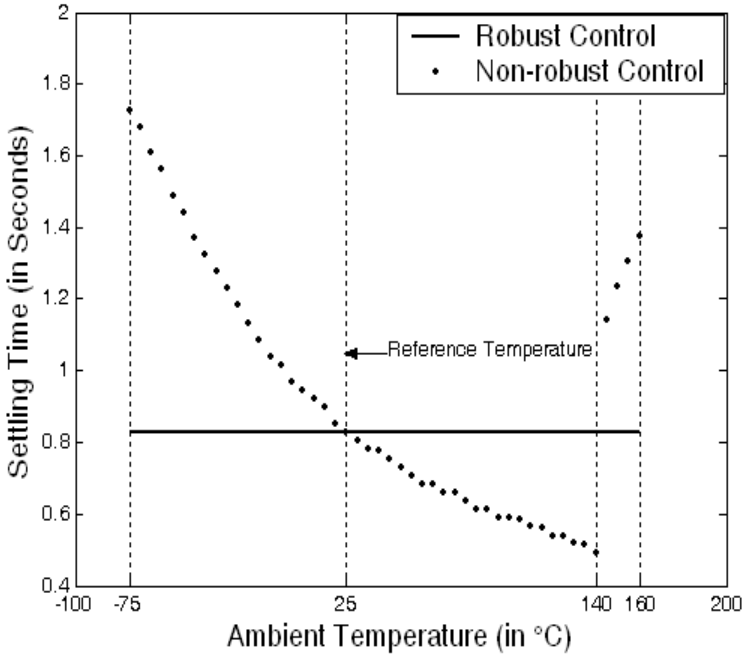

Figure 4.10: A variation of 'settling time' with 'ambient temperature' using (i) temperature non-robust and (ii) temperature robust control laws

4.6.7 *Settling Time*

Figure 4.10 shows variation of 'settling time' with 'ambient temperature'. Time taken to settle down first modal displacement upto $1/10^{th}$ of the peak value is considered as 'settling time'. As discussed in previous sub-section, control efforts applied on PZT-5H actuator are not accurate when control law is non-robust to temperature changes. It leads to deterioration in active vibration control performance. As a result, 'settling time' does not remain constant at all ambient temperatures and decreases non-linearly with temperature. Due to inadequate control efforts at higher temperatures, actual first modal velocity gets excited which leads to a sudden jump in settling time after 140°C**.** However when control law is robust to temperature changes, accurate control efforts are applied at all temperatures. Therefore, active vibration control performance is maintained and

settling time remains same at all ambient temperatures. In other words, active vibration control scheme becomes robust to temperature variations when temperature dependence of ' e_{31} ' and ' $\in_{33}$ ' is included in piezoelectric constitutive equations.

CHAPTER V

ACTIVE VIBRATION CONTROL OF SMART PIEZO PLATE: EXPERIMENTS

Simulation results given in previous chapter suggest that active vibration control performance can be maintained at ambient temperatures other than 'reference temperature' of the piezoelectric materials. To do so, temperature dependence of piezoelectric stress coefficient 'e_{31}' and permittivity '$\in_{33}$' need to be included in piezoelectric constitutive equations. It enables Kalman observer to estimate the modal state vectors accurately. Active vibration control law thus derived applies required control voltages on piezoelectric actuator at all temperatures according to the need of 'smart piezo structure'. This makes active vibration control technique robust to temperature variations. These findings encouraged the author to conduct experiments on active vibration control at elevated temperatures (temperatures higher than reference temperature). Therefore, experiments are planned to control the first vibration mode of cantilevered smart plate actively using a PZT-5H sensor-actuator patches pair at elevated temperatures ranging from 25°C to 75°C. For comparison, active vibration control technique has been applied at each temperature using two control schemes. First control scheme named as 'temperature non-robust control scheme', ignores temperature dependence of piezoelectric stress coefficient 'e_{31}' and permittivity '$\in_{33}$' in piezoelectric constitutive equations. Second control scheme named as 'temperature robust control scheme', considers temperature dependence of 'e_{31}' and '$\in_{33}$' in piezoelectric constitutive equations. It is found that active vibration control performance is not

maintained at elevated temperatures using ‘temperature non-robust control scheme’. It even fails when the temperature is significantly higher than the ‘reference temperature’ of the PZT-5H piezoelectric material. However, active vibration control performance is maintained at all elevated temperatures using ‘temperature robust control scheme’. This is the first successful attempt to achieve active structural vibration control of a ‘smart piezo structure’ at elevated temperatures. Following sections discuss experimental setup and the observations thereof.

5.1 Experimental Setup

A smart piezo plate structure was realized using various components namely:

1. A plate structure whose elastic properties are constant over the temperature range considered.
2. Two PZT-5H patches with length and breadth equal to that of one finite element of the plate.
3. Epoxy adhesive which can bond the PZT-5H patches perfectly to the host plate structure at least upto 80°C.
4. A mechanical clamp to cantilever one end of the plate structure.
5. A thermal chamber wherein any constant temperature between 25°C to 100°C can be maintained.
6. A signal conditioning system wherein the signal obtained from sensor can be conditioned.
7. A charge amplifier where the signal obtained from sensor can be amplified after conditioning.
8. A cathode ray oscilloscope wherein signals can be analyzed and stored.

9. A personal computer where the control algorithm is written in Lab VIEW 7.1 Real Time Software.

10. PXI Based Real Time System on which the control program can be downloaded from host PC and executed with minimal time delay.

11. Analog to digital data acquisition card.

12. Digital to analog data acquisition card.

13. A voltage amplifier to amplify the signal to be applied on actuator.

14. Connector box, ethernet cable, thin connecting wires etc.

Block diagram of the experimental setup is shown in Figure 5.1. Specially ordered square piezoceramic PZT-5H patches (composition: $PbZr_{0.53}Ti_{0.47}O_3$) of identical dimensions and material properties given in Table 5.1 were obtained from Central Electronics Limited (Figure 5.2a). A square isotropic galvanized iron plate with material properties given in Table 5.1 is considered as host structure. Elastic properties of piezoceramic PZT-5H and isotropic galvanized iron plate are constant over the temperature range considered. The plate structure is divided into 64 finite elements, each having dimension 2cm x 2cm and marked as per plan shown in Figure 4.3. Extra plate length is kept reserved for clamping purpose. Negative poling directions of both piezoceramic patches are fine soldered to thin connecting wires. Negative poling direction of the first PZT-5H patch assigned as sensor, is bonded to the plate structure at 'reference temperature' at location '12' using an epoxy adhesive. Negative poling direction of the second identical PZT-5H patch assigned as actuator, is bonded to the plate structure exactly opposite to the sensor patch at 'reference temperature' using epoxy adhesive. This forms a collocated sensor-actor pair (as shown in Figure 3.2b) which will

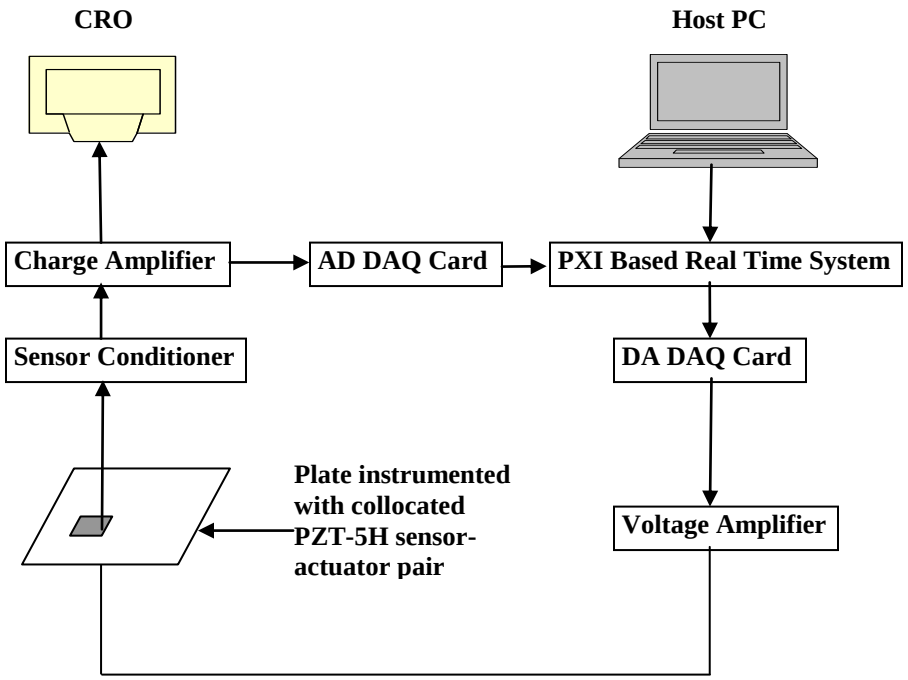

Figure 5.1: Block diagram of the experimental setup

ensure a stable active vibration control using 'negative velocity feedback' control law. Location '12' would be near the middle of cantilevered edge which is the optimal location to control the first vibration mode of a cantilevered plate structure [7]. Resulting piezo-plate structure is ready to be used for experimentation after curing time of 24 hours. Bonded negative poling directions of sensor-actuator pair act as common ground. Epoxy adhesive is able to bond the patches perfectly to the host structure upto 80°C after which it starts softening. Now, positive poling directions of both piezoceramic patches are also fine soldered to thin connecting wires carefully without adding any additional mass (Figure 5.2b). Plate so formed, is cantilevered along one edge with the help of a mechanical clamp (Figure 5.2c). Cantilevered plate is now inserted inside a thermal chamber wherein temperature between 25°C to 250°C (Figure 5.2d) can be maintained. Portions of connecting wires inside the thermal chamber are thermally insulated. Wires

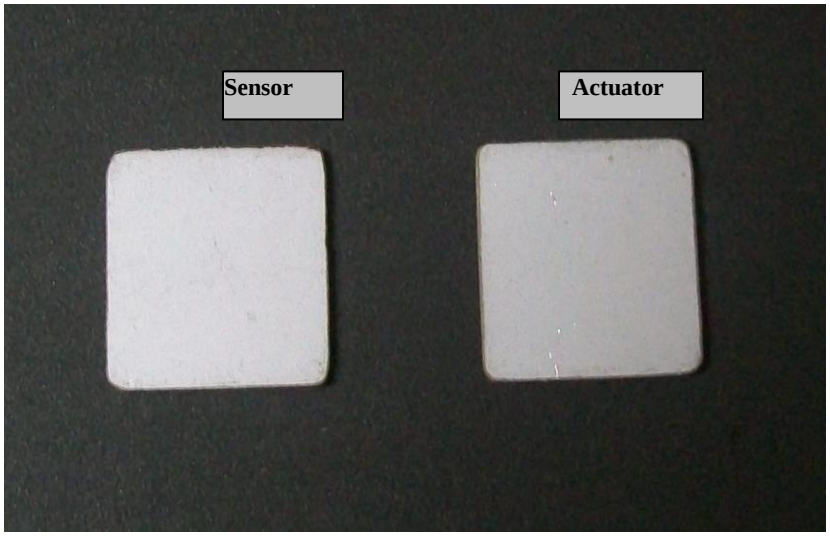

Figure 5.2a: Piezoceramic PZT-5H sensor-actuator pair

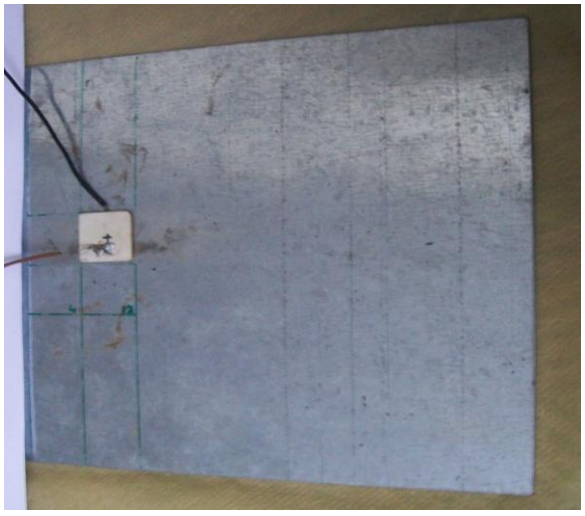

Figure 5.2b: Plate bonded with PZT-5H patch. Negative and positive poling directions are fine soldered to connecting wires

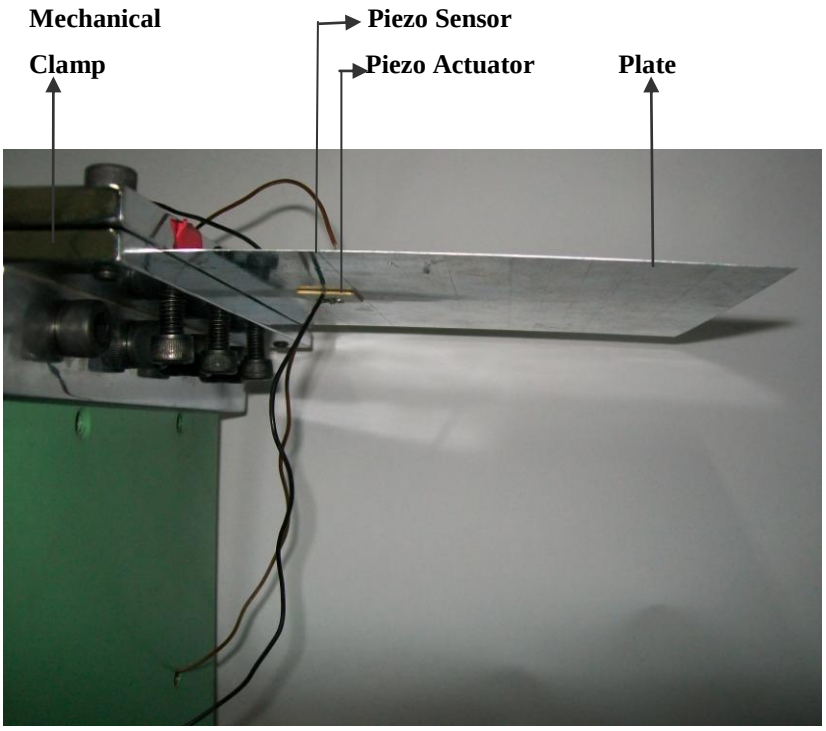

Figure 5.2c: Plate instrumented with collocated PZT-5H sensor-actuator pair cantilevered on a mechanical clamp

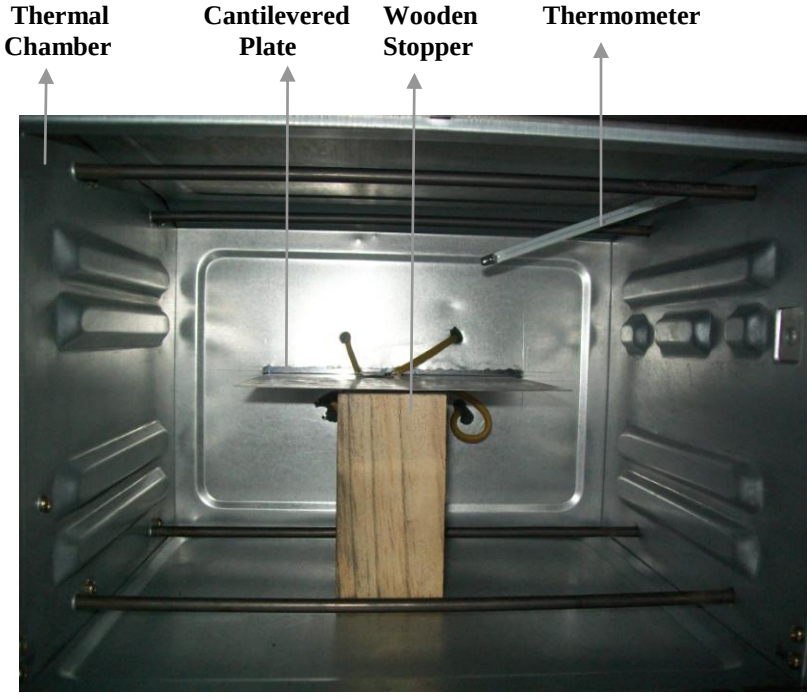

Figure 5.2d: Cantilevered plate placed inside thermal chamber (a wooden stopper is placed to ensure edge displacement of only 2mm)

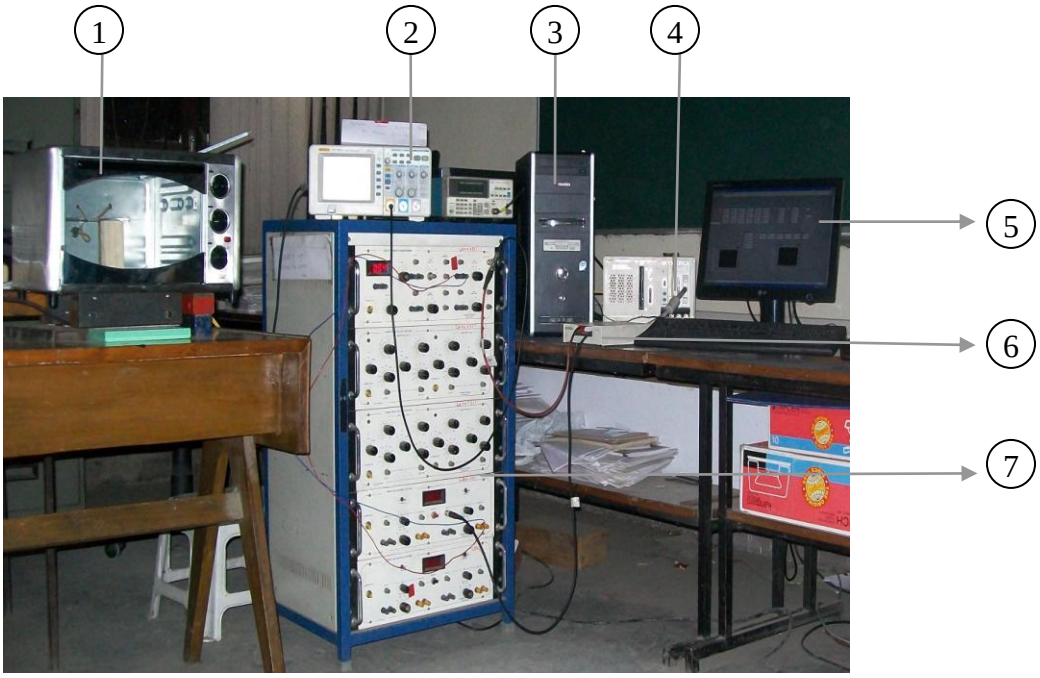

Figure 5.3: Experimental set up for realization of a smart piezo plate structure

1. **Thermal Chamber**
2. **Cathode Ray Oscilloscope**
3. **Central Processing Unit of Host PC**
4. **Real Time System with A/D and D/A DAQ Card**
5. **Monitor**
6. **Connector Box**
7. **Piezo-Sensor and Piezo-Actuator Signal Conditioner with Amplifiers**

coming out from the PZT-5H sensor are connected to the four channel sensor signal conditioning system (Spranktronics). A cathode ray oscilloscope (CRO) is also connected to the sensor signal conditioning system. Output of the signal conditioning system is connected to input channels of the connector box (National Instruments: SCB-68). Connector box is connected with 'PXI Based Real Time System' (National Instruments: PXI-1002) via ethernet cable and analog to digital data acquisition card (National Instruments: PXI-6040E). A host PC is connected to a 'Real Time System'. Out put of this Real Time System is connected to output channels of the connector box via digital to analog data acquisition card (National Instruments: PXI-6040E). Output channels of the connector box are connected to the four channel piezo actuator system equipped with voltage amplifier. Finally, the output wires from the voltage amplifier are connected to the PZT-5H actuator. This completes the desired electrical circuit. Figures 5.3 show a schematic photograph of so formed experimental set-up. A 'smart piezo structure' is now ready. We will show in the following sections how this 'smart piezo structure' can control the structural vibrations smartly!

5.2 Working of a 'Real Smart Piezo Structure'

When vibrations are generated in the 'smart structure' by means of some disturbance, PZT-5H sensor immediately generates an electric signal. Sensor signal from PZT-5H piezoceramic sensor patch goes to four channel sensor signal conditioning system where it is amplified using a piezoelectric charge amplifier after conditioning. Amplified sensor signal is obtained and stored on a cathode ray oscilloscope. Amplified sensor signal is assessed and manipulated by 'PXI Based Real Time System'. This Real Time System minimizes various time delays. A control program written in 'Lab VIEW 7.1 Real Time

Property	Units	Plate	PZT-5H
Length	m	0.16	0.02
Breadth	m	0.16	0.02
Thickness	m	0.00043	0.00106
Density	kgm^{-3}	7800	7500
Young's Modulus	Nm^{-2}	2.07×10^{11}	6.3×10^{10}
Poisson's Ratio	unitless	0.3	0.3
Coefficient of Thermal Expansion	$^oC^{-1}$	---	5×10^{-9}
Curie Temperature	^oC	---	190
Reference Temperature	^oC	25	25
Dielectric Constant	unitless	---	3200
Rayleigh Damping Coefficients	rad sec^{-1}	$\alpha = 0.01$	
	sec	$\beta = 0.00016$	

Table 5.1: **Material properties of galvanized steel plate and PZT-5H**

Natural frequency	Theoretical value (in Hz)	Experimental value (in Hz)
1st	15.01	14.51
2nd	36.45	40.96
3rd	87.49	87.04
4th	112.65	116.1
5th	130.90	132.3

Table 5.2: **First five theoretical and experimental frequencies of smart plate instrumented with collocated piezoceramic patches**

Software' on a host PC is downloaded into Real Time System and is executed there. After real time manipulation of sensor signal in Real Time System as per the control program, digital to analog data acquisition card outputs the desired control signal. This control signal reaches piezo actuator system where it is amplified using a voltage amplifier. Amplified control signal obtained from the piezo actuator system is applied on the actuator. On receiving the electrical signal, PZT-5H actuator expands and contracts in such a manner that vibrations of the 'smart structure' are forced to die.

5.3 Results and Discussions

In this section, experimental results on active vibration control of the first mode of a smart cantilevered plate instrumented with one PZT-5H sensor-actuator pair are presented. Experiments are conducted for ambient temperatures ranging from 25°C to 75°C. While performing the experiment at an elevated 'ambient temperature', following steps are taken care of:

1. Temperature of the thermal chamber is maintained at a particular value for twenty minutes before taking the readings so that smart plate uniformly achieves temperature equal to 'ambient temperature'.
2. Temperature of the thermal chamber is cooled down to 'reference temperature' each time after performing the experiment at an elevated temperature. It is kept at 'reference temperature' for at least half an hour before performing the experiment at next higher temperature.
3. At each 'ambient temperature', uncontrolled and controlled sensor signal is obtained for manual displacement of smart cantilevered plate against a vertical gap of 2mm at the edge opposite to cantilevered edge.

4. At each 'ambient temperature', first modal vibrations are controlled using: (i) 'temperature non-robust control scheme' and (ii) 'temperature robust control scheme' discussed in previous chapter.

First of all, uncontrolled sensor signal is obtained at 'reference temperature' and stored in the CRO. FFT of the sensor signal is done on the CRO and first five natural frequencies are noted. These experimental natural frequencies are compared with the theoretical natural frequencies obtained using finite element model derived in Chapter III. Experimental and theoretical natural frequencies so obtained, are shown in Table 5.2. It can be observed that both match well which experimentally proves the accuracy of present finite element model.

First modal vibrations are now controlled by applying 'temperature non-robust control scheme'. Controlled vibration response of smart cantilevered plate is stored in the CRO. Now, experiment is performed when 'ambient temperature' of the thermal chamber is 35°C. Uncontrolled sensor signal is stored in the CRO. First modal vibrations are controlled by applying 'temperature non-robust control scheme' and 'temperature robust control scheme' separately. Controlled vibration response of smart cantilevered plate for both the cases is stored in the CRO. This experiment is repeated at elevated ambient temperatures 45°C, 55°C, 65°C and 75°C.

Uncontrolled sensor signal at each elevated temperature is shown in Figure 5.4. It can be observed that uncontrolled sensor signal increases with temperature though the smart cantilevered plate is given the same displacement at each temperature. This can be attributed to the fact that: (i) sensor voltage is directly proportional to 'e_{31}' and inversely

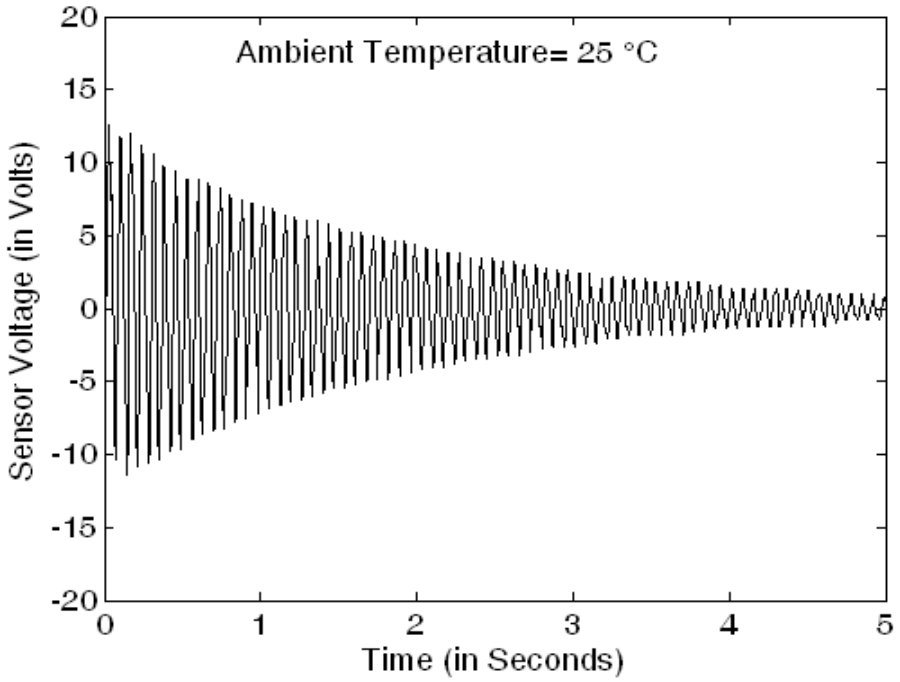

Figure 5.4a: Sensor signal at ambient temperature 25°C

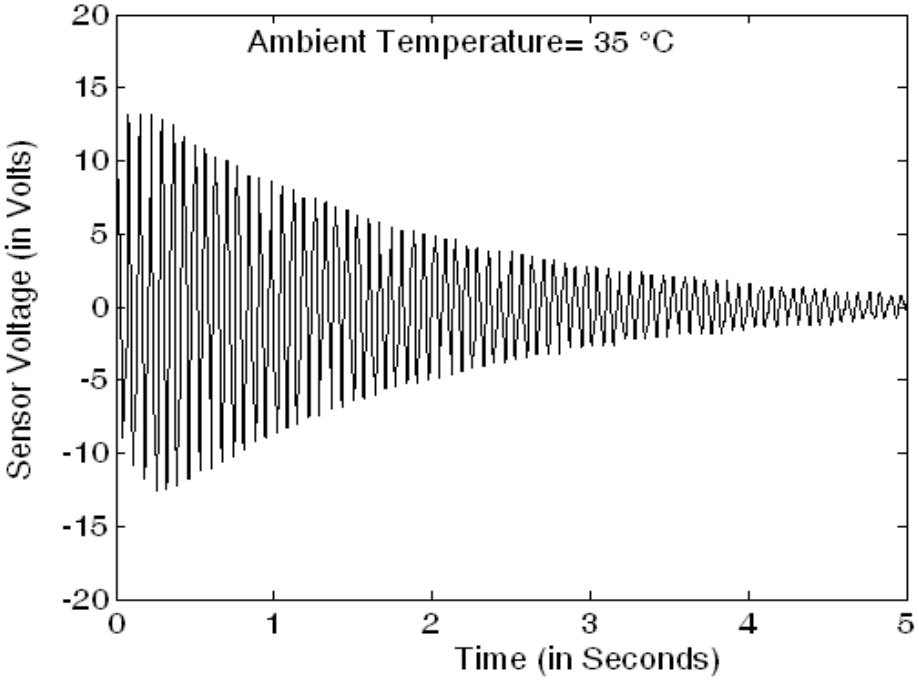

Figure 5.4b: Sensor signal at ambient temperature 35°C

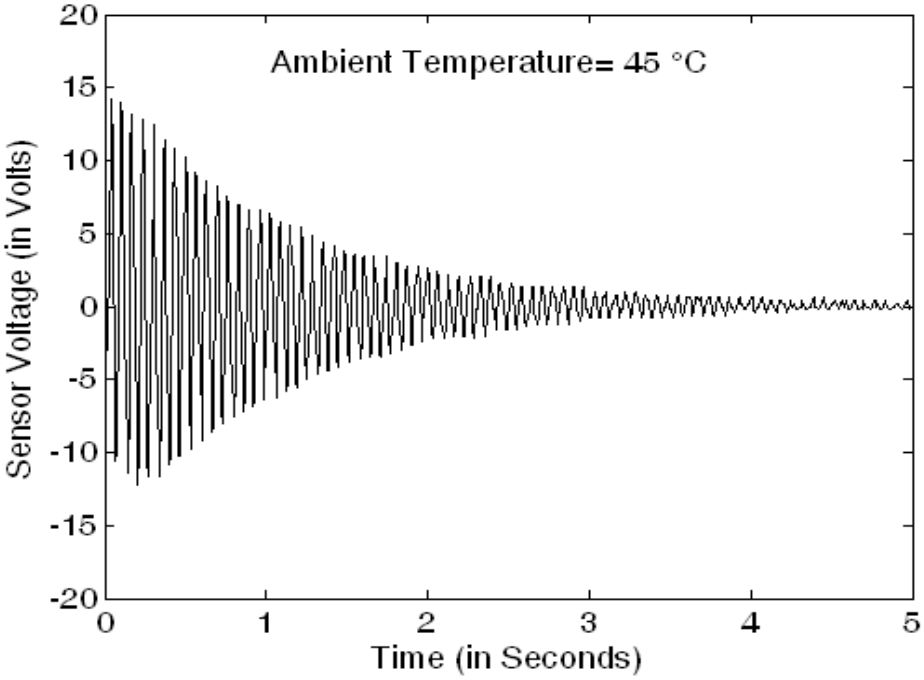

Figure 5.4c: Sensor signal at ambient temperature 45°C

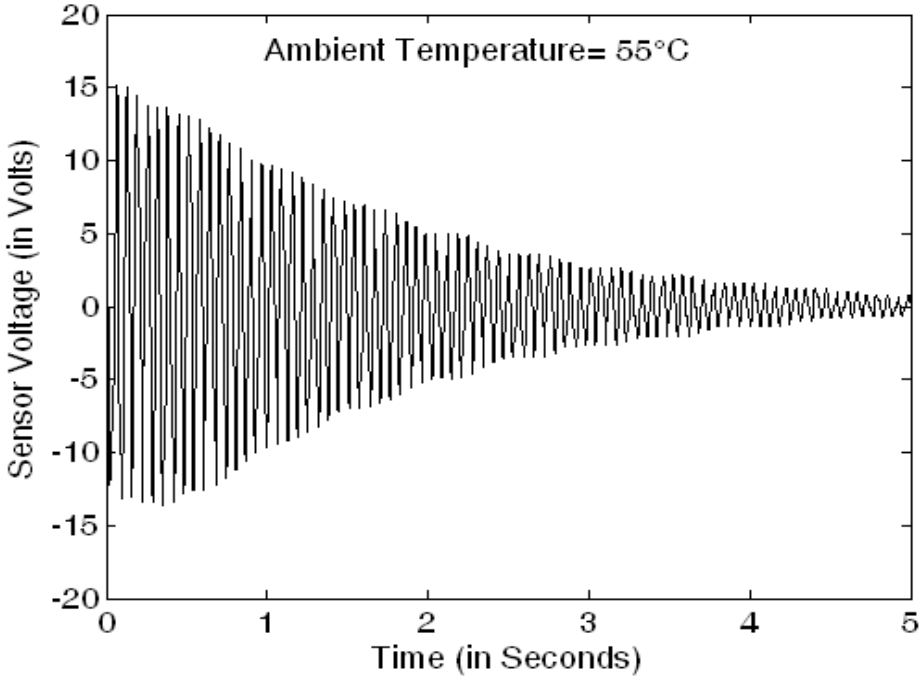

Figure 5.4d: Sensor signal at ambient temperature 55°C

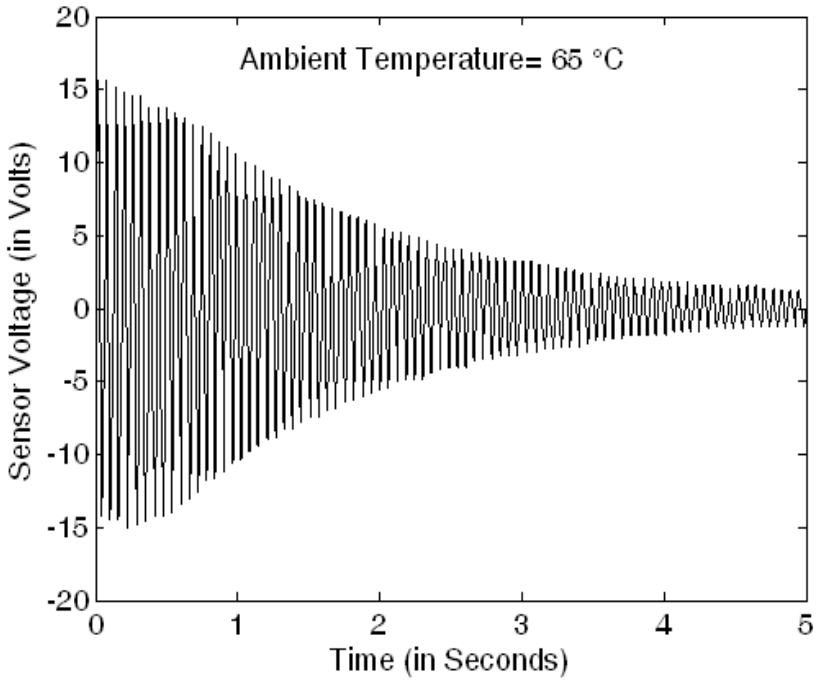

Figure 5.4e: Sensor signal at ambient temperature 65°C

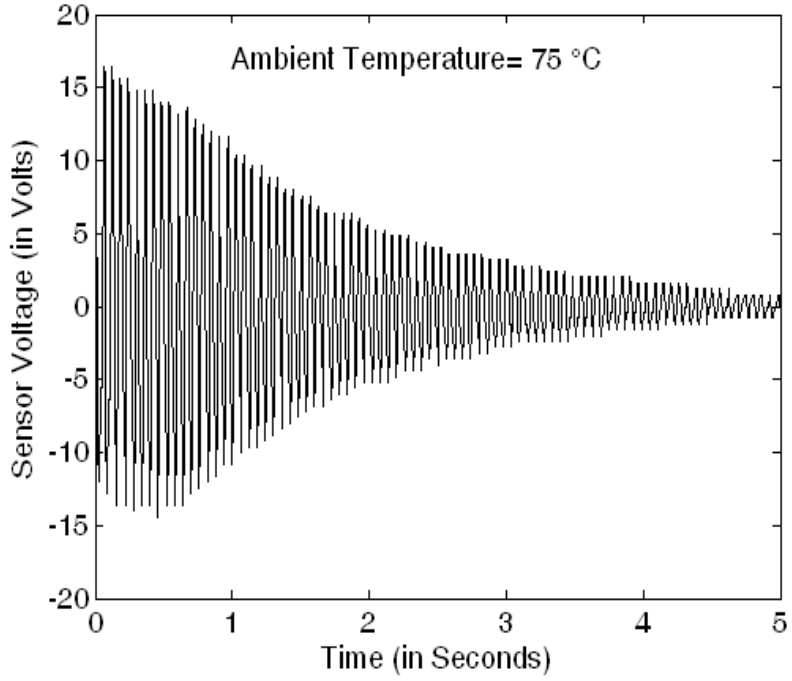

Figure 5.4f: Sensor signal at ambient temperature 75°C

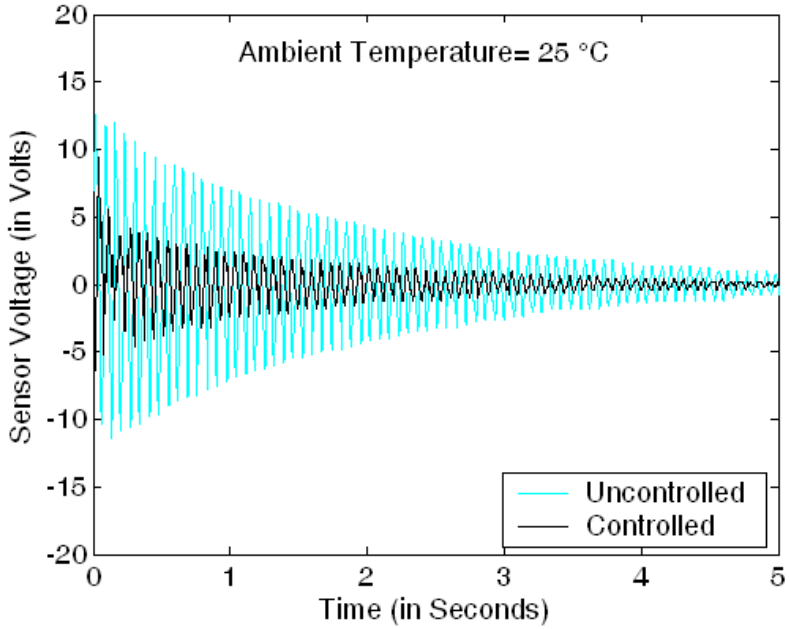

Figure 5.5: Active vibration control of a smart cantilevered plate using piezoceramic PZT-5H at 25°C using temperature non-robust and temperature robust control schemes

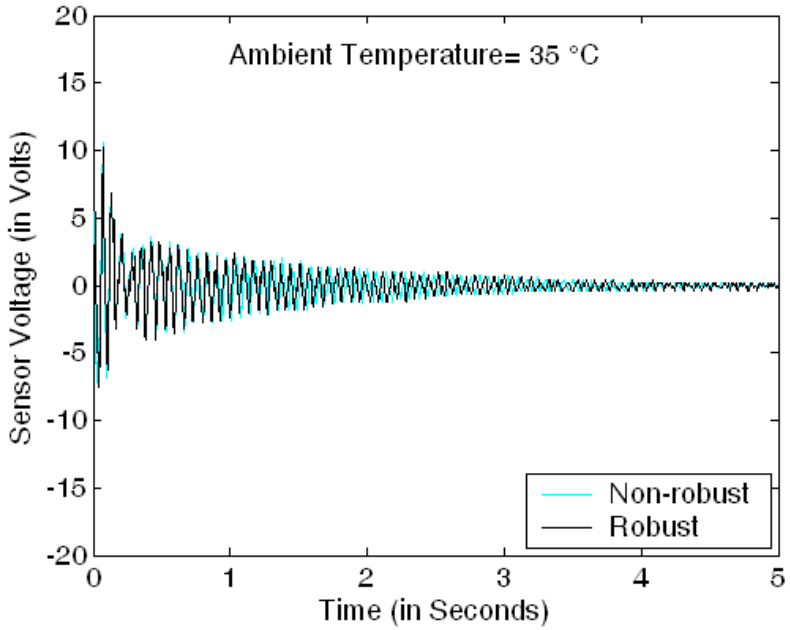

Figure 5.6a: Active vibration control of a smart cantilevered piezo plate at ambient temperature 35°C

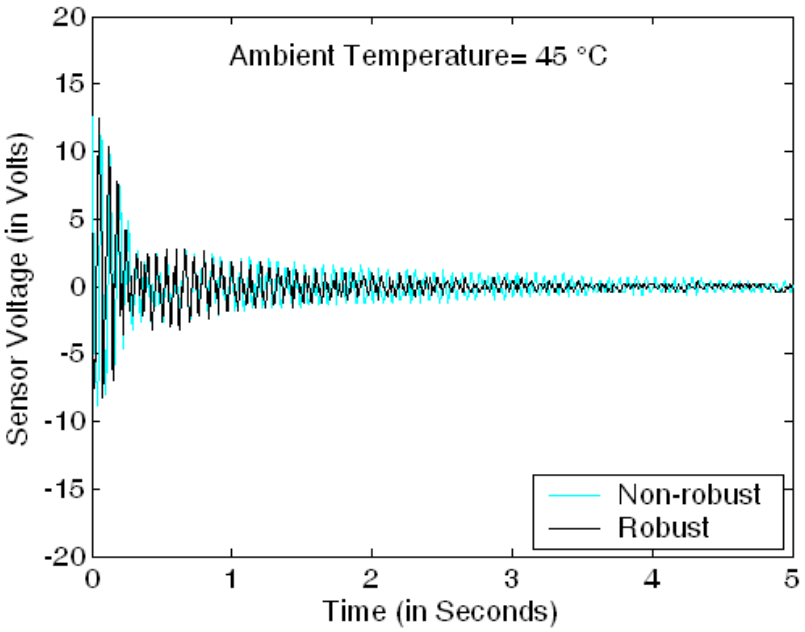

Figure 5.6b: Active vibration control of a smart cantilevered piezo plate at ambient temperature 45°C

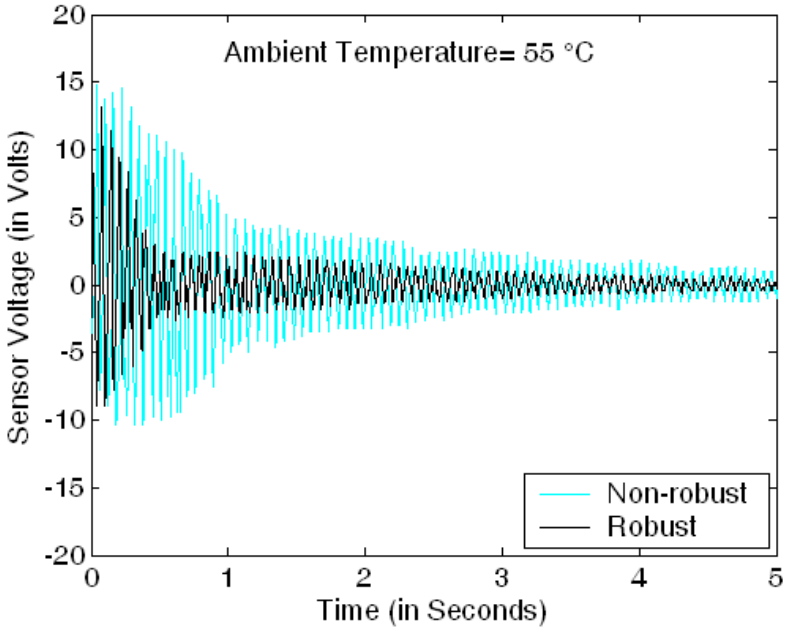

Figure 5.6c: Active vibration control of a smart cantilevered piezo plate at ambient temperature 55°C

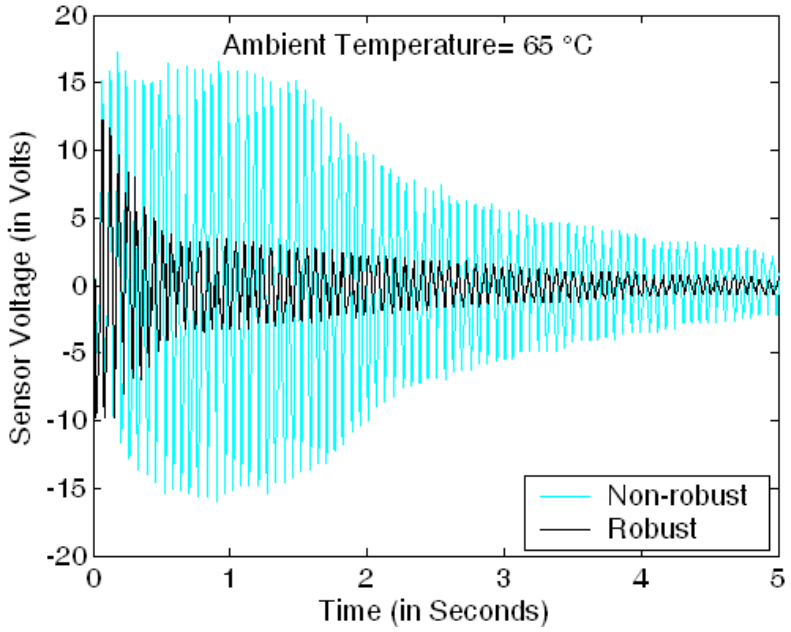

Figure 5.6d: Active vibration control of a smart cantilevered piezo plate at ambient temperature 65°C

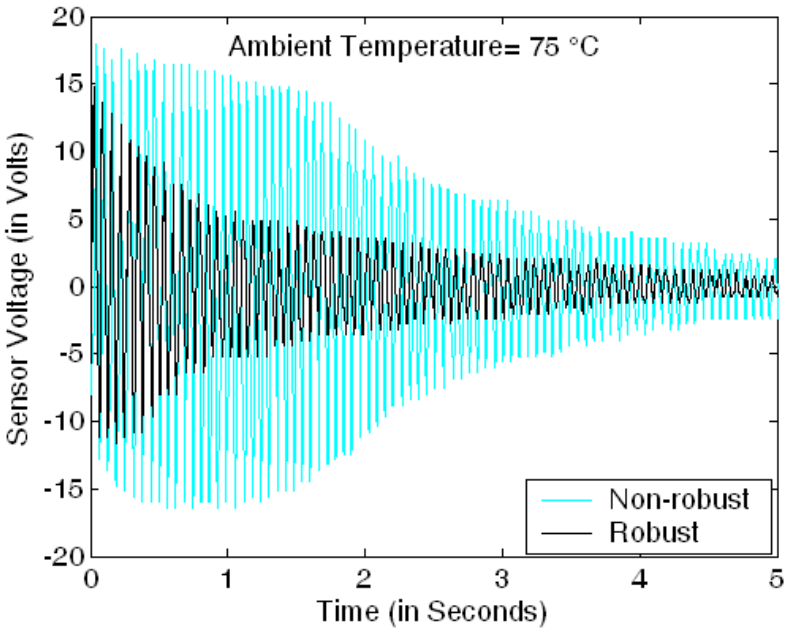

Figure 5.6e: Active vibration control of a smart cantilevered piezo plate at ambient temperature 75°C

proportional to '$\in_{33}$' (equation (4.10)) and (ii) 'e_{31}' increases more rapidly than '$\in_{33}$' within temperature range of 25°C to 75°C.

Controlled sensor signals at 'reference temperature' and at elevated temperatures are shown in Figure 5.5 and Figure 5.6. It can be observed that the active vibration control of the first vibration mode of smart cantilevered plate is achieved nicely at 'reference temperature' 25°C. Also, sensor signals using temperature non-robust and temperature robust control schemes are same (Figure 5.5). Controlled sensor signals at elevated temperatures are shown in Figure 5.6. At elevated temperatures, sensor signals obtained using temperature non-robust and temperature robust control schemes are compared. It is observed that 'temperature non-robust control scheme' fails to maintain active vibration control performance at elevated temperatures. When 'ambient temperature' exceeds 55°C, the system becomes unstable since controlled sensor signals (Figures 5.6(d)-(e)) are inferior to even uncontrolled signal (Figure 5.4) at 'reference temperature'. However, 'temperature robust control scheme' is able to maintain active vibration control performance at elevated temperatures too. These experimental results uphold author's point that actual values of piezoelectric stress coefficients and permittivity should be used in piezoelectric constitutive equations when 'smart piezo structure' is intended to be used at temperatures away from 'reference temperature' of the piezoelectric material. Hence, the newly proposed scheme for active vibration control at elevated temperatures is experimentally proved.

CHAPTER VI

CONCLUSIONS AND FUTURE SCOPE

Active vibration control technique using piezoelectric sensors and actuators is still an infant and restricted to laboratories only. This multidisciplinary field can emerge as a technology in future. To do so, researchers need to implement this technique on real life products and structures. Real life structures are generally complex and have to work in real life conditions where various factors like temperature, humidity etc. keep on changing. Piezoelectric materials are sensitive to these factors. So, in order to implement AVC in real life conditions, active vibration control technique should be robust to these factors. Present work is an attempt in this direction and suggests a new scheme to counter temperature effects. Simulation studies have shown that this new scheme is robust to temperature variations. This scheme has been tested experimentally at various elevated temperatures. Various conclusions drawn from this work are summarized in the following section.

6.1 Conclusions

Present work stresses the need to include temperature variations of piezoelectric strain/ stress and permittivity coefficients in piezoelectric constitutive equations. It would make the mathematical model of 'smart piezo structure' robust to temperature variations. Following conclusions are drawn from this work:

1. Sensor voltage is directly proportional to the piezoelectric stress coefficient and inversely proportional to the permittivity coefficient.

2. Modal state vectors estimated by Kalman observer depend upon both piezoelectric stress and permittivity coefficients.

3. Control voltage to be applied on piezoelectric actuator is directly proportional to modal velocity and inversely proportional to the piezoelectric stress coefficient.

4. Total control efforts applied by the piezoelectric actuator depend upon both piezoelectric stress and permittivity coefficients.

5. Piezoelectric stress coefficient and the permittivity have different values at different temperatures. Therefore, piezoelectric stress and permittivity coefficient values measured at 'reference temperature' can not be considered for all temperatures.

6. Static voltage as a result of 'thermal strain effect' is directly proportional to piezoelectric stress coefficient and inversely proportional to the permittivity coefficient. Due to different stress & permittivity coefficients of piezoelectric sensor and actuator patches under closed loop conditions, generation of static voltage as a result of 'thermal strain effect' induces a net static displacement in smart piezo plate. As a result, 'equilibrium position' of the smart piezo plate changes under closed loop conditions.

7. Static voltage as a result of 'pyroelectric effect' is inversely proportional to permittivity coefficient. Due to different stress & permittivity coefficients of piezoelectric sensor and actuator patches under closed loop conditions, generation of static voltage as a result of 'pyroelectric effect' induces a net static displacement in smart piezo plate. As a result, 'equilibrium position' of the smart piezo plate changes under closed loop conditions.

8. If temperature dependence of piezoelectric stress and the permittivity coefficients is ignored in constitutive equations at temperatures other than 'reference temperature', then:

(i) sensor and actuator behaviour can not be accurately predicted (ii) modal state vectors of the 'smart piezo structure' are wrongly estimated by Kalman state observer (iii) static sensor voltages generated as a result of thermal strain and pyroelectric effects are wrongly calculated and (iv) 'equilibrium position' of the 'smart piezo structure' is also wrongly estimated. As a result, the controller applies wrong control voltages on the actuator.

9. Active vibration control performance is not maintained and it eventually fails at temperatures substantially away from 'reference temperature' if temperature dependence of piezoelectric stress and the permittivity coefficients is ignored in piezoelectric constitutive equations.

10. Active vibration control performance is maintained at all temperatures when temperature dependence of piezoelectric stress and the permittivity coefficients is included in piezoelectric constitutive equations. In other words, the AVC scheme becomes robust to temperature variations.

11. Temperature dependence of piezoelectric stress and the permittivity coefficients is material specific and there is no reliable analytical expression for this so far. Therefore, temperature dependence of these coefficients can be determined using experimental characterization of the piezoelectric material to be used.

12. The variation of piezoelectric stress and the permittivity coefficients with temperature can be included in the piezoelectric constitutive equations using curve fit technique to match the experimental values. It updates piezoelectric constitutive equations at each 'ambient temperature'.

6.2 Scope for Future Work

Before active vibration technique is implemented on real life products and structures, researchers will have to make it robust to various factors present in the real life environment. A scheme to counter temperature effects in 'smart piezo structure' has been proposed and experimentally proved in present work. This sets the stage for future work in this direction so that AVC technique is finally implemented on real products and structures. Some of the important future research directions are:

1. Electromechanical interaction of piezoelectric sensors and actuators in real life environment is not completely understood. Their performance is sensitive to thermal, hygro, non-linearities, fatigue, ageing effects etc. In order to implement AVC on real life products and structures, future work in AVC should be carried out to cope with these effects.

2. Real life structures are generally complex and it is difficult to model them mathematically. However, very less research has been carried out on the online system identification of smart structures. Therefore in the present world of fast processors, researchers should look for finding the equations of motion of smart piezo structures using online system identification techniques.

3. Boundary conditions assumed in the mathematical model of real life structures may change during its working. Therefore, robust model updating methods are required which can update the mathematical model of 'smart piezo structure' during its operation.

With this contribution to the multidisciplinary field of active vibration control using piezoelectric sensors and actuators, authors hope that the research in coming years shall enable this field to serve the mankind !

REFERENCES

1. Cady W G 1964 *Piezoelectricity* vol I (New York: Dover)
2. Jaffe B *et al* 1971 *Piezoelectric Ceramics* (London: Academic)
3. Roberts S 1947 Dielectric and piezoelectric properties of Barium Titanate *Phy. Rev*. **71** 890-895
4. Jaffe B *et al* 1954 *Journal of Applied Physics* **25** 809-810
5. Fukada E 2000 History and recent progress in piezoelectric polymers *IEEE Transactions on Ultrasonics, Ferroelectrics and Frequency Control* **47** 1277-1290
6. Ikeda T 1996 *Fundamentals of Piezoelectricity* (Oxford: Oxford University Press)
7. Crawley E and de Luis J 1987 Use of piezoelectric actuators as elements of intelligent structures *AIAA J.* **25** 1373-85
8. Sun C T and Zhang X D 1995 Use of thickness shear mode in adaptive sandwich structures *Smart Mater. Struct.* **4** 202-206
9. Raja S *et al* 2004 Thermally induced vibration control of composite plates and shells with piezoelectric active damping *Smart Mater. Struct.* **13** 939-950
10. Fahy F J and Walker J G 1998 *Fundamentals of noise and vibration control* (Spon: London)
11. Brennan M J and Ferguson N S 2004 *Vibration control: Advanced application in acoustics, noise and vibration* (London: Spon)

12. Lam K Y and Ng T Y 1999 Active control of composite plates with integrated piezoelectric sensors and actuators under various dynamic loading conditions *Smart Mater. Struct.* **8** 223-237

13. Chantalakhana C and Stanway R 2000 Active constrained layer damping of plate vibrations: a numerical and experimental study of modal controllers *Smart Mater. Struct.* **9** 940-952

14. Fuller C R *et al* 1997 *The active control of vibration* (New York: Academic)

15. Fabunni J A 1980 Forced vibration of single stage axial compressor rotor *Journal of Engg. for Power* **102** 322-328

16. Bailey T and Hubbard J E Jr 1985 Distributed piezoelectric-polymer active vibration control of a cantilevered beam *J. Guidance, Control, Dynam.* **8** 605-11

17. Hanagud S *et al* 1985 Electronic damping techniques and active vibration control *AIAA* **85-0752** 443-453

18. Baz A and Poh S 1988 Performance of an active control system with piezoelectric actuators *Journal of Sound and Vibration* **126** 327-343

19. Chandrashekhara K and Tanneti R 1995 Thermally induced vibration suppression of laminated plates with piezoelectric sensors and actuators *Smart Mater. Struct.* **4** 281-290

20. Raja S *et al* 2002 Active vibration control of composite sandwich beams with piezoelectric extension-bending and shear actuators *Smart Mater. Struct.* **11** 63-71

21. Li F X *et al* 2008 Quasi-static thermo-electro-mechanical behaviour of piezoelectric stack actuators *Smart Mater. Struct.* **17** 015049

22. Lahtinen R *et al* 2007 A piezopaint based sensor for monitoring structure dynamics *Smart Mater. Struct.* **16** 2571-2576

23. Glynne-Jones P *et al* 2001 A method to determine the ageing rate of thick-film PZT layers *Smart Mater. Struct.* **12** 663-670

24. Yang J and Xiang H J 2007 Thermo-electro-mechanical characteristics of functionally graded piezoelectric actuators *Smart Mater. Struct.* **16** 784-797

25. Tzou H S and Fu H Q 1994 A study of segmentation of distributed piezoelectric sensors and actuators Part I:Theoretical analysis *Journal of Sound and Vibration* **172** 247-259

26. Dosch J J *et al* 1992 A self-sensing piezoelectric actuator for collocated control *J. Intell. Mater. Syst. Struct.* **3** 166-84

27. Anderson E H *et al* 1992 Self-sensing piezoelectric actuation: analysis and application to controlled structures *33rd SDM Conference* AIAA-92-2465-CP.

28. Simmers Jr G E *et al* 2004 Improved piezoelectric self-sensing actuation *J. Intell. Mater. Syst. Struct.* **15** 941-953

29. Yang S M and Chiu J S 1994 Dither motor design with concurrent sensing and actuating piezoelectric materials *Smart Mater. Struct.* **3** 248-53

30. Yang S M and Jeng C A 1996 Structural vibration suppression by concurrent piezoelectric sensor and actuator *Smart Mater. Struct.* **5** 806-813

31. Zhang Wenfeng *et al* 2004 Robust vibration control of a plate using self-sensing actuators of piezoelectric patches *J. Intell. Mater. Syst. Struct.* **15** 923-931

32. Simmers Jr G E *et al* 2007 Thermal protection for a self-sensing piezoelectric control system *Smart Mater. Struct.* **16** 2492-2500

33. Zhang X D and Sun C T 1996 Formulation of an adaptive sandwich beam *Smart Mater. Struct.* **5** 814-23

34. Benjeddou A *et al* 2000 Piezoelectric actuation mechanisms for intelligent sandwich structures *Smart Mater. Struct.* **9** 328-335

35. Wang S Y *et al* 2001 Vibration control of smart piezoelectric composite plates *Smart Mater. Struct.***10** 637-644

36. Shaik Dawood M S I *et al* 2008 Three-dimensional static shape control analysis of composite plates using distributed piezoelectric actuators *Smart Mater. Struct***. 17** 025002

37. Sharma M *et al* 2007 Modal control of a plate using fuzzy logic controller *Smart Mater. Struct***. 16** 1331-1341

38. Meirovitch L *et al* 1983 A comparison of control techniques for large flexible systems *Journal of Guidance Control and Dynamics* **6** 302-310

39. Meirovitch L 1988 *Control of distributed systems large space structures: Dynamics and control* (Berlin: Springer)

40. Proulx B and Cheng L 2000 Dynamic analysis of piezoceramic actuation effects on plate vibrations *Thin Walled Structures* **37** 147-162

41. Lee C K and Moon F C 1990 Modal sensors/actuators *ASME J. Appl. Mech*. **57** 434-441

42. Tzou H S and Hollkamp J J 1994 Collocated independent modal control with self-sensing orthogonal piezoelectric actuators (theory and experiment) *Smart Mater. Struct.* **3** 277-284

43. Chen C Q and Shen Y P 1997 Optimal control of active structures with piezoelectric modal sensors and actuators *Smart Mater. Struct.* **6** 403-409

44. Fripp M L and Atalla M J 2001 Review of modal sensing and actuation techniques *Shock and Vibration Digest* **33** 3-14

45. Hwang W S and Park H C 1993 Finite element modeling of piezoelectric sensors and actuators *AIAA Journal* **31** 930-937

46. Yang S M and Lee Y J 1994 Interaction of structure vibration and piezoelectric actuation *Smart Mater. Struct.* **3** 494-500

47. Kim J *et al* 1996 Finite element modeling of smart cantilevered plate and comparison with experiments *Smart Mater. Struct.* **5** 165-170

48. Mindlin R D 1961 On the equations of motion of piezoelectric crystals *Problems of Continuum Mechanics* (*N.I. Muskhelishvili 70th Birthday Volume*) 2nd edn (Philadelphia, PA: SIAM) 282–90

49. Tiersten H F 1971 On the nonlinear equations of thermoelectroelasticity *Int. Journal of Engg. Sc.* **9** 587-604

50. Mindlin R D 1974 Equations of high frequency vibrations of thermopiezoelecric crystal plates *Int. J. Solids Struct.* **10** 625-37

51. Nowacki W 1978 Some general theorems of thermopiezoelectricity *J Thermal Stresses* **1** 171-82

52. Nowacki J P 1982 Steady state problems of thermopiezoelectricity *J Thermal Stresses* **5** 183-194

53. Sunar M and Rao S S 1992 Distributed thermopiezoelectric sensors and actuators in structural design *33rd AIAA-ASME-ACSE-AHS-ASC Structures, Structural Dyn and Mat Conf* 890-95

54. Tzou H S and Ye R 1994 Piezothermoelasticity and precision control of piezoelectric systems: Theory and finite element analysis *ASME Journal of Vibration and Acoustics* **116** 489-495

55. Sunar M and Rao S S 1997 Thermopiezoelectric control design and actuator placement *AIAA J.* **35(3)** 534-539

56. Rao S S and Sunar M 1993 Analysis of distributed thermopiezoelectric sensors and actuators in advanced intelligent structures *AIAA J.* **31** 1280-1286

57. Tzou H S and Howard R V 1994 A piezothermoelastic shell theory applied to active structure *ASME Transactions Journal of Vibration and Acoustics* **116** 295-302

58. Bao Y *et al* 1998 Analysis of non-linear piezothermoelastic laminated beam with electric and temperature effects *Journal of Sound and Vibration* **209** 505-18

59. Raja S *et al* 1999 Piezothermoelastic modeling and active vibration control of laminated composite beams *J. Intell. Mater. Syst. Struct.* **10** 890-899

60. Balamurugan V and Narayanan S 2001 Active vibration control of smart shells using distributed piezoelectric sensors and actuators *Smart Mater. Struct.* **10** 173-180

61. Gornandt A and Gabbert U 2002 Finite element analysis of thermopiezoelectric smart structures *Acta Mechanica* **154** 129-140

62. Jiang J P and Li Dong Xu 2008 Finite element formulations for thermopiezoelastic laminated composite plates *Smart Mater. Struct.* **17** 015027

63. Saravanos D A and Heylinger P R 1999 Mechanics and computational models for laminated piezoelectric beams, plates and shells *Appl. Mech. Rev.* **52** 305-20

64. Sunar M and Rao S S 1999 Recent advances in sensing and control of flexible structures via piezoelectric materials *Appl. Mech. Rev.* **52** 1-16

65. Tauchert T R *et al* 2000 Developments in thermopiezoelasticity with relevance to smart composite structures *Composite Structures* **48** 31-38

66. Tzou H S and Ye R 1993 Piezothermoelasticity and control of piezoelectric laminates exposed to a steady state temperature field *ASME Intelligent Struct Mat and Vibrations* **58** 27-34

67. Tzou H S and Ye R 1996 Pyroelectric and thermal strain effects of piezoelectric (PVDF and PZT) devices *Mech. Sys. and Signal Processing* **10** 459-469

68. Friswell M I *et al* 1997 Active damping of thermally induced vibrations *J. Intell. Mater. Syst. Struct.* **8** 678-685

69. Narayanan S and Balamurugan V 2003 Finite element modeling of piezolaminated smart structures for active vibration control with distributed sensors and actuators *Journal of Sound and Vibration.* **262** 529-562

70. Jiang J P and Li Dong Xu 2007 A new finite element model for piezothermoelastic composite beam *Journal of Sound and Vibration* **306** 849-864

71. Kumar R *et al* 2008 Thermally induced vibration control of cylindrical shell using piezoelectric sensor and actuator *Int J Adv Manuf Technol* **38** 551-562

72. Roy T and Chakraborty D 2009 Genetic algorithm based optimal control of smart composite shell structures under mechanical loading and thermal gradient *Smart Mater. Struct.* **18** 115006

73. Giannopoulos G and Vantomme J 2006 A thermal-electrical-mechanical coupled FE formulation using discrete layer kinematics for the dynamic analysis of smart plates *Smart Mater. Struct.* **15** 1846-1857

74. Birman V 1996 Thermal effects on measurements of dynamic processes in composite structures using piezoelectric sensors *Smart Mater. Struct.* **5** 379-385

75. Schulz Mark J *et al* 2003 Piezoelectric materials at elevated temperatures *J. Intell. Mater. Syst. Struct.* **14** 693-705

76. Bronowicki A J *et al* 1996 Mchanical validation of smart structures *Smart Mater. Struct.* **5** 129-139

77. Elsoufi L *et al* 2007 Modeling the thermal behavior of PZT patches during the manufacturing process of smart thermoplastic structures *Smart Mater. Struct.* **16** 1076-1082

78. Wang D *et al* 1998 Infuence of temperature on the electromechanical and fatigue behavior of piezoelectric ceramics *Journal of Applied Physics* **83** 5342-5350

79. Joshi S *et el* 2003 Numerical characterization of functionally graded active materials under electrical and thermal fields *Smart Mater. Struct*. **12** 571-579

80. Apte D A and Gauguli R 2009 Influence of temperature and high electric field on power consumption by piezoelectric actuated integrated structure *Comput. Mater. Continua* **10** 139–162

81. Luck R and E I Egba 1998 On the design of piezoelectric sensors and actuators *ISA Transactions* **37** 65-72

82. Perry M A *et al* 2008 A finite-element-based formulation for sensitivity studies of piezoelectric systems *Smart Mater. Struct.* **17** 015015

83. Smittakorn W and Heyliger P R 2000 A discrete-layer model of laminated hygrothermopiezoelectric plates *Mechanics of Composite Materials and Structures* **7** 79-104

84. Alberada A *et al* 2000 Characterization of the mechanical non-linear behavior of piezoelectric ceramics *IEEE Trans. Ultrason. Ferroelectr. Freq. Control.* **47** 844-853

85. Garcia J E *et al* 2001 High electric field measurement of dielectric constant and losses of ferroelectric ceramics *J. Phys. D: Applied Physics* **34** 3279-84

86. Masys A J *et al* 2003 Piezoelectric strain in lead zirconate titanate ceramics as a function of electric field, frequency and dc bias *J. Appl. Phys.* **94** 1155-62

87. Perez R *et al* 2004 Extrinsic contribution to the non-linearity in a PZT disc *Smart Mater. Struct.* **37** 2648-2654

88. Fleming A J and Moheimani S O R 2004 Improved current and charge amplifiers for driving piezoelectric loads, and issues in signal processing design for synthesis of shunt damping circuits *J. Intell. Mater. Syst. Struct.* **15** 77-92

89. Ge P and Jouaneh M 1996 Tracking control of a piezoceramic actuato *IEEE Trans. Control Syst. Technol.* **4** 209-216

90. Vautier B J G and Moheimani S O R 2005 Charge driven piezoelectric actuators for structural vibration control: issues and implementation *Smart Mater. Struct.* **14** 575-586

91. Liu Y C and Yang S M 1993 Three simple and effective methods for vibration control of slewing flexible structures *Journal of Dynamic Systems, Measurement and Control* **115** 725-30

92. Yang S M and Lee Y J 1993 Optimization of non-collocated sensor/actuator location and feedback gain in control systems *Smart Mater. Struct.* **2** 96-102

93. Reklaitis G V *et al* 1983 *Engineering optimization: method and applications* (New York: John Wiley)

94. Vanderplaasts G N 1984 An efficient feasible directions algorithm for design synthesis *AIAA Journal* **22** 1633-1640

95. Kirkpatrick S *et al* 1983 Optimization by simulated annealing *Science* **220** 671-680

96. Glover F and Laguna M 1997 *Tabu Search* (Kluwer: Academic Publishers)

97. Mitchell M 1996 *An Introduction to Genetic Algorithms* (Cambridge MA: MIT Press)

98. Conte J P *et al* 2003 Consistent finite-element response sensitivity analysis *J. Eng. Mech.* **129** 1380-1393

99. Haftka R T and Gurdal Z 1993 *Elements of structural optimization* (Kluwer: Academic Publishers)

100. Mehrabian A R and Lucas C 2006 Novel numerical optimization algorithm inspired from weed colonization *Ecological Informatics* **1** 355-366

101. Padula S L and Kincaid R K 1999 Optimization strategies for sensor and actuator placement *NASA* **CASI 301 621-0390**

102. Frecker M I 2003 Recent advances in optimization of smart structures and actuators *J. Intell. Mater. Syst. Struct.* **14** 207-216

103. Bin Li *et al* 2000 Maximal modal force rule for optimal placement of piezoelectric actuators for plates *J. Intell. Mater. Syst. Struct.* **11** 512-515

104. Main J A *et al* 1994 Optimal placement and sizing of paired piezo-actuators in beams and plates *Smart Mater. Struct.* **3** 373-381

105. Bruch Jr J C *et al* 2000 Optimal piezo-actuator locations/lengths and applied voltage for shape control of beams *Smart Mater. Struct.* **9** 205-211

106. Correia V M F *et al* 2000 Modeling and design of adaptive composite structures *Computer Methods in Applied Mechanics & Engg.* **185** 325-346

107. Correia V M F *et al* 2001 Refined models for the optimal design of adaptive structures using simulated annealing *Composite Structures* **54** 161-167

108. Moita J S M *et al* 2006 Optimal design in vibration control of adaptive structures using a simulated annealing algorithm *Composite Structures* **75** 79-87

109. Sunar M *et al* 2001 Robust design of piezoelectric actuators for structural control *Computer Methods in Applied Mechanics & Engg.* **190** 6257-6270

110. Zhang J *et al* 2008 A LQR controller design for active vibration control of flexible structures *IEEE Pacific-Asia Workshop on Computational Intelligence and Industrial Application* 127-132

111. Ip K H and Tse P C 2001 Optimal configuration of a piezoelectric patch for vibration control of isotropic rectangular plates *Smart Mater. Struct.* **10** 395-403

112. Barboni R *et al* 2000 Optimal placement of PZT actuators for the control of beam dynamics *Smart Mater. Struct.* **9** 110-120

113. Yang Y and Zhang L 2006 Optimal excitation of a rectangular plate resting on an elastic foundation by a piezoelectric actuator *Smart Mater. Struct.* **15** 1063-1078

114. Quek S T *et al* 2003 Vibration control of composite plates via optimal placement of piezoelectric patches *J. Intell. Mater. Syst. Struct.* **14** 229-245

115. Zhang J *et al* 2009 Study of optimal location and size of piezoelectric actuators in smart structures *IEEE Int. Asia Conf. on Informatics in Control, Automation and Robotics* 42-46

116. Kim T W and Kim J H 2005 Optimal distribution of an active layer for transient vibration control of a flexible plate *Smart Mater. Struct.* **14** 904-916

117. Yang F *et al* 2005 Optimal placement of active bars in smart structures *Proc. of IEEE International Conf. on Mechatronics & Automation* **1** 1-6

118. Yang S M and Lee Y J 1993 Vibration suppression with optimal sensor/actuator location and feedback gain *Smart Mater. Struct.* **2** 232-239

119. Yang Y *et al* 2005 Integrated optimal design of vibration control system for smart beams using genetic algorithms *Journal of Sound and Vibration* **282** 1293-1307

120. Gaudiller L and Hagopian J D 1996 Active control of flexible structures using a minimum number of components *Journal of Sound and Vibration* **193** 713-741

121. Bruant I *et al* 2001 A methodology for determination of piezoelectric actuator and sensor location on beam structures *Journal of Sound and Vibration* **243** 861-882

122. Livine W S and Athans M 1970 On the determination of the optimal constant output feedback gains for linear multivariable systems *IEEE Trans. Automatic Control* **AC-15** 44-48

123. Changho N *et al* 1996 Optimal sizing and placement of piezo-actuators for active flutter suppression *Smart Mater. Struct.* **5** 216-224

124. Fahroo F and Wang Y 1997 Optimal location of piezoceramic actuators for vibration suppression of a flexible structure *Proc. of 36th IEEE Conf. on Decision and Control* 1966-1971

125. Demetriou M A 2000 A numerical algorithm for the optimal placement of actuators and sensors for flexible structures *Proc. of American Control Conference, AACC* 2290-2294

126. Young L I *et al* 2002 Simultaneous optimization of piezoelectric actuator placement and feedback for vibration suppression *Acta Astronautica* **50** 335-341

127. Gao W *et al* 2003 Optimal placement of active bars in active vibration control for piezoelectric intelligent truss structures with random parameters *Computers & Structures* **81** 53-60

128. Si H *et al* 2003 Optimization of the number and locations of the actuators in smart structures *Proc. of IEEE Int. Conf. Robotics, Intell. Sys. Sig. Processing* 841-846

129. Kumar K R and Narayanan S 2007 The optimal location of piezoelectric actuators and sensors for vibration control of plates *Smart Mater. Struct.* **16** 2680-2691

130. Lammering R *et al* 1994 Optimal placement of piezoelectric actuators in adaptive truss structures *Journal of Sound and Vibration* **171** 67-85

131. Inman D J 2006 *Vibration with control* (West Sessex: John Wiley & Sons)

132. Hac A and Liu L 1993 Sensor and actuator location in motion control of flexible structures *Journal of Sound Vibration* **167** 239-61

133. Peng F *et al* 2005 Actuator placement optimization and adaptive vibration control of plate smart structures *J. Intell. Mater. Syst. Struct.* **16** 263-271

134. Bruant I and Proslier L 2005 Optimal location of actuators and sensors in active vibration control *J. Intell. Mater. Syst. Struct.* **16** 197-206

135. Grace A *et al* 1990 *Control system toolbox for use with MATLAB* (Natick, MA: The MathWorks)

136. Sadri A M *et al* 1999 Modeling and optimal placement of piezoelectric actuators in isotropic plates using genetic algorithms *Smart Mater. Struct.* **8** 490-498

137. Kermani M R *et al* 2004 Parameter selection and control design for vibration suppression using piezoelectric transducers *Control Engg. Practice* **12** 1005-1015

138. Hamden A M and Nayfeh A H 1989 Measures of modal controllability and observability for first and second order linear systems *AIAA J. Guidance, Contr. Dynam.* **12** 421-8

139. Sadri A M *et al* 1998 Robust strategies for active vibration control of strain actuated plate like structures *UKACC Int. Conf. on Control* 213-218

140. Aldraihem O J *et al* 2000 Optimal size and location of piezoelectric actuator/sensors: practical considerations *AIAA Journal of Guidance, Control and Dynamics* **23** 509-515

141. Gopal M 2008 *Digital control and state variable methods* 3rd ed (New Delhi: Tata McGraw Hill)

142. Wang Q and Wang C M 2001 A controllability index for optimal design of piezoelectric actuators in vibration control of beam structures *Journal of Sound Vibration* **312** 210-233

143. Wang Q and Wang C M 2000 Optimal placement and size of piezoelectric patches on beams from the controllability perspective *Smart Mater. Struct.* **9** 558-567

144. Dhuri K D and Sheshu P 2006 Piezo-actuator placement and sizing for good control effectiveness and minimal change in original system dynamics *Smart Mater. Struct.* **15** 1661-1672

145. Dhuri K D and Sheshu P 2009 Multi-objective optimization of piezo-actuator placement and sizing using genetic algorithms *Journal of Sound Vibration* **323** 495-514

146. Moheimani S O R and Ryall T 1999 Considerations on placement of piezoelectric actuators that are used in structural vibration control *Proc. of 38th IEEE Conf. on Decision and Control* 1118-1123

147. Moheimani S O R and Fu M 1998 Spatial H_2 norm of flexible structures and its application in modal order election *Proc. of 37th IEEE Conf. on Decision and Control* 3623-3624

148. Halim D and Moheimani S O R 2003 An optimization approach to optimal placement of collocated piezoelectric actuators and sensors on a thin plate *Mechatronics* **13** 27-47

149. Liu W *et al* 2006 A computational scheme for optimal sensor/actuator placement of flexible structures using spatial H_2 measures *Mechanical Systems and Signal Processing* **20** 881-895

150. Qui Z *et al* 2007 Optimal placement and active vibration control of piezoelectric smart flexible cantilever plate *Journal of Sound Vibration* **301** 521-543

151. Dhuri K D and Sheshu P 2007 Favorable locations for piezo actuator in plates with good control effectiveness and minimal change in system dynamics *Smart Mater. Struct.* **16** 2526-2542

152. Guney M and Eskinat E 2008 Optimal actuator and sensor placement in flexible structures using closed-loop criteria *Journal of Sound Vibration* **312** 210-233

153. Demetriou M A and Armaou A 2005 Optimal actuator placement and model reduction for a class of parabolic partial differential equations using H_2 norm *Proc. of American Control Conference, AACC* 4569-4574

154. Li Z N *et al* 2004 Optimal sensor locations for structural vibration measurements *Applied Acoustics* **65** 807-818

155. Baruh H 1992 Placement of sensors and actuators in structural control *Control and Dynamic Systems* **52** 359-390

156. Kim Y and Junking J L 1991 Measure of controllability for actuator placement *AIAA Journal of Guidance, Control and Dynamics* **14** 895-902

157. Aldraihem O J *et al* 1997 Realistic determination of the optimal size and location of piezoelectric actuators/sensors *IEEE Int. Conf. on Control Applications* 435-440

158. Sun D and Tong L 2001 Modal control of smart shells by optimized discretely distributed piezoelectric transducers *Int. Journal of Solids and Structures* **38** 3281-3299

159. Han J H *et al* 1997 An experimental study of active vibration control of composite structures with a piezo-ceramic actuator and a piezo-film sensor *Smart Mater. Struct.* **7** 549-558

160. Preumont A 2002 *Vibration control of active structures: An introduction* 2nd ed (Kluwer: Academic Publishers)

161. Joshi S M 1989 *Control of large flexible space structure* (Berlin: Springer)

162. Han J H and Lee In 1999 Optimal placement of piezoelectric sensors and actuators for vibration control of a composite plate using genetic algirithms *Smart Mater. Struct.* **8** 257-267

163. Lee C K *et al* 1991 Piezoelectric modal sensor/actuator pairs for critical active damping vibration control *J Acoust Soc Am.* **90** 374-384

164. Dimitriadis E K *et al* 1991 Piezoeletric actuators for distributed vibration excitation of thin plates *Journal of Vibration and Acoustic* **113** 100-107

165. Yang S M and Lee Y J 1994 Modal analysis of stepped beams with piezoelectric materials *Journal of Sound and Vibration* **176** 289-300

166. Yang S M and Jeng C A 1996 Structural vibration suppression by concurrent piezoelectric sensor and actuator *Smart Mater. Struct.* 806-813

167. Aoki Y *et al* 2008 Modeling of a piezoceramic patch actuator for velocity feedback control *Smart Mater. Struct.* **17** 015052

168. Chandrashekhara K and Agarwal A N 1993 Active vibration control of laminated composite plates using piezoelectric devices: a finite element approach *J. Intell. Mater. Syst. Struct.* **4** 496-508

169. Reddy J N 2005 *An introduction to the finite element method* 3rd ed (New York: Tata McGaw-Hill)

170. Huang D J *et al* 2007 Piezoelasticity solutions for functionally graded piezoelectric beams *Smart Mater. Struct.* **16** 687-695

171. Geradin M and Rixen D 1993 *Theories des vibrations-Application a la Dynamique des Structures* (Paris: Mason)

172. Kargarnovin M H *et al* 2007 Vibration control of a functionally graded material plate patched with piezoelectric actuators and sensors under a constant electric charge *Smart Mater. Struct.* **16** 1252-1259

173. Petyt M 1990 *Introduction to finite element vibration analysis* 2nd ed (New York: Cambridge University Press)

174. Lin C C and Huang H N 1999 Vibration control of beam-plates with bonded piezoelectric sensors and actuators *Computers and Structures* **73** 239-248

175. Huang D and Sun B 2001 Approximate analytical solutions of smart composite Mindlin beams *Journal of Sound and Vibration* **244** 379-394

176. Mirzaeifar R *et al* 2008 Active control of natural frequencies of FGM plates by piezoelectric sensor/actuator pairs *Smart Mater. Struct.* **17** 045003

177. Akella P *et al* 1994 Modeling and control of smart structures with bonded piezoelectric sensors and actuators *Smart Mater. Struct.* **3** 344-353

178. Oh Jinho *et al* 2007 Enhanced lower-order shear deformation theory for fully coupled electro-thermo-mechanical smart laminated plates *Smart Mater. Struct.*, **16** 2229-2241

179. Allik H and Hughes J R 1970 Finite element method for piezoelectric vibration *Int. J. Num. Methods in Engg.* **2** 151-157

180. Tzou H S and Tseng C I 1991 Distributed vibration control and identification of coupled elastic/piezoelectric systems: Finite element formulation and application *Mechanical Systems and Signal Processing* **5** 215-231

181. Ha S K *et al* 1992 Finite element analysis of composite structures containing distributed piezoelectric sensors and actuators *AIAA Journal* **30** 772-780

182. Manna M C *et al* 2009 Static analysis of rubber components with piezoelectric patches using nonlinear finite element *Smart Structures and Systems* **5** 23-42

183. Bathe K J 1996 *Finite element procedures in engineering analysis* (Englewood Cliffs, NJ: Prentice-Hall)

184. MacNeal R H 1987 A theorem regarding locking of tapered four-node membrane elements *Int. J. Numer. Methods Eng.* **24** 1793-1799

185. Sze K Y 2000 On immunizing five-beta hybrid stress elements from trapezoidal locking in practical analysis *Int. J. Numer. Methods in Engg.* **47** 907-920

186. Kim *et al* 1997 Finite element modeling of structures with piezoelectric active devices *Int. J. Numer. Methods in Engg.* **40** 817-832

187. Varadan V V *et al* 1996 Closed loop finite-element modeling of active/passive damping in structural vibration control *Smart Mater. Struct.* **5** 685-694

188. Ghandi K and Hagood N W 1997 A hybrid finite element model for phase transitions in non-linear electro-mechanically coupled material *Mathematics and control in smart structures Proc. of SPI,* **3039** 97-112

189. Sze K Y and Pan Y S 1999 Hybrid finite element models for piezoelectric materials *Journal of Sound and Vibration* **226** 519-547

190. Sze K Y and Yao L Q 2000 A hybrid stress ANS solid shell elements and its generalization to smart structure modeling *Int. J. Numer. Methods in Engg.* **48** 545-582

191. Bathe K J and Dvorkin E N 1986 A formulation of general shell elements–the use of mixed interpolation of tensorial components *Int. J. Numer. Methods in Engg.* **22** 697-722

192. Stolarski H S 1991 On a formulation of the quadrilateral with highly accurate in-plane bending behavior *First U.S. National Congress on Computational Mechanics, Chicago*

193. Sze K Y and Yao L Q 2000 Modeling smart structures with segmented piezoelectric sensors and actuators *Journal of Sound and Vibration* **235** 495-520

194. Zheng S *et al* 2004 The formulation of a refined hybrid enhanced assumed strain solid shell element and its application to model smart structures containing distributed piezoelectric sensors/actuators *Smart Mater. Struct.* **13** N43-N50

195. Simo J C and Armero F 1992 Geometrically non-linear enhanced strain mixed methods and the method of incompatible modes *Int. J. Numer. Methods Eng.* **33** 1413-49

196. Chen W and Cheung Y K 1992 Three dimensional 8-node and 20-node refined hybrid isoparametric elements *Int. J. Numer. Methods Eng.* **35** 11871-89

197. Sharma M *et al* 2005 Fuzzy logic based modal space control of a cantilevered beam instrumented with piezoelectric patches *Smart Mater. Struct.* **14** 1017–1024

198. Guyan R J 1965 Reduction of stiffness and mass matrices *AIAA J.* **3** 380

199. Baz A 2000 Spectral finite-element modeling of the longitudinal wave propagation in rods treated with active constrained layer damping *Smart Mater. Struct.* **9** 372-377

200. Ochoa O O and Reddy J N 1992 *Finite element analysis of composite laminates* (Dordrecht: Kluwer Academic)

201. Mitchell J A and Reddy J N 1995 A refined plate theory for composite laminates with piezoelectric laminae *J. Solids Struct.* **32** 2345-2367

202. Griffiths D J 1999 *Introduction to electrodynamics* 3rd ed (Prentice Hall)

203. Wang F *et al* 2007 Accurate modeling of a piezoelectric composite beam *Smart Mater. Struct.* **16** 1595-1602

204. Robbins D H and Reddy J N 1991 Analysis of piezoelecrically actuated beams using a layer-wise displacement theory *Computers and Structures* **41** 265-279

205. Han J H and Lee In 1998 Analysis of composite plates with piezoelectric actuators for vibration control using layerwise displacement theory *Composite Part B* **29** 621-632

206. Han J H *et al* 1999 Vibration and actuation characteristics of composite structures with a bonded piezo-ceramic actuator *Smart Mater. Struct.* **8** 136-143

207. Benjeddou A 2000 Advances in piezoelectric finite element modeling of adaptive structural elements: a survey *Computers and Structures* **76** 347-363

208. William Saunders R *et al* 1994 Experiments in piezostructure modal analysis for MIMO feedback control *Smart Mater. Struct.* **3** 210-218

209. Bruant I *et al* 2001 Active control of beam structures with piezoelectric actuators and sensors: modeling and simulation *Smart Mater. Struct.* **10** 404-408

210. Meirovitch L 1989 Dynamics and Control of Structures (New York: John Wiley & Sons)

211. Lee Y Y and Yao J 2003 Structural vibration suppression using the piezoelectric sensors and actuators *Journal of Vibration and Acoustics* **125** 109-113

212. Singh S P *et al* 2003 Efficient modal control strategies for active control of vibrations *Journal of Sound and Vibration* **262** 563-575

213. Yang S M and Bian J J 1996 Vibration suppression experiments on composite laminated plates using an embedded piezoelectric sensor and actuator *Smart Mater. Struc.,* **5** 501-507

214. Chen S.H. *et al* 1997 Active vibration control and suppression for intelligent structures *Journal of Sound and Vibration* **200** 167-177

215. Lim Y H *et al* 1999 Finite element simulation of smart structures using an optimal output feedback controller for vibration and noise control *Smart Mater. Struct.* **8** 324-337

216. Zhabihollah A *et al* 2007 Active vibration suppression of smart laminated beams using layerwise theory and asn optimal control strategy *Smart Mater. Struct.* **16** 2190-2201

217. Friswell M I and Inman D J 1999 The relationship between positive position feedback and output feedback controllers *Smart Mater. Struct.* **8** 285-291

218. Manning W J *et al* 2000 Vibration control of a flexible beam with integrated actuators and sensors *Smart Mater. Struct.* **9** 932-939

219. Kumar R and Khan M 2007 Pole placement techniques for active vibration control of smart structures: A feasibility study *Journal of Vibration and Acoustics* **129** 601-615

220. Miller S E *et al* 1995 Active distributed vibration control of anisotropic piezoelectric laminated plates *Journal of Sound and Vibration* **179** 797-817

221. Amant Y S and Cheng L 2000 Simulations and experiments on active vibration control of a plate with integrated piezoceramics *Thin Walled Structures* **38** 105-123

222. Kim Y S and Wang K W 1993 On the sliding mode control of structural vibrations via variable damping *Mechanical Systems and Signal Processing* **7** 335-347

223. Choi S B *et al* 1995 Sliding mode control of vibration in a single-link flexible arm with parameter variations *Journal of Sound and Vibration* **179** 737-748

224. Rao V *et al* 1994 The adaptive control of smart structures using neural networks *Smart Mater. Struct.* **3** 354-366

225. Smyser C P and Chandershekhara K 1997 Robust vibration control of composite beams using piezoelectric devices and neural networks *Smart Mater. Struct.* **6** 178-189

226. Li Y Y *et al* 2003 Modeling and vibration control of a plate coupled with piezoelectric material *Composite Structures* **62** 155-162

227. Wang D A and Huang Y M 2002 Robust vibration control of a beam using the H_∞ based controller with model error compensator *Journal of Sound and Vibration* **254** 877-895

228. Kar I N *et al* 2002 Multimode vibration control of a flexible structure using H_∞ based control *IEEE Transactions on Mechatronics* **5** 23-30

229. Yu W and Hodges D H 2004 A simple thermopiezoelastic model for smart composite plates with accurate stress recovery *Smart Mater. Struct.* **13** 926-938

230. Abramovich H and Pletner B 1997 Actuation and sensing of piezolaminated sandwich type structures *Composite Structures* **38** 17-27

231. Karagulle H *et al* 2004 Analysis of active vibration control in smart structures by ANSYS *Smart Mater. Struct.* **13** 661-667

232. Malgaca L and Karagulle H 2009Simulation and experimental analysis of active vibration control of smart beams under harmonic excitation *Smart Structures and Systems* **5** 55-68

233. Benjeddou A 2009 New insights in piezoelectric free-vibrations using simplified modeling and analyses *Smart Structures and Systems* **5** 591-612

234. Reaves C M and Horta L G 2003 Piezoelectric actuator modeling using MSC/NASTRAN and MATLAB *NASA* **TM-2003-212651**

235. Marinkovic D *et al* 2007 Accurate modeling of the electric field within piezoelectric layers for active composite structures *J. Intell. Mater. Syst. Struct.* **18** 503-513

236. Kumar R and Singh S P 2006 Adaptive hybrid control of smart structures subjected to multiple disturbances *Smart Mater. Struct.* **15** 1345-1357

237. Blanguernon A *et al* 1999 Active control of a beam using a piezoceramic element *Smart Mater. Struct.* **8** 116-124

238. Reddy J N 2007 *Theory and Analysis of Elastic Plates and Shells* 2nd ed (Boca Raton, FL: CRC Press)

239. Ling *et al* 1997 An impedence method for dynamic analysis of active material systems *J. Intell. Mater. Syst. Struct.* **8** 323-334